Summer 2016

Identification And Characterization Of DNA Repair Snf2/Swi2 Atpases In Tetrahymena Thermophila

Andrew Francis Morin

IDENTIFICATION AND CHARACTERIZATION OF DNA REPAIR SNF2/SWI2 ATPASES IN TETRAHYMENA THERMOPHILA

A Masters Thesis

Presented to

The Graduate College of

Missouri State University

In Partial Fulfillment

Of the Requirements for the Degree

Master of Science, Cell and Molecular Biology

By

Andrew Francis Morin

July 2016

IDENTIFICATION AND CHARACTERIZATION OF DNA REPAIR SNF2/SWI2 ATPASES IN TETRAHYMENA THERMOPHILA

Biomedical Sciences

Missouri State University, July 2016

Master of Science

Andrew Morin

ABSTRACT

The Snf2/Swi2 ATPases Rad5 and Rad16 have been shown to play vital roles in a number of DNA repair pathways. In both *Saccharomyces cerevisiae* and human cell lines, Rad5 homologs (SHPRH, HLTF) have been shown to function in DNA double strand break (DSB) repair along with pathways that repair damage after replication. The function of Rad16, unlike Rad5, has been found only in lower eukaryotes such as *Saccharomyces*, despite the fact that it plays an essential role in nucleotide excision repair (NER), and more specifically in the repair of silenced areas of the genome. In order to more fully understand the function of Rad16, this work focuses on using a model organism, *Tetrahymena thermophila*, to identify and characterize the functional aspects of both Rad5 and Rad16. To do this, qPCR analyses of the potential Rad5/16 homologs were conducted to determine their expression, while shRNA constructs were designed to inhibit their expression to assess the phenotypic consequences of DNA damage in deficient cells. Expression analyses showed that three of the potential homologs (Rad16, Rad5.2, and Rad5.1) have damage-depended expression, and that the levels of one can have substantial effects on levels of the others. Moreover, two of the homologs, Rad16NH and Rad5.1, show altered survival after genotoxic stress. The data showed that the functions of Rad16 and Rad5 homologs in *Tetrahymena* may diverge greatly from those in lower eukaryotes.

KEYWORDS: rad16, rad5, nucleotide excision repair, genome stability, snf2/swi2 atpase

This abstract is approved as to form and content

_____

Joshua J. Smith
Chairperson, Advisory Committee
Missouri State University

IDENTIFICATION AND CHARACTERIZATION OF DNA REPAIR SNF2/SWI2 ATPASES IN TETRAHYMENA THERMOPHILA

By

Andrew Morin

A Masters Thesis
Submitted to the Graduate College
Of Missouri State University
In Partial Fulfillment of the Requirements
For the Degree of Master of Sciences, Cell and Molecular Biology

July 2016

Approved:

_____
Joshua J. Smith, PhD

_____
Colette M. Witkowski, PhD

_____
Amanda C. Brodeur, MD, PhD

_____
Julie Masterson, PhD: Dean, Graduate College

ACKNOWLEDGEMENTS

I would like to thank the following people for their support during the course of my graduate studies. Dr. Joshua Smith, for his constant guidance and support, along with the freedom he gave to plan and execute experiments. I can honestly say that I would not have made it without him. All the members of Smith Lab; especially Kyle Cottrell for his assistance with the shRNA sequence design, Emily Nischwitz and Rachel Mullner for their help with one of the RNA extraction procedures, and Allie Maltzman for her initial bioinformatic search for Rad16. I would also like to thank my family for their constant support and fiancé, Arielle Simpson, for always pushing me to be a better person and scientist.

TABLE OF CONTENTS

LIST OF FIGURES

INTRODUCTION

Snf2/Swi2 ATPases

There are many distinct families of proteins which have been identified based on structural similarities, and while the proteins in these groups are related by sequence, more often than not, they have distinctly different functions. One such group of proteins is the family of Snf2/Swi2 ATPases, which are initially classified based on the presence of a specific ATPase motif which was originally characterized in the *Saccharomyces cerevisiae* Snf2 protein (Davis et al., 1992). The ATPase domains that this protein family contains are structurally related to DEAD box helicases, but lack any of the traditional helicase activity seen in that motif (Eisen et al., 1995). Despite this, the vast majority of Snf2-like proteins have been shown to interact with DNA in different ways, and a number of them are involved in DNA repair and transcriptional regulation.

The defining hallmark of this class of proteins are the characteristic ATPase domains which have been studied across the family of proteins in great depth. The ATPase consists of seven specific sequence blocks however the spacing, placement, and sequence of these domains can still vary between members of this family of proteins (Flaus et al., 2006). In general, this series of domains has the ability to catalyze ATP in a DNA dependent manner (Caruthers and McKay, 2002). The energy created by the reaction can allow the protein containing the domain to interact with other proteins to facilitate their binding to a substrate; or that same energy can be utilized to allow the domain containing protein to overcome pre-existing binding to the substrate (Becker and Horz, 2002). In the second case, an ATPase will use the energy derived from the

conversion of ATP to ADP to displace proteins which are already interacting with a substrate (such as histone proteins on DNA), so that the other proteins may take their place (Flaus and Owen-Hughes, 2001).

The way in which helicase and helicase-like domains (including the Snf2/Swi2 ATPases) were arranged along with their sequence homology led to the initial classification of these proteins into a specific superfamilies (SF). There are multiple SFs, with the Snf2/Swi2 ATPases falling into SF2, along with the DEAD box helicases (Durr et al., 2006). The largest similarities between these very diverse proteins comes from the spacing and sequence of the domains, where there are two clusters of the ATPase sequences; one, the N-terminal which contains the first, second, third, and fourth sequences and the second cluster, the C-terminal, consisting of the fifth and sixth sequences (Ding et al., 1999).

The SF2 proteins are further divided into a number of families, which are separated based on the structure and function of the proteins as a whole. The Snf2/Swi2 ATPases fall into the Snf2 family. In *Saccharomyces*, there are 17 Snf2 family members, which can be classified further into 12 distinct subfamilies, again based on their structure and function (Flaus et al., 2006). These subfamilies include: the Rad54 subfamily (named for the primary member Rad54, which is a well-studied protein involved in homologous recombination (HR)), the Snf2 subfamily (which are known to be involved in transcriptional activation), and the Rad5/16 subfamily (composed of Rad5 and Rad16, which play direct roles in the processes of post replication repair (PRR) and nucleotide excision repair (NER), respectively).

Rad5 and Rad16

Rad5 and Rad16 are particularly interesting since they share extremely close homology but have been shown to operate in independent pathways in distinct manners. Aside from the ATPase domains, Rad5 and Rad16 share another interesting functional domain, a cullin-RING ubiquitin ligase domain. This domain is situated between the N-terminal and C-terminal ATPase domains; which is considered embedded due to its placement. Much like the ATPase domains, the RING domain has been shown to serve a distinct and important function, it serves as an E3 ubiquitin conjugating enzyme.

Ubiquitin is a small protein modifier which, as the name suggests, is utilized by many different cellular proteins. In order to attach ubiquitin to a substrate a specific enzymatic cascade is utilized. The first step of this cascade involves activating the ubiquitin, this is carried out by a class of E1 ubiquitin activating enzymes. There are only a small number of E1 enzymes because they are general purpose and will act on ubiquitin to modify the C-terminus by forming a thiolester bond between the ubiquitin and the E1. In *Saccharomyces* the E1 enzyme responsible for most of the ubiquitin activation is Uba1 (McGrath et al., 1991). At this point the E1 will transfer the ubiquitin to an E2 ubiquitin conjugating enzyme, which acts to displace the E1 at the bonding site and bind in its place. The E2 enzymes are also a small class, because their main function is to transfer ubiquitin from E1 enzymes to the substrate protein with the help of E3 enzymes. However, there are instances where an E2 enzyme can transfer the ubiquitin molecule directly to a substrate, but these instances are by far the minority.

The final step in the enzymatic cascade is the transfer of the ubiquitin from the E2 to an E3 ubiquitin ligase. Again, this transfer occurs at the thiolester bond, with the E3

removing the ubiquitin from the E2 enzyme. The E3 enzymes are by far the most numerous and diverse class of proteins involved in the process. The E3 enzymes confer specificity to the process, their job is to facilitate the transfer of the ubiquitin from the E2 enzyme to specific lysine residues on a target protein. The E3 proteins are localized to the target ubiquitin substrates either through their own actions or through the actions of proteins with which they complex (Li et al., 2008). It is this step, the transfer from an E2 to the substrate via an E3, which makes up the majority of the cases in which ubiquitin is transferred to a substrate. It is important to note that ubiquitin molecules can also be a substrate which gets ubiquitinated, leading to polyubiquitination of a target lysine residue.

Ubiquitin has very important dual roles in protein function within the cell; it can function to signal for proteasomal degradation of proteins, or it can protect proteins from degradation. The ubiquitin proteasome pathway has been studied in depth, and much like the modification of histones, there are a variety of different ways that a protein can be ubiquitinated. An amino acid residue can be modified with a single ubiquitin or with a chain of ubiquitin molecules; and a protein can be modified with ubiquitin at a number of different residues. This variability allows for a great amount of diversity in the way that proteins can be modified, changing their stability and longevity.

In addition to the ATPases and E3 ubiquitin ligase Rad5 contains a domain which is not present in Rad16 or any of the other Snf2 family of ATPases, this is the HIRAN domain. The HIRAN domain is a Rad5 characteristic protein motif which serves as a DNA binding domain, which may serve to recognize damaged DNA or stalled replication forks (Iyer et al., 2006). This function would serve to localize Rad5 to damaged DNA

without the need for other protein factors. Interestingly enough, the HIRAN domain has been found as a standalone protein in bacteria, or as a part of an endonuclease containing proteins in some eukaryotes (Iyer et al., 2006). It is important to note that the proposed function of the HIRAN domain is based largely on bioinformatic analysis, as it was more recently discovered and there has not been a large amount of analysis of its function.

DNA Damage and Repair

Rad5 and Rad16 share very close homology and domain architecture, and despite this fact they have been shown to function in very different processes. Rad16 has been shown to function in only one process, nucleotide excision repair. The process of NER is necessary for the repair of bulky adducts on DNA. There are two major types of lesions which are repaired by NER; cyclobutane pyrimidine dimers (CPDs) and 6-4 photoproducts (6-4 PPs). In general, CPDs occur between adjacent thymines on the same strand of DNA, and result in the creation of a cyclobutane ring between the 5' and 6' carbons in the six membered ring structure of the thymines (Lukin and de Los Santos 2006). In contrast the 6-4 PPs will form between any two adjacent pyrimidines creating a single bond between the 6' carbon of one and the 4' carbon of the other (Lukin and de Los Santos 2006). Both types of lesions have an effect on the local structure of the DNA, where they can cause bulging of the helical structure and prevent hydrogen bonding of complementary base pairs across the helix.

Other than their ability to affect the local structure of DNA there are also a number of other detrimental outcomes that can result from these bulky DNA adducts. If a large number of them are clustered in the same general area on the DNA then the large

scale structure of the DNA can be affected which may cause single strand or double strand breaks. If these lesions are not repaired immediately they can prevent the proper function of other proteins, such as DNA or RNA polymerase, causing stalling of replication or transcription machinery (Limoli et al., 2002). If the machinery for replication or transcription does not stall then the damaged bases may be recognized as purines, which leads to mutations in the new strand of DNA or RNA.

The primary cause of this type of damage is ultraviolet (UV) radiation, which provides the energy that leads to the structural changes. The distribution of the two types of damage is not even, with CPDs composing about 75% of the UV induced lesions and 6-4 PPs making up the remaining percentage of the lesions (Sinha and Häder, 2002). Another factor which affects the severity of the damage is the location in which the damage occurs. If it occurs in an area of the genome where transcription is actively occurring, it has the potential to induce the errors mentioned above; while damage occurring in silenced areas of the genome would induce errors during replication.

There are two distinct pathways of NER, the use of which depends on where the damage occurs. Damage in actively transcribed areas of the genome is repaired by transcription coupled NER (tcNER); while damage in silenced areas of the genome is repaired by global genome NER (ggNER). The primary difference in the two types of NER is at the recognition step. In areas that are being transcribed a lesion in the DNA will stall RNA polymerase, this acts as the recognition and recruitment step due to the "bubble" created by the stalled polymerase (Tapias et al., 2004). This bubble is an area on the DNA where the two strands are separated, when the bubble lingers, in this case

due to the RNA polymerase being unable to advance, the process of NER can begin when the bubble is recognized by transcription factor 2-H ($TF_{II}H$).

In ggNER, RNA polymerase is not present at the site of damage and so does not create the bubble needed for NER, so in this case the recognition step is more targeted. The lesion in DNA is recognized by two proteins that are present in the cell, Rad4 (XPC) and Rad23 (HR23). During ggNER Rad4 and Rad23 recognize and bind to the lesion, shortly after Rad14 (XPA) localizes to the site of damage through an affinity for damaged DNA (Shuck et al., 2008). This complex attracts $TF_{II}H$ which acts to melt the DNA which separates the two strands of DNA. After this point, the processes occur in the same way and utilize the same series of proteins.

Once the DNA helicase activity of $TF_{II}H$ melts the DNA, other factors are able to assemble at the melted region of DNA which is between 24 and 32 nucleotides. Two endonucleases, Rad2 (XPG) and the Rad10-Rad1 complex (ERCC1-XPF), cut the 3' and 5' sides of the damaged strands; Rad2 acts at the 3' and Rad10-Rad1 act at the 5' end of the melted DNA (Le May et al., 2010). The damaged strand is removed while DNA polymerases fill the gap left and DNA ligase seals the final nick left after the XP complex leaves the DNA. In NER there are four major nucleotide excision repair factors (NEFs) that have been identified in yeast and are conserved among other eukaryotes; these NEFs are made of distinctive functional units. NEF1 is composed of the proteins Rad1, Rad10, and Rad14, NEF2 is composed of Rad4 and Rad23, NEF3 includes Rad2 and $TF_{II}H$, and NEF4 is Rad7, Rad16 and Elc1.

Functionally speaking the process is highly conserved between eukaryotic species with the main differences being in the damage detection step and the overall number of

proteins involved in the process. However, it should be noted that no human homologs of Rad16 or Rad7 have yet been identified. Despite the fact that no homolog has been found, the function that Rad16 serves is vital to the process of ggNER, and as such it is highly likely that a functional homolog of Rad16 exists.

While Rad16 has only been shown to be involved in ggNER, Rad5 is involved in a number of different processes. Originally, the proposed purpose to Rad5 was its activity in the regression of stalled replication forks, in complex with its partners Mms2, Ubc13, and Rad18 (Gangavarapu et al., 2006). This activity occurs via the E3 ubiquitin ligase domain, and requires the activity of its E2 partner, the Mms2/Ubc13 complex. This pathway also requires the activity of Rad18 to mono-ubiquitinate the processivity clamp (PCNA), without which there can be no classical Rad5 activity (Gangavarapu et al., 2006).

Post-replication repair (PRR) is used as an umbrella term to describe a number of different processes which do not repair damaged DNA at the time it is recognized. There are many different pathways which fall into the category of PRR, they include trans-lesion synthesis (TLS) and template switching. The process of TLS occurs when a DNA polymerase stalls at the site of damage due to physical changes in DNA structure (Lehmann and Fuchs, 2007). Template switching is a general term which is used to refer to any process that uses a homologous DNA sequence as a template in the place of one which is damaged, but whose mechanism does not seek to repair or replace the damaged strand (Smirnova and Klein, 2003). As such, this excludes processes such as homologous recombination (HR) which uses a homologous chromosome to synthesize a new strand which replaces the damaged one (Zhao et al., 2007).

It is important to understand that while these processes are considered part of DNA repair they do not actually repair the initial lesion (Lehmann 2007). More appropriately they can be considered damage avoidance mechanisms, which allow the normal process of DNA replication to occur without prolonged stalling and worsening the effects of the current damage (Lehmann et al., 2006). In most cases this is accomplished through the use of specialized DNA repair polymerases which have higher fidelity when working with chemically altered bases (Hoege et al., 2002).

DNA damage has the potential to induce more damage in one of two ways; either directly or indirectly. Damage is induced directly when abnormalities in the DNA structure, such as CPDs, are clustered in one area and cause strain on the DNA backbone, this strain can lead to separation of the strands or to breaks in the backbone of the DNA molecule (Wang and Smith, 1986). Damage is caused indirectly when another protein attempts to interact with already damaged DNA (Wang and Smith, 1986). In these instances, the damaged DNA has the potential to prevent interactions with other proteins, such as stalling DNA or RNA polymerases, or the damage can be misinterpreted by polymerases which interact with the damage (Satoh et al., 1993). This type of interaction can lead to synthesis of a new strand of DNA or RNA which has improperly placed nucleotides, which can cause various mutations such as frameshifts, deletions, or insertions (Nouspikel, 2009).

UV radiation can induce errors in replication which require replication fork regression; in *Saccharomyces* Rad5Δ and Rad5 E3 mutated strains the survivability is greatly decreased after exposure to UV light when compared to wild type cells (Chen et al., 2005). When exposed to ionizing radiation, which induces double-strand damage and

subsequent repair, the Rad5Δ and Rad5 ATPase mutant showed almost identically low survival rates (Chen et al., 2005). These data suggest that Rad5, specifically the ATPase activity, has an important function in a double-strand break repair pathway. This repair is hypothesized to occur via interaction with the Mre11-Rad50-Nbs1 (MRN complex) as Rad5 activity was decreased only when the Rad51 pathway was inhibited (Gangavarapu et al., 2006). While the exact method and process of this repair remains elusive the data shows that both domains in Rad5 are conserved and maintain diverse, independent activity.

Rad5 Higher Eukaryotic Homologs: HLTF and SHPRH

In humans and other higher eukaryotes there are two homologs of Rad5, helicase-like transcription factor (HLTF) and Snf2 histone linker PHD RING helicase (SHPRH). Interestingly, there are a number of ways in which SHPRH and HLTF can work together as well as independently of each other. Both proteins will interact with Rad18, and these reactions will lead, in both cases, to the ubiquitination of the PCNA (Lin et al., 2011). Where the two differ is in the way they ubiquitinate the PCNA, and how that change in ubiquitination appears to lead to utilization of the different arms of PRR, specifically the trans-lesion synthesis (TLS) pathway. Additionally, the choice of which is used depends largely on the type of agent which generates the damage.

There are two types of damage which can lead to the use of PRR, there is DSB damage, or bulky adducts caused by UV damage. Since transcription and replication are processes that alter the structure of DNA they must occur quickly to return the DNA to its normal state. As such, the recognition of the damage in either case occurs when a

polymerase stalls. The first step of the process involves the ubiquitination of PCNA, this is facilitated by two proteins, Rad6 and Rad18 which are E2 and E3 ubiquitin enzymes, respectively. As discussed previously, these two proteins fill the role of conjugating the ubiquitin and conferring specificity to the substrate, in this case lysine 63 (K63) or164 (K164) of PCNA (Motegi et al., 2008).

Prior to damage, Rad18 can be found conjugated to both HLTF and SHPRH in the cell, and at the same relative frequency (Lin et al., 2011). It is after a specific type of damage that Rad18 begins to primarily associate with either HLTF or SHPRH. Data has shown that when treated with MMS which induces DSBs, the HLTF itself can become ubiquitinated and marked for degradation (Lin et al., 2011). As a result, SHPRH becomes the only functional factor bound to Rad18, and this complex can act to transfer a polyubiquitin chain to PCNA at K63. This results in dissociation of PCNA from the polymerase and DNA, which, in turn, allows dissociation of the normal polymerase and replacement with polymerase kappa (Polκ) (Motegi et al., 2008). This polymerase will synthesize the new strand across the lesion created by MMS, and once clear of the lesion it will dissociate and the normal polymerase complex will be reconstituted at the site to allow continuation of the replication or transcription.

The process occurs in much the same way, however using different players after UV damage. Cellular response to UV can lead to two specific outcomes, the first is that HLTF gains the ability to bind to SHPRH, this interaction prevents SHPRH interaction with Rad18, and this leaves HLTF-Rad18 complexes as the primary player that can act on the PCNA at the stalled polymerase (Lin et al., 2011). The HLTF-Rad18 complex acts to monubiquitinate the PCNA at the same lysine residue, this signals for dissociation

of PCNA and the polymerase. It is at this point that another repair polymerase, polymerase eta (Polη) associates at the site of the lesion and synthesizes the new strand by inserting nucleotides across from the lesion (Krijger et al., 2011). Shortly after, Polη dissociates from the DNA and it is replaced by a reassembly of the original polymerase complex. It is important to note that Polη is actually less error prone than Polκ, as Polη has very high fidelity when replicating strands across from CPDs and tends to induce less mutations (Lin et al., 2011).

Data has shown that Mms2 and Ubc13 may be responsible for recognizing the type of ubiquitination on the PCNA, and for helping to facilitate the creation of the polyubiquitin chain at K63 (Kumar et al., 2014). The physical localization of the Mms2-Ubc13 complex may serve as a signal that helps to localize the correct repair polymerase to the site of damage (Sun and Chen, 2004). Traditionally, Mms2-Ubc13 act in tandem as an E2 ubiquitin conjugating enzyme which is capable of producing polyubiquitin chains (Sun and Chen, 2004). While this would indicate it in functioning in the recruitment of Polκ; it would be unable to account for recruitment of Polη which is recruited in the presence of monoubiquitinated K163. As such, it is hypothesized that there may be another factor involved in the selection, or that the lack of Mms2-Ubc13 may be the defining factor (Lin et al., 2011).

Since complexes of Rad18 and HLTF or SHPRH are present during normal cellular conditions it is likely that they will act on PCNA any time that they can come into contact with it (Lee and Myung, 2008). Polymerase and PCNA move very quickly, which would decrease the chances that the complexes of Rad18 could come into contact with PCNA. As a result, there may not be an actual signal that detects the stalled

polymerase, instead it may be that a stalled polymerase complex simply becomes accessible to the ubiquitination (Kumar et al., 2014). In this way, the prevalence of a Rad18 partner would make the interaction more specific and would explain the necessity of the programed degradation of HLTF (Lin et al., 2011).

Apart from its DNA repair activity HLTF has also been shown to act as a transcription factor promoting basal expression of other genes which contain an enhancer sequence, the B-box sequence (5'-(A/G)G(C/T)(G/A/T)G(A/T)(A/T)(T/C/A)-3') which is situated before the TATA box (Ding et al., 1999). This activity is mediated by a DNA binding domain which is located before of the first ATPase cluster (Ding 1996). This activity has been shown to promote expression of PAI-1, which binds and inactivates plasminogen factors (Ding et al., 1999).

Initial study of the Rad5/16 subfamily of Snf2/Swi2 ATPases was conducted in *Saccharomyces cerevisiae*, and a significant amount of data about their roles and interactions has been collected in that organism. However, there are two constraints in *Saccharomyces* that cannot be overlooked when using it as a model for Rad5 and Rad16. The first constraint is in regard solely to Rad16, and it relates to where Rad16 functions, namely, that the process of ggNER functions in silenced areas of the genome. These areas are typically arranged as very tightly compacted heterochromatin. *Saccharomyces* has only one such locus, the mating type (MAT) locus, meaning that analyzing the function of Rad16 in ggNER is very limited.

The second constraint plays a role in the study of Rad5 and Rad16, and it has to do with how these proteins relate to higher eukaryotic proteins which should serve the main function. As mentioned previously, there are two Rad5 homologs in higher

eukaryotes, SHPRH and HLTF, and while SHPRH is thought to be the closest homolog to Rad5 that does not account for the actions of HLTF, a protein which does not seem to be present in *Saccharomyces* unless Rad5 does play the roles of both HLTF and SHPRH in yeast. This problem is also seen in Rad16, which currently has no human or higher eukaryotic homolog, even though it has been shown to serve essential functions in the repair of the silenced portion of the yeast genome. One would expect that as genomes became more compacted and had larger silenced areas the need for a protein which has the functionality of Rad16 would increase.

Tetrahymena thermophila

The way to address both of the constraints listed above is to attempt to study the Rad5/16 subfamily in another organism; one which would provide a better platform and give higher translational value when comparing to higher eukaryotic organisms. Along those lines *Tetrahymena thermophila* is an excellent choice to carry out study of Rad5 and Rad16. *Tetrahymena* has been used to uncover a variety of different biologically important processes which are well conserved among eukaryotes, these include the study of the histone code and the activity of telomerase (Strahl et al., 1999, Greider and Blackburn, 1985).

There are a number of features of *Tetrahymena* which have strong similarities to humans. These similarities allow for the translational study of *Tetrahymena* and humans which provides insight into both evolutionary modeling and current cellular functions. Both *Tetrahymena* and humans have similar nuclear architecture, specifically the interactions of the histones and DNA, and the way in which modifications of those

histones leads to alterations in the chromatin structure (Strahl et al., 1999). Moreover, the ciliated nature of *Tetrahymena* has allowed comparative study of ciliary dynamics and assembly in ciliated human cells, and has been able to elucidate a number of different ciliary processes (Rajagopalan et al., 2009).

Tetrahymena is a ciliated protist which has two nuclei; a transcriptionally active macronucleus (MAC) and a transcriptionally silenced micronucleus (MIC). A large number of studies have been conducted in this organism, and it has served as an important model for understanding a variety of different proteins, and protein modification pathways. There are several benefits to using this organism for biomedical research. The most basic include the ease of maintenance of the cells and a large number of different techniques which have been developed to work with them. Particularly useful are the number of different techniques which can be used to introduce specific DNA directly into the genome for long term expression of target genes (Chalker, 2012).

The nuclear dimorphism seen in *Tetrahymena* is a result of the way in genetic information is passed on to the next generation. *Tetrahymena* are able to reproduce asexually during vegetative growth, this is done by replication of both the MIC and MAC, however genetic assortment varies between the two (Yao et al., 1979). The MIC always contains five diploid chromosomes, while the MAC contains approximately 221 chromosomes and 45n copies of the genome (Orias and Newby, 1975). It is important to note that sexual reproduction can only occur between cells of different mating types, of which there are seven, meaning that cultures of one specific cell line will never undergo sexual reproduction without the introduction of an entirely different cell line (Arslanyolu and Doerder, 2000). Additionally, mating must be triggered by some environmental

stress such as starvation, because the process of sexual reproduction is time consuming and halts other functionalities from the cells (Arslanyolu and Doerder, 2000).

The MIC plays a primary role during the process of sexual reproduction, or meiosis, where it functions as the means of transfer for the genetic information. At the start of sexual reproduction, the MIC will recombine and assort into chromosome pairs, which condense once assortment is done (Cole, 2006). At this stage the MIC will undergo meiotic division producing four different MICs, three of which are degraded in much the same way as the polar bodies from oogenesis (Cole, 2006). The new MIC will undergo meiotic division which results in two new nuclei, one of which remains in the parent cell while the other transfers across a cytoplasmic junction to the other cell in the mating pair, resulting in two cells which have two haploid micronuclei (Sugai and Hiwatashi, 1974).

It is at this stage that the new MIC and old MIC will fuse and become a new diploid micronucleus (Sugai and Hiwatashi, 1974). That micronucleus will undergo two mitotic divisions, producing 4 nuclei, two of which will become new MACs and the other two become new MICs. As this phase of reproduction concludes two things occur, the cells break off their attachment and the old MAC condenses and degrades, allowing the new MAC to function. After the end of the sexual reproduction the new cells are poised to divide creating two cells with new genetic information, allowing for a more robust means of surviving and adapting to environmental stress.

The similarities of *Tetrahymena* do not relate only to higher eukaryotes, but also to lower eukaryotes such as *Saccharomyces cerevisiae*. The study of a number of different mechanisms and proteins have occurred in both *Saccharomyces* and

Tetrahymena, which show that protein structure and function can be highly related between the organisms. These relationships have value in regard to both basic understanding of protein-protein and protein-DNA dynamics, as well as evolutionary relationships (Collins and Gorovsky, 2005).

Other than the general benefits of using *Tetrahymena* there are benefits that are specific to the study of Rad16 in this organism. Since Rad16 has been shown to be active in ggNER, the best chance to characterize the action and importance of the protein comes when there is potential for a large amount of damage to occur in silenced areas of the genome. The fact that *Tetrahymena* has an entire nucleus which is silenced provides a very large platform to study the function of potential Rad16 homologs; since a deficiency in Rad16 would be especially detrimental to a nucleus which does not undergo transcription.

Purpose Statement

This work seeks to identify homologs of both Rad5 and Rad16 in *Tetrahymena thermophila* so that their interactions and functions can be examined in a more complex organism which is more closely related to humans. The study of these proteins, particularly Rad16, will be greatly aided by analysis in *Tetrahymena* which has nuclear structure that has been more homologous to humans than that of *Saccharomyces*. Due to the previously described functions of Rad5 and Rad16 it is very likely that functional homologs of these proteins exist in *Tetrahymena*; and that identification of a Rad16 homolog in this organism will lead to discovery of a homolog in higher eukaryotic organisms.

In narrowing scope, the goals of this work are as follows; first, to use bioinformatics to identify potential Snf2/Swi2 ATPases that resemble Rad5 and Rad16. Second, determining the response of these homologs to different types of DNA damaging agents to elucidate the functions that the proteins serve. Third, to decrease the expression of these homologs to assess any phenotypic consequences linked to decreased effectiveness of DNA repair.

MATERIALS AND METHODS

Strains and Maintenance

Vegetative growth of *T. thermophila* was done in 2% PPY media (0.02 g/mL protease peptone, 0.002 g/mL yeast extract) supplemented with 10 µM $FeCl_3$ and 1X PSF (100 µg/mL penicillin, 100 µg/mL streptomycin, and 0.25 µg/mL amphotericin B, Thermo Fisher Scientific). All vegetatively growing cultures were incubated at 30˚C while shaking at 100 RPM. For long term storage cells were inoculated into 10 mL of 1% PPY media and were stored at room temperature for two to four months before beginning a new culture. The strains used in this research are described in Appendix A. Strains with the designation CU were obtained from the *T. thermophila* stock center at Cornell University.

RNA Isolation

Tetrahymena strains were grown to a concentration of $1x10^5$ cells/mL on the day of isolation. Cells were then mock treated or treated in 10 mL cultures with either 100 j/m^2 UV or 10 mM (MMS) as described previously. After treatment, samples were taken at designated timepoints from both the treated and untreated cells; cellular RNAs were isolated with the Qaigen RNeasy® mini kit according to the manufacturer's instructions. Briefly, 10 mL of cells were centrifuged at 3500 RPM for three minutes (Marathon 21000R, Fisher Scientific), media was decanted and cells were resuspended in 600 µL of buffer RLT supplemented with 143 mM β-mercaptoethanol (βME) and vortexed for one minute to homogenize the cells. Sample was transferred to a spin-column assembly and

centrifuged at 13300 RPM (Spectrafuge 24D, Labnet International) for 30 seconds and flow through was discarded.

Column was washed once with 700 µL of buffer RW1 followed by two washes with 500 µL of buffer RPE. Column was centrifuged at 13300 RPM for two minutes to remove any remaining buffer and 50 µL of nuclease-free water was added to the column which was allowed to incubate at room temperature for two minutes and then transferred to a new collection tube. The column was then centrifuged at 13300 RPM for one minute to remove RNA from the column; and the resulting sample was quantified using the Nanodrop 2000 and then stored at -80˚C until use in Reverse Transcriptase PCR.

Reverse Transcriptase Reaction

Previously isolated RNA was used to conduct reverse transcriptase PCR (RT-PCR) in order to produce cDNA. RNA was added to the reaction to a final concentration of 2 µg (as measured by the NanoDrop 2000 Spectrophotometer, Thermo Scientific) into the 20 µL reaction. The remainder of the reaction included: 4 µL of 5X AMV buffer, 4 µL of 25 mM $MgCl_2$, 2 µL of 10 mM dNTPs, 1 µL of 40 U/µL RiboLock RNase inhibitor (Thermo Fisher Scientific), 1 µL of 10 U/µL AMV reverse transcriptase (Promega), RNase-free water to bring the total reaction volume to 18 µL, and finally 2 µL of either 50 µM oligo dTVN or random hexamer (IDT). Samples were incubated at 42˚C for 25 minutes followed by incubation at 99˚C for five minutes and finally incubation at 4˚C for five minutes. After the incubations the samples were diluted with 20 µL of nuclease-free water and stored at -20˚C until use.

qRT-PCR

Quantitative real time PCR (qRT-PCR) was conducted using the cDNA which was generated from RNA isolation and RT-PCR protocols. The cDNAs were added at 1 µL to each well in a 96 well qPCR plate, to that cDNA 19 µL of cocktail consisting of 10 µL SsoFast EvaGreen 2X master mix (Bio-Rad), 8 µL of nuclease-free water, and 0.5 µL of each a specific reverse and forward qPCR primer depending on the target molecule or the control molecule (See Appendix A2). Construction of a standard curve based on starting quantity of DNA was created from a set of standards consisting of gDNA at concentrations of: 1 µg/µL, 0.1 µg/µL, 10 ng/µL, 1 ng/µL and occasionally 0.1 ng/µL. HHP1 was used as a template and loaded in duplicate to generate a set of controls to compare back to the standard curve to determine a normalized starting quantity for each sample.

The plate was then briefly centrifuged to pool all reagents at the bottom of the wells. The plate containing samples was then placed into the BioRad Mj mini Personal thermocycler and run under the following conditions: an initial cycle of 98˚C for two minutes, followed by 39 cycles of 95˚C for five seconds, 56˚C for 20 seconds and reading of the wells. The cycling was followed by a 56˚C incubation for 10 seconds and an increase of 0.5˚C from 56˚C to 95˚C with measurements taken at each half degree increment. Samples were then held at a temperature of 4˚C until removal and storage at -20˚C. A single sample from each different template with each different set of primers was run via agarose gel electrophoresis as previously described to validate product size, band number, and melt curve measurements (Appendix B).

shRNA Plasmid Construction

Oligonucleotides for the shRNA constructs (Appendix A) were obtained from IDT and were utilized in generation of the shRNA constructs for the three potential Rad5/Rad16 homologs. Oligonucleotides were resuspended to a concentration of 200 pmol/µL in water. Both the sense and antisense oligonucleotides were phosphorylated by adding 1 µL of each into a reaction consisting of 29 µL of water, 4 µL of 10 mM ATP, 1 µL of T4 Polynucleotide Kinase (10,000 U/mL, NEB), and 4 µL of PNK buffer (NEB). The reactions were allowed to incubate at 37˚C for one hour, before incubating at 70˚C for 10 minutes to denature the enzyme. In order to anneal the oligonucleotides, 10 µL of the phosphorylation reaction was mixed with 2.5 µL of 10X SSC (1.5 M NaCl, and 0.15 M Sodium Citrate at pH 8.0) and 12.5 µL of water. The reaction was heated to 75˚C for 5 minutes before being allowed to cool down to room temperature.

The resulting products were then ligated into the *BglII* (NEB) and *HindIII* (NEB) digested pBT1-YFG plasmid (generated previously by Joshua J. Smith) as follows. Reactions were done at a molar ratio of 1:3 vector: insert, with 3 µL of annealed oligonucleotides to 1 µL of pBT1-YFG. The vector and insert (or vector alone) were added to a reaction consisting of 2 µL of 10X DNA ligase buffer (NEB), 0.6 µL T4 DNA Ligase (400,000 U/mL, NEB) and 13.4 µL of water (16.4 µL of water for reactions without the insert used as a negative control). Reactions were incubated at 14˚C for 12 hours prior to transformation of *E. coli*.

Electroporation Transformation of *E. coli* and Plasmid DNA Isolation

Electroporation of *E. coli* (DH10B electrocompetent cells) for introduction of shRNA plasmids was conducted as follows. A reaction consisting of 50 µL of DH10B cells and 2 µL of ligation reaction product was mixed and placed into a 2 mm electroporation cuvette (Fisher). The samples were then electroporated at 2.5 kV, 25 µF, and 200 Ω using the BIO-RAD Gene Pulser II Electroporation System. Cells were transferred into 1 mL of SOC media (2% w/v bacto-tryptone, 8.56 mM NaCl, 2.5 mM KCl, 0.5% w/v yeast extract, 10 mM $MgCl_2$, and 20 mM glucose in water) and allowed to recover for one hour at 37˚C. After recovery, 100 µL of cells were plated onto LB-AMP plates (1% w/v bacto-tryptone, 1% NaCl, 0.5% yeast extract in water with 100 µg/mL ampicillin) and allowed to grow overnight at 37˚C. Surviving colonies were screened by plasmid isolation and restriction enzyme digests.

Cultures of *E. coli* containing the plasmids of interest (2 mL) were grown in LB+AMP media (1% w/v bacto-tryptone, 0.5% yeast extract, 1% NaCl in water with 100 µg/mL ampicillin) at 37˚C while shaking at 220 RPM. Cells were centrifuged (Spectrafuge 24D, Labnet International) at 13300 RPM for 2 minutes and the media was removed. Cells were resuspended in 350 µL of Sucrose Lysis Buffer (8% sucrose, 0.5% Triton X-100, 50 mM EDTA, 10 mM Tris pH 8.0 in water) and 25 µL of 10 mg/mL lysozyme was added. Samples incubated for 5 minutes and were then placed in 99˚C water for one minute. The samples were then centrifuged at 13300 RPM for 15 minutes and the pellet of cell debris was removed and discarded. The samples were then mixed with 220 µL of isopropanol and 40 µL of 3 M sodium acetate (pH 5.1). Plasmid DNA was allowed to precipitate out by incubating at room temperature for five minutes,

followed by centrifugation at 13300 RPM for 10 minutes. The supernatant was removed and the pellets were washed with 1 mL of 70% ethanol and allowed to air dry before being resuspended in nuclease-free water.

Biolistic Transformation of *Tetrahymena*

Tetrahymena cultures of strain CU522 were grown to a concentration of $1x10^5$ cells/mL for biolistic transformation. Cells were centrifuged at 3000 RPM for three minutes (Marathon 21000R, Fisher Scientific) and the media was removed and replaced with 10 mM Tris-HCl pH 7.5, and were allowed to starve at 30˚C for 18 hours. The cells were then counted and brought to a concentration of $1x10^7$ cells/mL for transformation. The linearized plasmid constructs (5 µg) for transformation were coated onto 1 µm gold beads (25 µL of 1.5 mg of beads in 50% glycerol) with the addition of 25 µL of 2.5 M $CaCl_2$ and 10 µL of 100 mM spermidine. The mix was then vortexed at 4˚C for 30 minutes before being centrifuged briefly for 5 seconds at 13300 RPM (Spectrafuge 24D, Labnet International). The supernatant was removed and the beads were washed with 100 µL of 70% ethanol once followed by a wash with 100 µL of 100% ethanol. Finally, the beads were suspended back into 25 µL of 100% ethanol and were then added to a macrocarrier and allowed to dry.

Cells (1 mL) were added onto Grade 3 or 4 Whatman filter paper which had been pre-treated with 2 mL of 10 mM HEPES, inside of a petri dish which was inserted into the chamber of the gene gun (PDS-1000/He™ Biolistic Particle Delivery System, BIO-RAD) along with the coated macrocarrier. The chamber was placed under a vacuum (~26 mmHg) and the gene gun was fired at a pressure of ~900 psi. The cells and filter

paper were transferred into 50 mL of 2% PPYF with 1X PSF and were allowed to recover at 30˚C for 5 hours. Cells were treated with Paclitaxel (LKT Laboratories) at a final concentration of 20 µM and were plated onto 3 96-well plates at 100 µL per well. Cells were monitored for 72 hours before being re-plated into new 2% PPYF with 1X PSF in 24-well plates (500 µL per well) in 40 µM Paclitaxel.

Polymerase Chain Reaction

Polymerase chain reaction (PCR) was utilized with either Phusion DNA polymerase (Thermo Fisher Scientific) or GoTaq DNA polymerase (Promega). GoTaq DNA polymerase reactions were utilized for primer annealing temperature checks or shRNA confirmation and consisted of 12.5 µL of GoTaq Green 2X master mix, and 1-2 µL of template (either DNA or whole cells) with specific primers (Appendix A2) added at concentrations of 20 pmol/µL in volumes of 0.5 µL. Finally, nuclease-free water added to a total volume of 25 µL with all reagents at a final concentration of 1X. Reactions were placed in a thermocycler (BioRad Mj mini personal thermocycler) and run on program GOTAQ32, which consists of an initial cycle at 95˚C for two minutes followed by 32 cycles of 95˚C for 45 seconds, the primer specific annealing temperature for 45 seconds, and 72˚C one minute and forty-five seconds. Finally, samples were incubated at 72˚C for five minutes and then analyzed immediately by agarose gel electrophoresis or stored at -20˚C until further use.

Phusion PCR was conducted as follows to amplify genomic DNA of target genes for use in the *in vitro* NER assay: reactions consisted of 0.5 µL of each specified forward and reverse oligonucleotide primer (20 pmol/µL, IDT), 0.2 µL of 10 mM dNTPs

(Promega), 0.2 µL of Phusion polymerase (2 U/µL), 5 µL of GC buffer (Thermo Fisher Scientific), 5 µL of 5 M betaine, 0.5-2 µL of template DNA, and nuclease-free water to a total reaction volume of 25 µL. Samples were placed in a thermocycler (BioRad Mj mini personal thermocycler) and run on program PHUS2KB as follows: 98˚C for one minute, followed by 35 cycles of 98˚C for 20 seconds, the primer specific annealing temperature for 25 seconds, 72˚C for one minute and thirty seconds. Finally, samples were incubated at 72˚C for ten minutes and then stored at -20˚C until further use.

DNA Damage Survivability

Tetrahymena strains were grown to a concentration of $1x10^5$ cells/mL on the day of treatment. To ensure concentration cells were counted and adjusted to $1x10^5$ cells/mL prior to treatment. Cells were then mock treated or treated in 10 mL cultures with either 75 j/m^2 UV or 10 mM methyl methanesulfonate (MMS). For UV, cells were centrifuged at 3000 RPM (Marathon 21000R, Fisher Scientific) for 3.5 minutes, the media was decanted and the cells were resuspended in approximately 10 mL of 10 mM Tris-HCl (pH 7). The cells were then centrifuged a second time at the same settings to remove any residual media, and the Tris was decanted. The cell pellet was again resuspended into 10 mL of 10 mM Tris-HCl (pH 7). The cells were then added to clear 100 mm x 15 mm plastic petri dishes which were placed in the UV Stratolinker (CL-1000 Ultraviolet Crosslinker, UVP) with the lids removed. Samples were then treated or left untreated and 1 mL was transferred from the petri dish to 9 mL of sterile 10 mM Tris-HCl (pH 7) in glass 15 mL test tubes placed which were shielded from light after addition of the cells. From this point forward any dilution or growth of UV samples was protected from

exposure to light. For MMS treatment, 10 mL of cells in media were transferred to new 50 mL flasks with the addition or absence of 10 mM MMS. Samples were allowed to incubate at 30˚C and shaking at 100 RPM for one hour. At the end of the hour 1 mL from each sample was added to 9 mL of sterile 10 mM Tris-HCl (pH 7) in glass 15 mL test tubes.

For both UV and MMS, tubes containing 9 mL of Tris and 1 mL of cells were vortexed briefly to mix cells and 1 mL of the solution was transferred to a new test tube containing 9 mL of sterile 10 mM Tris-HCl (pH 7) which was again vortexed briefly to mix the solution. From this test tube 600 µL of the suspension was transferred to 29.4 mL of 2% PPY + $FeCl_3$ and 1X PSF. The media was mixed by inversion and 100 µL of the mixture was plated into three 96 well cell culture plates for each sample resulting in a concentration of 2 cells/well. The plates were then placed into a humidity chamber and incubated at 30˚C for 5 days for MMS and 10 days for UV treatment with counting of living wells conducted every day starting at the third day after damage until the end of the incubation time period.

DNA Purification

DNA obtained by Phusion PCR was purified before use in a number of downstream applications. In order to purify the samples, an equal volume of phenol: chloroform: isoamyl alcohol (25:24:1) was added and samples were vortexed for 30 seconds. The samples were centrifuged at 13300 RPM (Spectrafuge 24D, Labnet International) for five minutes. After centrifugation the aqueous (top) layer was removed and placed into a new microcentrifuge tube and mixed with $1/10^{th}$ volume of 3 M sodium

acetate. To that mix 2.5 volumes of 100% ethanol was added and the samples were mixed by inversion and incubated overnight at -20˚C. The following day, samples were centrifuged at 13300 RPM and 4˚C for 10 minutes. The ethanol was discarded and samples were washed with 70% ethanol and centrifuged again under the same conditions. Residual ethanol was removed and samples were allowed to dry before being resuspended in nuclease-free water. Samples were quantified by NanoDrop (NanoDrop 2000 Spectrophotometer, Thermo Scientific) and stored at -20˚C for later use as *in vitro* NER Assay substrates.

DNA Damage with $AgNO_3$ and Analysis by *Ase1* Digestion

Induction of cyclobutane pyrimidine dimers (CPDs) into target DNA was conducted using $AgNO_3$ and a UV Stratolinker (CL-1000 Ultraviolet Crosslinker, UVP) as follows. The DNA sequence of interest (PCR amplified BTU1 genomic DNA) was quantified by NanoDrop and diluted to a concentration of 10 ng/µL, and 10 µL of DNA at this concentration was treated. Silver Nitrate was added at a 1:2 ratio of silver ions to backbone phosphates on the target DNA molecules based on the number of DNA molecules in 100 ng (5 µL of 0.2912 mM $AgNO_3$). Reactions were incubated at 4˚C for 30-120 minutes before exposure to UV radiation. To induce damage, the full reaction from above was pipetted onto Parafilm and treated in the Stratolinker with varying doses (0 j/m^2, 50 j/m^2 repetitively to a total dosage of 600 j/m^2, or at individual doses of 50 j/m^2, 100 j/m^2, 200 j/m^2, and 400 j/m^2) of UV radiation at 254 nm. Treated samples were digested with *AseI* (NEB) or mock digested.

To analyze DNA damage by impaired restriction enzyme digest, the enzyme *Ase*I (NEB) which cleaves at palindromic ATTAAT sites between the adjacent thymines, was utilized. Reactions consisted of 0.2 µL of *AseI* (10,000 U/mL), 5 µL of 10X NEBuffer 3.1 (NEB), 44.3 µL of nuclease-free water and 10.5 µL of the damaged DNA template (mock reactions were the supplemented with an additional 0.2 µL of nuclease-free water in the place of AseI). Reactions were incubated at 37˚C for 20 minutes and loaded onto 1% agarose gels to be visualized by gel electrophoresis using the KODAK Gel Logic 200 Imaging System. Band intensities for both the uncut product and the digested fragments were obtained using the KODAK Molecular Imaging Software V.4.0.5 (Kodak). Induction of damage was determined by plotting the intensities of the uncut and cut fragments in each lane and comparing the total relative fluorescent unit (RFU) values to mock digested controls (for undigested band intensities) and undamaged digested controls (for digested band intensities) (Appendix C).

RESULTS

Bioinformatics

To initially identify potential homologs of Rad16 and Rad5 in *Tetrahymena thermophila* the genomic sequences of those genes were taken from the Saccharomyces Genome Database (SGD) and run through BLAST software searching for homology in *Tetrahymena*. The Tetrahymena Genome Database (TGD) BLAST returned four potential homologs: TTHERM_00298220 (Rad5.1), TTHERM_00037210 (Rad5.2), TTHERM_00933250 (Rad16.1), and TTHERM_00420480 (Rad16NH). Rad16 and Rad5 have certain characteristic domains; both contain paired N-terminal and C-terminal ATPase domains, with an E3 ubiquitin ligase domain situated between the ATPases. In addition to these domains, Rad5 also contains a HIRAN domain, which is located before the N-terminal ATPase.

The potential homologs along with the *Saccharomyces cerevisiae* proteins were analyzed to determine if they contained similar domains utilizing the InterPro protein analysis tool (Figure 1). It was found that Rad5.1 contains an N-terminal ATPase domain from amino acids 637-851, an E3 ubiquitin ligase domain from 1063-1119, and a C-terminal ATPase domain from 1161-1316. Analysis of Rad5.2 revealed a HIRAN domain from 391-504, an N-terminal ATPase from 787-1084, an E3 ubiquitin ligase from 1295-1352, and a C-terminal ATPase from 1371-1525.

Examination of Rad16.1 identified an N-terminal ATPase from 324-644, an E3 ubiquitin ligase from 780-822, and a C-terminal ATPase from 843-987. Rad16NH also

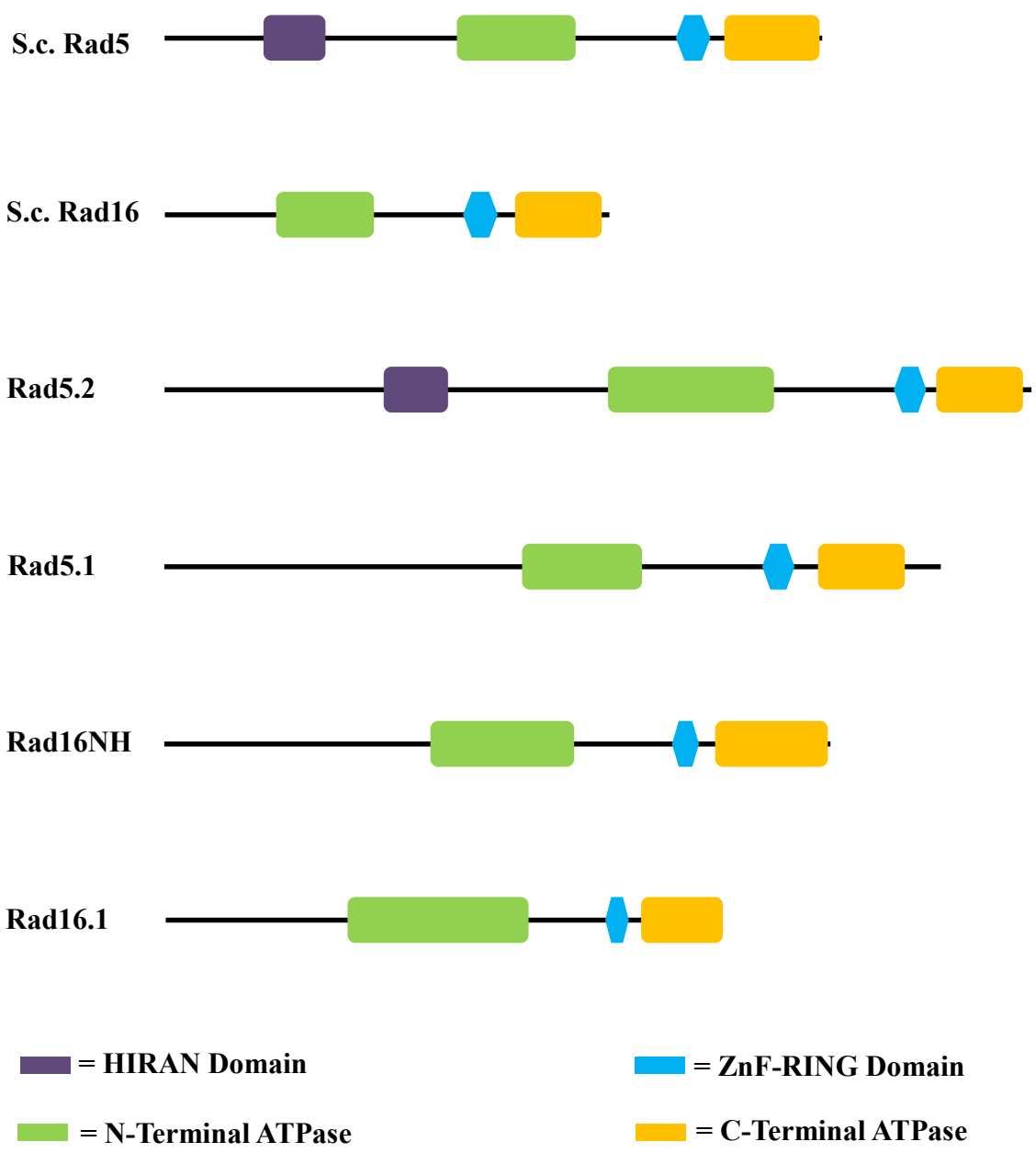

Figure 1: Domain and Motif Predictions of Rad5/Rad16 Homologs**.** Using Interpro, motifs for each potential homolog were identified, with lengths of the lines and shapes being relative to the protein size. Homologs contain the Zn-finger Ring domain, as well as the two ATPase domains; only Rad5.2 and *Saccharomyces* Rad5 contained the Rad5 characteristic HIRAN domain.

contained these domains; with an N-terminal ATPase situated from 472-728, an E3 ubiquitin ligase domain from 901-949, and finally a C-terminal ATPase from 979-1178.

Phylogenic analyses of the homologs by the Unweighted Pair Group Method with Arithmetic Mean (UPGMA) was utilized to compare protein similarities between the four potential homologs and the *Saccharomyces* proteins as well as similarities to higher eukaryotic Rad5 homologs (SHPRH, HLTF, SM3L1-3) (Figure 2). When compared to the yeast homologs alone Rad5.2 and Rad5.1 show close similarity and branch more closely to Rad16, while Rad16NH is close to yeast Rad5. Rad16.1 branches the farthest away from all of the other homologs, including the yeast proteins.

When compared to homologs of Rad5 in other eukaryotes (SHPRH) or Rad5-like proteins (HLTF, or SM3L1-3 in plants), the relationships of the proteins differ from the comparisons to the yeast proteins alone. Rad5.2 branches closely to the Rad5-like proteins from other organisms, while Rad5.1 branches most closely to the yeast Rad5 and Rad16. Rad16NH branches closely to Rad5.1 and Rad16.1 branches more distantly from all other Rad5-like proteins and more closely to the SHPRH proteins.

It has been found that HLTF can act as a transcription factor and has a DNA binding domain at the N-terminus, this domain can interact with a B-box promoter element with the consensus sequence 5'-(A/G)G(C/T)(G/A/T)G(A/T)(A/T)(T/C/A)-3'. Analyses of the N-terminal portions before the ATPase domain in the Rad5.1, Rad5.2, and Rad16NH homologs comparing them to the DNA binding domain of HLTF were conducted (Figure 3). All three homologs showed areas of high similarity to the DNA binding domain of HLTF. Further analysis of the regions spanning approximately 500

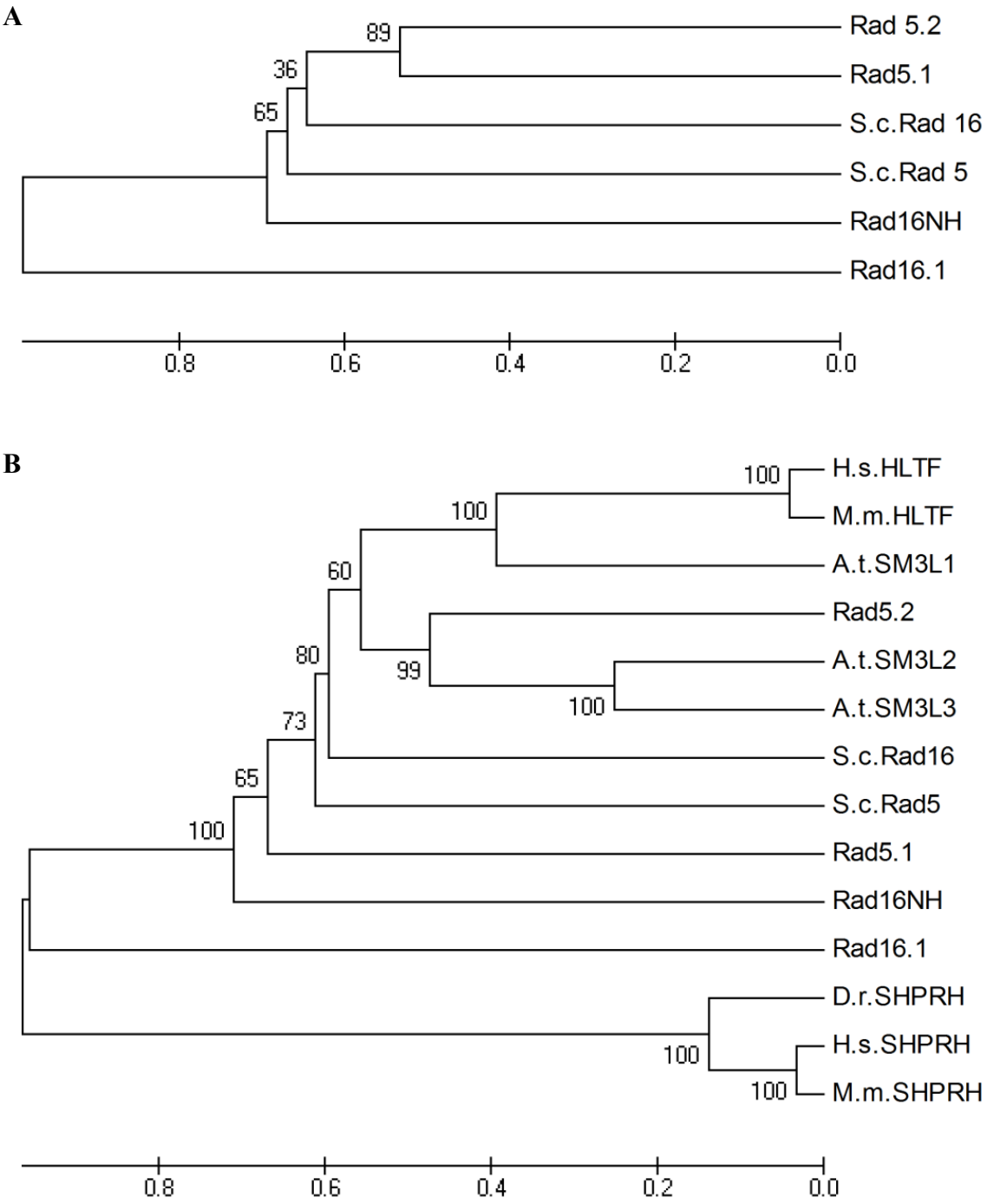

Figure 2: Unweighted Pair Group Method with Arithmetic Mean (UPGMA) Bootstrapped Phylogenetic trees for possible T. *thermophila* Rad16 homologs**.** Trees compare possible Tetrahymena Rad16 homolog protein sequences with Saccharomyces Rad16 and Rad5 along with other Rad5-like (HLTF/SM3L1-3) or Rad5 homologs (SHPRH) from various species. A bootstrap test of phylogeny was conducted for each tree. A**)** UPGMA tree of the potential Rad16/Rad5 homologs compared solely to the Saccharomyces Rad5 and Rad16. B**)** UPGMA tree comparing the potential Rad16/Rad5 homologs of Tetrahymena to the Rad5 or Rad5-like homologs from various species.

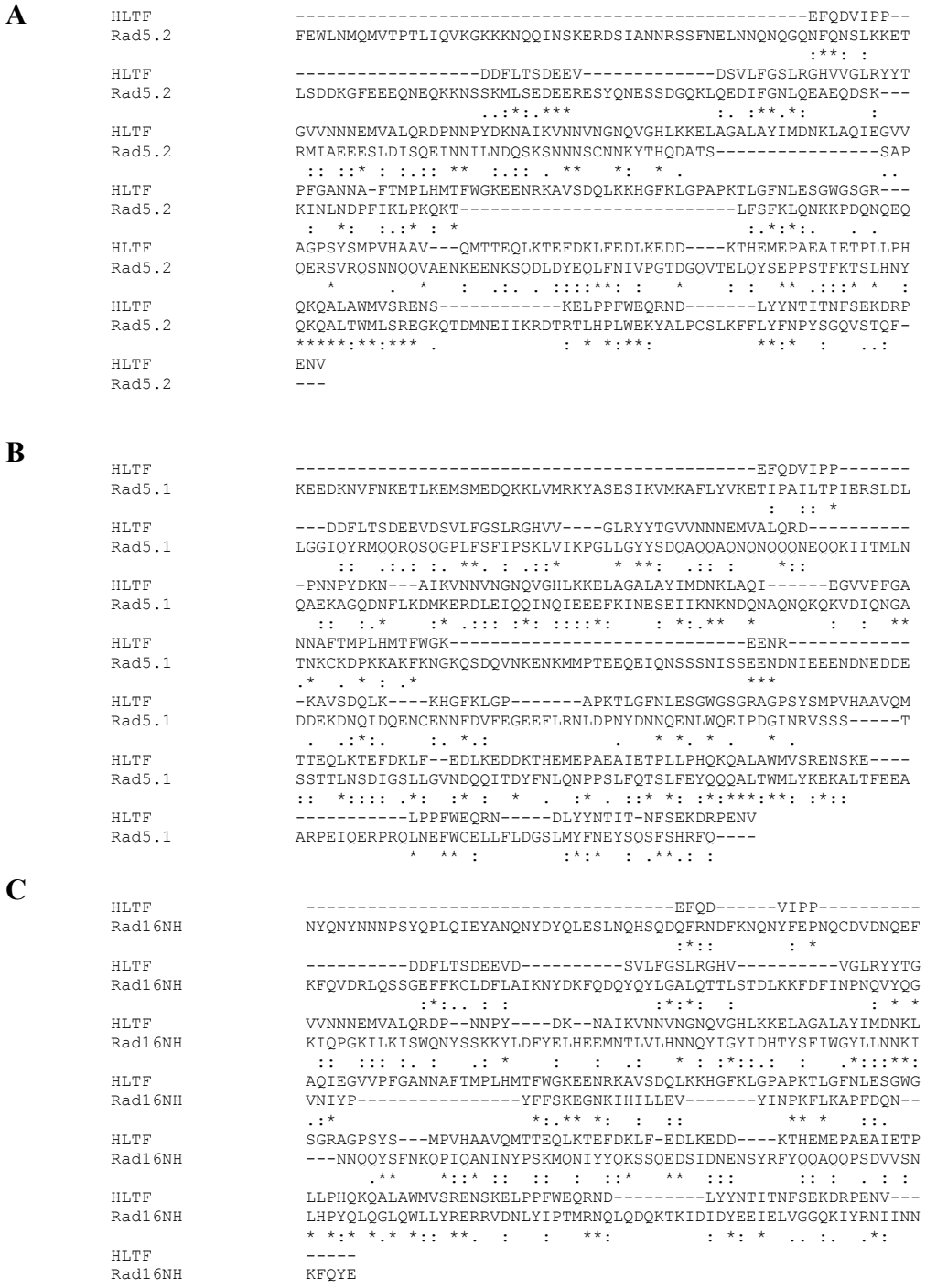

Figure 3: Alignment of HLTF DNA Binding Domain to Homolog N-terminal Protein Regions. The sequence of the *Homo sapiens* HLTF DNA binding domain was compared individually to each of the three main homologs of Rad5/Rad16. A) ClustalW alignment of Rad5.2 and HLTF DNA binding domain. B) ClustalW alignment of Rad5.1 and HLTF DNA binding domain. C) ClustalW alignment of Rad16NH and HLTF DNA binding domain. * denotes identical amino acids, : denotes amino acids with strongly similar properties, · denotes amino acids with weakly similar properties.

base pairs upstream of the start codon for each gene revealed several potential B-box promoter elements for the homologs (Figure 4)

Expression Profiles

In order to analyze the potential function of the four putative homologs, quantitative real-time polymerase chain reaction (qRT-PCR) was conducted using cDNA which was generated from the CU725 strain. These RNAs were collected before treatment, at the time of treatment, and every hour for four hours after treatment with either 100 j/m^2 of UV radiation, 10 mM methyl methanesulfonate (MMS), or 0.5 mM Hydrogen Peroxide (H_2O_2). To determine activity in nucleotide excision repair (NER) UV was utilized, as this type of damage leads to a high percentage of lesions which must be repaired by NER machinery. The MMS treatment was used to stimulate the formation of DNA double strand breaks (DSBs) which can be repaired through a number of different mechanisms, including homologous recombination (HR) which utilizes a complex of proteins, the MRN complex, which is shuttled to the site of damage with the help of Rad5. To induce base excision repair (BER) H_2O_2 was used; this type of damage affects individual bases on the DNA, which can also stall replication which calls for translesion synthesis (TLS) where both SHPRH and HLTF are involved.

Under H_2O_2 damage conditions, all of the homologs except Rad16.1 exhibited the same pattern of expression (Figure 5-7), with expression peaking at one hour after exposure and decreasing rapidly by the two hour time point. In the case of Rad5.1, expression peaked at approximately 40-fold of the untreated expression, decreasing to 10-fold expression at two hours post exposure and leveling off at 3-fold expression for the

Rad5.2

TCTTTAAAATAGAATGGATAAATAATAATATAATTAGCTCAAATTTTTAAAAATAAATTTAAATGA
TTTCCAAATTTCATTTTATTATTATTAATGTGCCTTATTTTTCAGCAAAAAAAATTTTCGCTCCAAT
AAAATTCAATTTTAAATTTTCAATAGACTCTAAAATAGAATCTTTTTATGAATATTTATAAAAAGT
GAGCCAAAGTAGAGTTTGATTTTAGAATGTTATTACTCTTCATTGGCTATAGATTAATTAACATTCA
AAAGTATTGTTAAAGGCAAAGATATTAATTCGTGAATTAAAATCTGAATTCTTATTGAAGTTTATT
AGCACTGATTTATTTTTAAAAAGTAAAAGTATAAACATATCAAAAAATCAAATTAAGACTTAGAT
TGATTTTTGATAGATAATTTTTTTAAGATACTTTTTAAACTAGTATTAAAAACGAAGTAAAACTTTT
CATAGATTTTGCATATCTTTTATTACTCAATAGATG

Rad16NH

TTAAAATGTATATTATTTTTATTATTTTAAAGAATTTTTATAAAATAAAATATTTTTTCTTAAAAATAA
TATACCAAAAATTTGAAATTGCGTAAAAAGAGTTAAGAGCAGTgAGGATCTAACTAATTAAATAAAT
GTATTTTTTTTACTTAATTTTGAGACATTTATTAGAATAGGGTAATGGCTAGTAAAATTTAAAGATAG
AAAATGAGATAAAAATATTTTTTTTTAAACTTTTATTATTTGTACCTTAAATAGATATTTATCTATTCT
CAAGGTTGcTATTAGAATATAAAGTGATGATAGTTTAGAATTTTCAATCAATATACTAAAAGAGAAAA
CAAGAGAAAAATAAAATTTTTTTATTTTTTGATTCGCATTAAAATAAGAAAATAAATAGTTCAAAAAG
AGGAAAAGAAAAAATTATTGATTAATTTTATTAATTAATTTTTCGAAAAAAATACAAAAAATAAAAA
TAATAACTAAAAAAAGAAGAAATG

Rad5.1

TATCAGACTATATAAAAAACTTTATACTGTGTAAAATTCTGATGATAACCACCTTATTTGTATATTTAT
TAACACTTTTATTTCTTCTTCATAAATTCAATGATATTTTATAGAATTCTGGATATGAAGACGCAGcAT
GATTTTTTAGTTTCATATTACTACCTTCATCATATTAGTTTTAAGGATTTTTTTGTATTTTTTATGACGA
ATAGGGAAAATTTTTTCGTCTTTCTATTTATATACTATGCGAAGTCGCAGTcAGAATTTTTCAAAATTT
TTTATAAGAATAACTATTTTTAATTAAAAGTAGTTTGATAGAAGTATATAAAAGTTATTACTGTTTTGA
TTCTATTTACACACTGGTAAGATACGAATACGATTTATTTTATG

Figure 4: Presence of B-box or B-box-like Promoter Elements in Rad5/16 Homologs. Sequences for 497 bp upstream of the ATG start codon for *T. thermophila* Rad5.2, Rad16NH, and 387 bp upstream of the ATG start codon of *T. thermophila* Rad5.1 were obtained from the Tetrahymena Genome Browser. Sequences which have either an exact match to the known B-box consensus sequence (5'-(A/G)G(C/T)(G/A/T)G(A/T)(A/T)(T/C/A)-3') or are different by only one nucleotide are highlighted in blue. Lowercase letters denote the nucleotides which do not fit the consensus sequence. Start codons are underlined at the end of each sequence.

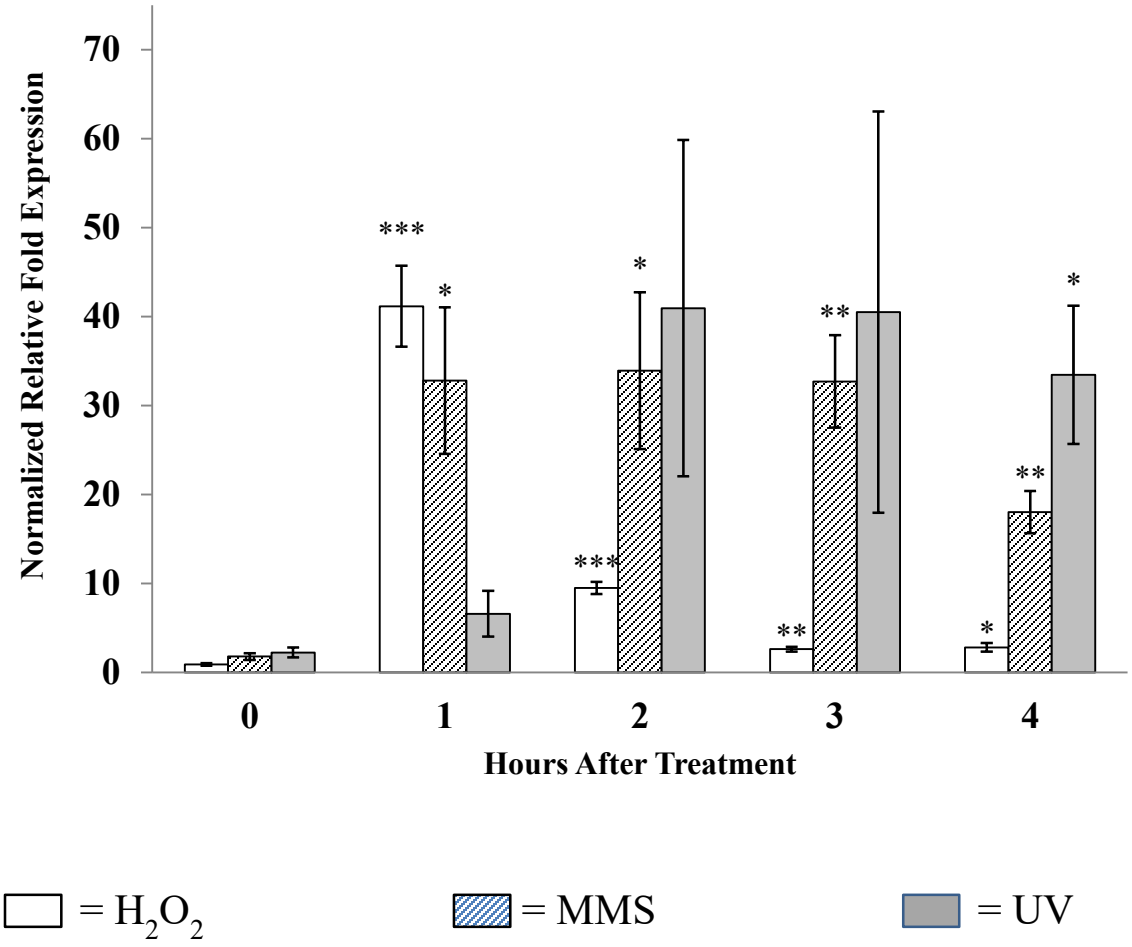

Figure 5: qRT-PCR expression profile analysis of the transcription of Rad5.1 following damage induction with MMS, UV, or H_2O_2**.** Expression profiles of Rad5.1. White bars represent treatment with 10 mM H_2O_2; striped represents MMS treatment, and gray represents UV treatment. All samples were normalized to HHP1 levels in treated samples at matching time points and set relative to untreated cDNA samples with the same primers. Values represent mean of five trials with error bars of ±SEM. *p<0.05, **p<0.01, ***p<0.001 vs. untreated samples as measured by two-tailed, paired sample t-test.

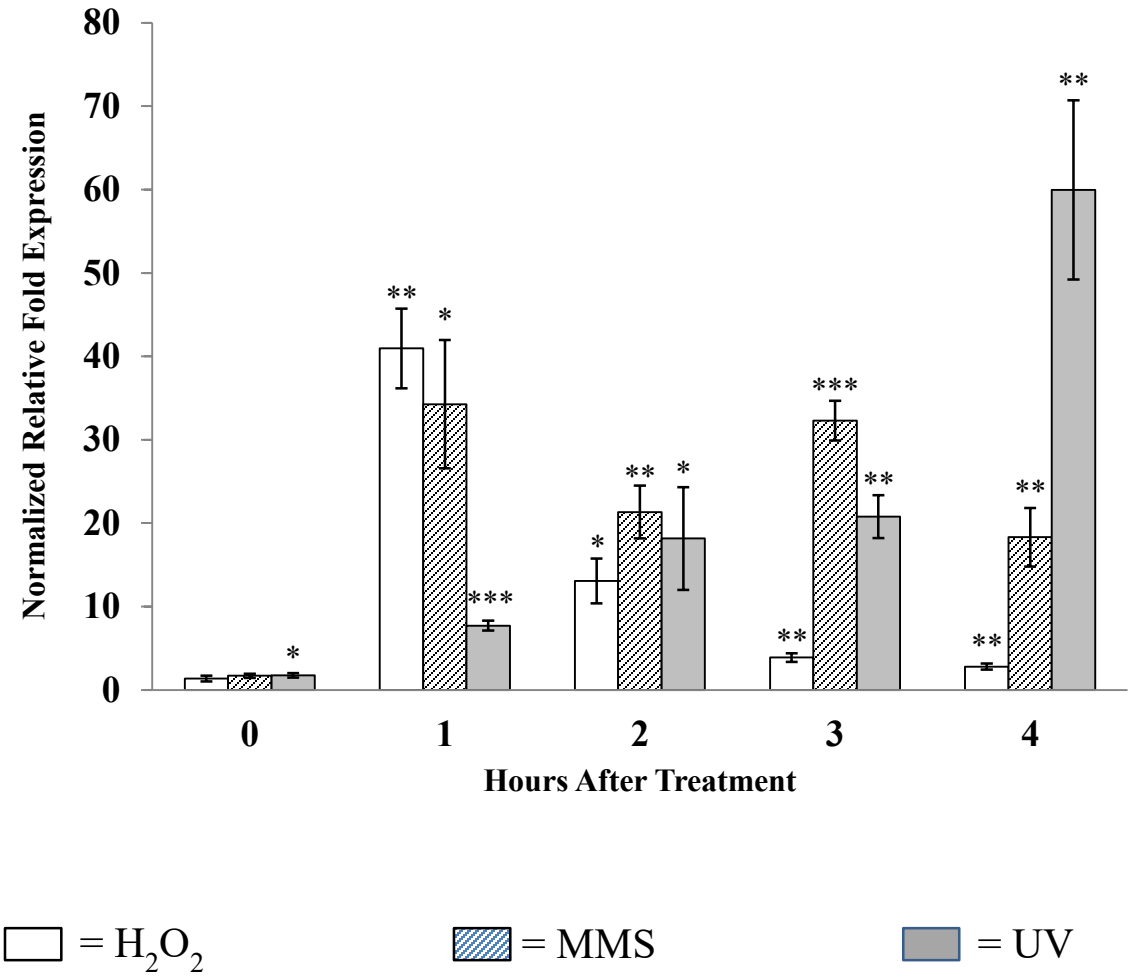

Figure 6: qRT-PCR expression profile analysis of the transcription of Rad5.2 following damage induction with MMS, UV, or H_2O_2**.** Expression profiles of Rad5.2. White bars represent treatment with 10 mM H_2O_2; striped represents MMS treatment, and gray represents UV treatment. All samples were normalized to HHP1 levels in treated samples at matching time points and set relative to untreated cDNA samples with the same primers. Values represent mean of five trials with error bars of ±SEM. *p<0.05, **p<0.01, ***p<0.001 vs. untreated samples as measured by two-tailed, paired sample t-test.

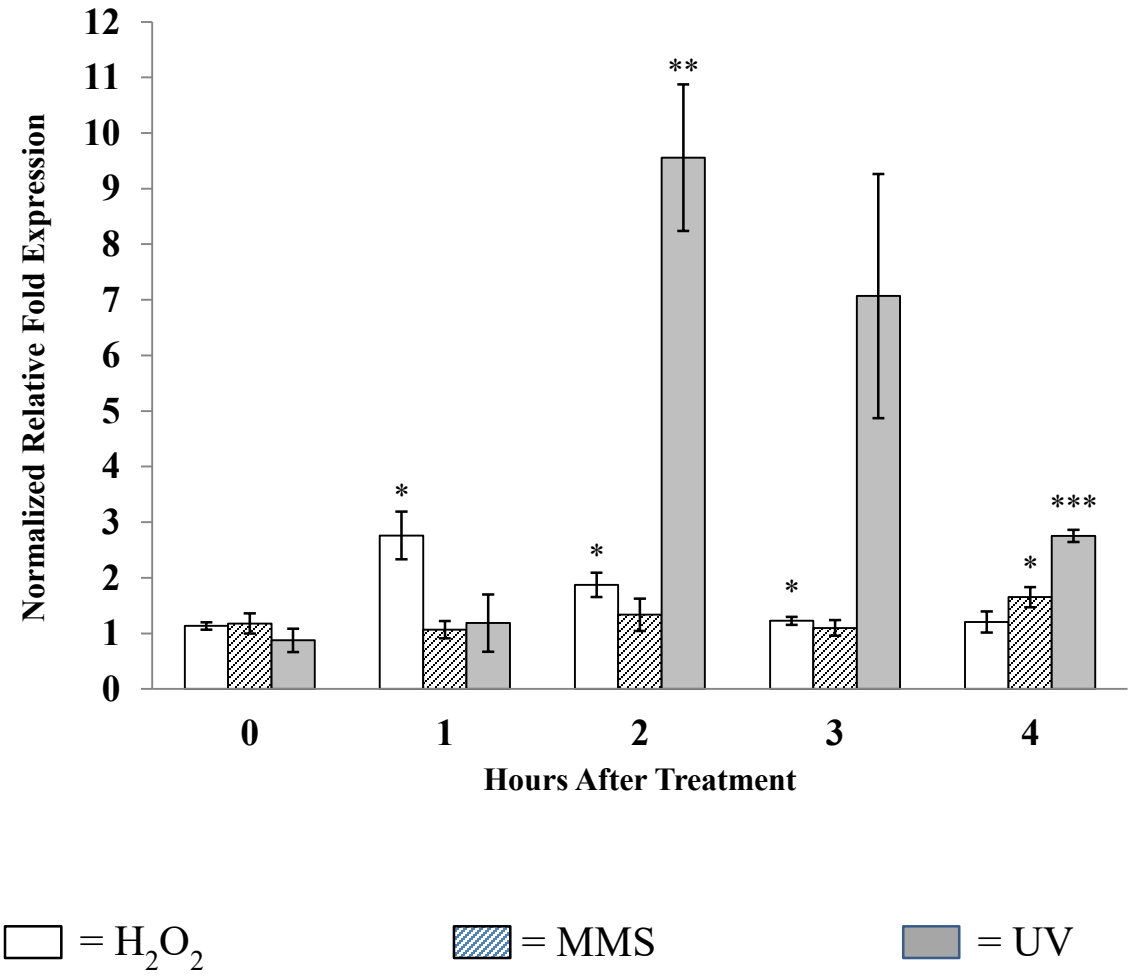

Figure 7: qRT-PCR expression profile analysis of the transcription of Rad16NH following damage induction with MMS, UV, or H_2O_2. Expression profiles of Rad16NH. White bars represent treatment with 10 mM H_2O_2; striped represents MMS treatment, and gray represents UV treatment. All samples were normalized to HHP1 levels in treated samples at matching time points and set relative to untreated cDNA samples with the same primers. Values represent mean of five trials with error bars of ±SEM. *$p<0.05$, **$p<0.01$, ***$p<0.001$ vs. untreated samples as measured by two-tailed, paired sample t-test.

third and fourth hours after treatment (Figure 5). This pattern was repeated for Rad5.2, with expression peaking at one hour after exposure at a 40-fold increase, dropping to 13-fold at two hours after treatment and leveling off at approximately 3-fold expression during the third and fourth hours after treatment (Figure 6). This pattern also held for Rad16NH, although the degree of the increase was much smaller. One hour after exposure, Rad16NH expression peaked at approximately 3-fold, decreasing to around 2-fold expression at two hours after damage and finally returning to undamaged levels at the three and four hour times (Figure 7). Rad16.1 was the only homolog which diverged from the trend above (Figure 8). Expression began to decrease at two hours after exposure to 60% of untreated levels. Expression continued to fall during the three and four hour times to approximately 30% of untreated levels.

Treatment with MMS yielded much more diverse results across the four homologs. Levels of Rad5.1 increased to roughly 33-fold of untreated expression at one hour after treatment, and levels remained increased at that level until four hours after treatment when they decreased to an 18-fold expression increase (Figure 5). Expression of Rad5.2 peaked to a 34-fold expression increase one hour after exposure to MMS; the levels then decreased to a 21-fold increase two hours after treatment (Figure 6). Three hours after treatment levels of expression increased again to 32-fold of untreated expression and finally decreased to an 18-fold expression change at four hours after treatment. After MMS treatment expression of Rad16NH remained largely unchanged with no significant increases until four hours after treatment, where an increase of 1.65-fold in expression versus the untreated levels was observed (Figure 7). Expression of Rad16.1 decreased to 66% of untreated expression when tested immediately after

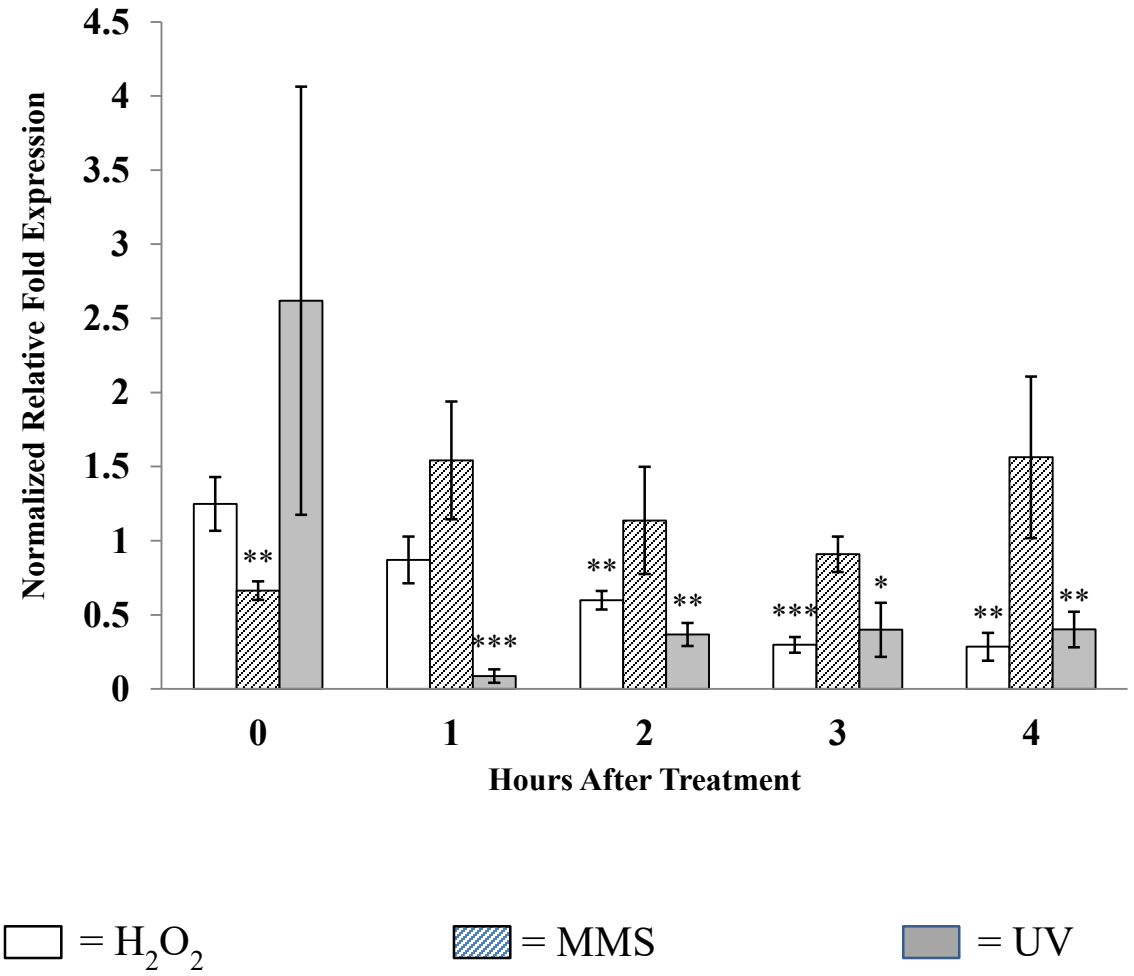

Figure 8: qRT-PCR expression profile analysis of the transcription of Rad16.1 following damage induction with MMS, UV, or H_2O_2**.** Expression profiles of Rad16.1. White bars represent treatment with 10 mM H_2O_2; striped represents MMS treatment, and gray represents UV treatment. All samples were normalized to HHP1 levels in treated samples at matching time points and set relative to untreated cDNA samples with the same primers. Values represent mean of five trials with error bars of ±SEM. *$p<0.05$, **$p<0.01$, ***$p<0.001$ vs. untreated samples as measured by two-tailed, paired sample t-test.

treatment but then showed no significant changes from untreated levels for the rest of the times after MMS treatment (Figure 8).

After UV treatment Rad5.1 levels were significantly increased at four hours to approximately 33-fold, no other time measured showed a statistically significant increase for Rad5.1 (Figure 5). Levels of Rad5.2 began to increase immediately after UV treatment with a 1.76-fold increase. Expression of Rad5.2 continued to increase as time progressed, increasing to approximately 8-fold at one hour after treatment, 18-fold two hours after treatment, 21-fold three hours after treatment, and finally peaking at a 60-fold increase over untreated levels four hours after treatment (Figure 6). Expression of Rad16NH after UV peaks at roughly a 10-fold increase at two hours after treatment, and decreases down to roughly a 2.8-fold increase over untreated levels at four hours after treatment (Figure 7). Expression of Rad16.1 decreases to approximately 8% of untreated levels one hour after treatment; at two hours after treatment the expression increases to roughly 36% of untreated levels. Expression then plateaued at approximately 40% of untreated levels for both three and four hours after treatment (Figure 8).

Knockdown Strains

In order to assess the consequences of a loss of three of the potential homologs (Rad5.1, Rad5.2, and Rad16NH), small-hairpin RNA (shRNA) constructs were designed and transformed into the CU522 strain of *Tetrahymena thermophila*. The constructs were transformed into the *btu1-1* beta-tubulin locus. This puts the constructs under constant expression and makes transformants resistant to a microtubule stabilizing agent,

paclitaxel. Seven days after transformation, the potential transformants were selected in paclitaxel containing media. The resulting transformant strains were then analyzed by whole-cell PCR using primers situated on either side of the *btu1-1* locus. Figure 9 shows agarose gel electrophoresis of these PCR products from the knockdown strains. Lane 1 contains the 100 bp DNA ladder, while lanes 2 and 3 contain samples from CU522 and CU522NC strain 8, respectively. PCR products from shRad5.1 strain 6, shRad5.2 strain 6, and shRad16 strain 2 are shown in lanes 4, 5, and 6 respectively. No PCR product can be seen in lanes 2 or 3, while PCR products of approximately 500 bp in size are present in lanes 4, 5, and 6.

Knockdown Survivability

Once strains were selected and confirmed, the following strains were utilized to assess the phenotypic consequences of a loss in gene expression for each of the homologs after genotoxic stress with either MMS or UV. The Rad16NH knockdown strain (shRad16) number two was utilized, along with the Rad5.2 knockdown strain (shRad5) number six and the Rad5.1 knockdown strain (shRad5.1) number six. For these experiments a CU522 strain which had spontaneously developed paclitaxel resistance, CU522NC strain number 8, was utilized as a wild type (WT) control. The cells were exposed to either 20 mM MMS or 75 j/m^2 UV and allowed to recover for 10 days after UV or five days after MMS treatment. The number of wells showing live cells in untreated samples were set as 100% and the percentages for all treated samples were calculated in relation to their untreated counterparts.

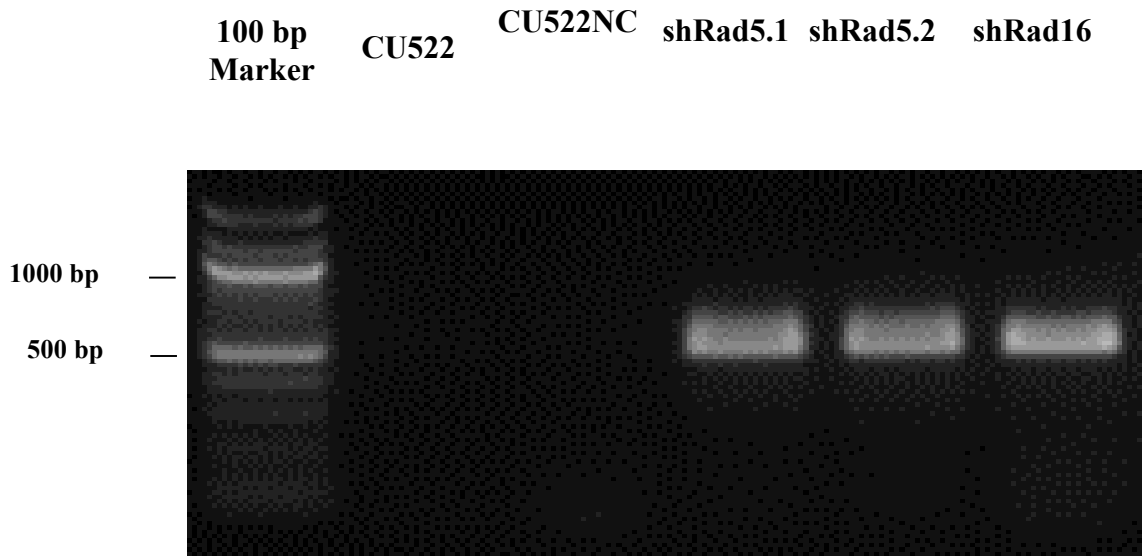

Figure 9: Confirmation of shRNA Knockdown Transformation. PCR primers specific to the flanking region of the *btu1-1* locus were used in whole cell PCR to determine if the potential transformant strains were transformed. Lane 1 contains NEB 100 bp Marker, lane 2 contains WT CU522 as a negative control, along with the spontaneously paclitaxel resistant strain in lane 3. Lanes 4-6 contain the potential transformants, specifically strains 6, 6, and 2 respectively. Bands can be visualized in lanes 4-6 at approximately 500 bp.

Figure 10A shows the after UV treatment for all of the strains utilized. The CU522NC strain had a 57% survival rate when compared to untreated cells. The shRad5 strain had roughly a 56% survival rate, which did not differ significantly from the wild-type strain. Survivability was diminished after UV for the shRad5.1 strain which had a 10.5% survival rate. This decrease in survivability was also seen in the shRad16 strain, with only 4.6% of cells surviving UV damage.

Although the degrees of severity differed between the two types of damage, these trends were also seen after treatment with MMS (Figure 10B). The CU522NC strain had a survival rate of roughly 94% when compared to untreated cells. The shRad5 strain had a survival rate of approximately 90% which was not significantly altered when compared to the wild-type strain. Survivability was significantly decreased to roughly 54% in the shRad5.1 strain when compared to untreated cells. There was also a significant decrease in the survivability of the shRad16 strains, which had approximately 62% of cells surviving treatment with MMS.

Knockdown Expression Profiles

In an attempt to elucidate what effect the shRNA constructs were having on the RNA levels in the knockdown strains, RNA isolates were taken from each knockdown strain along with the CU522NC strain at two hours after 100 j/m^2 UV damage and at three hours after 10 mM MMS treatment. Quantitative Reverse-Transcriptase PCR (qRT-PCR) was utilized, as previously described, to analyze the expression of all three genes in each knockdown strain in both the presence and absence of each type of damage.

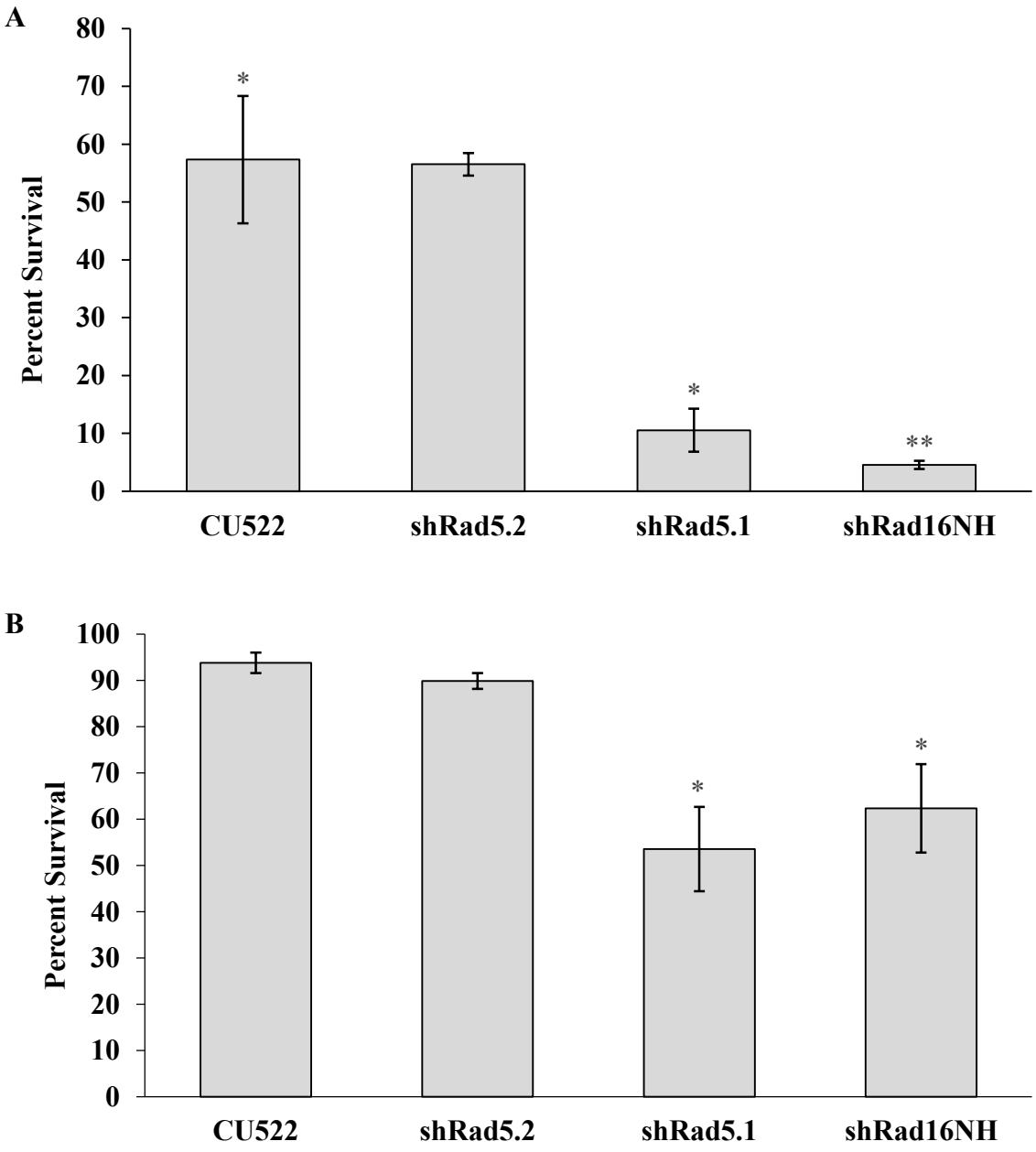

Figure 10: Knockdown Strain Survivability**.** A) Percent survival of shRNA strains after exposure to 75 J/m^2 UV damage. B) Percent survival of shRNA strains after treatment with 20mM MMS. Values for both graphs represent the average of three individual trials with error bars of ± SEM. *p<0.05, **p<0.01 vs. untreated samples as measured by two-tailed, equal variance t-test. Samples were plated at 2 cells/well on three 96 well plates and visualized for growth 72-240 hours after treatment for UV or 72-120 hours after treatment for MMS.

Knockdown Expression Profiles

In an attempt to elucidate what effect the shRNA constructs were having on the RNA levels in the knockdown strains, RNA isolates were taken from each knockdown strain along with the CU522NC strain at two hours after 100 j/m^2 UV damage and at three hours after 10 mM MMS treatment. Quantitative Reverse-Transcriptase PCR (qRT-PCR) was utilized, as previously described, to analyze the expression of all three genes in each knockdown strain in both the presence and absence of each type of damage.

Under undamaged and growing conditions the shRad5.2 strain showed no decreases in the RNA expression levels for Rad5.2, Rad5.1, or Rad16NH (Figure 11). However, after MMS damage, the levels of Rad16NH dropped to 27% of WT Rad16NH levels after MMS damage. There was no decrease in the levels of either Rad5.1 or Rad5.2 after MMS damage. This effect was also evident after UV damage where Rad16NH levels were decreased to 57% of WT levels while Rad5.1 levels were unaffected and Rad5.2 expression increased to roughly 1.5-fold over the WT Rad5.2 levels.

The untreated shRad5.1 strain showed differential decreases in expression of multiple genes (Figure 12). Untreated levels of Rad5.1 were down to 72% of WT three hours after mock MMS treatment, and down to 45% of WT two hours after mock UV treatment. Untreated levels of Rad5.2 were down to 67% of WT after mock MMS treatment, and down to 55% of WT after mock UV treatment. Finally, untreated levels of Rad16NH were down to 48% of WT after mock MMS treatment and were not significantly decreased after mock UV treatment. After MMS treatment levels of Rad5.2 and Rad5.1 were not significantly different from WT levels after MMS treatment.

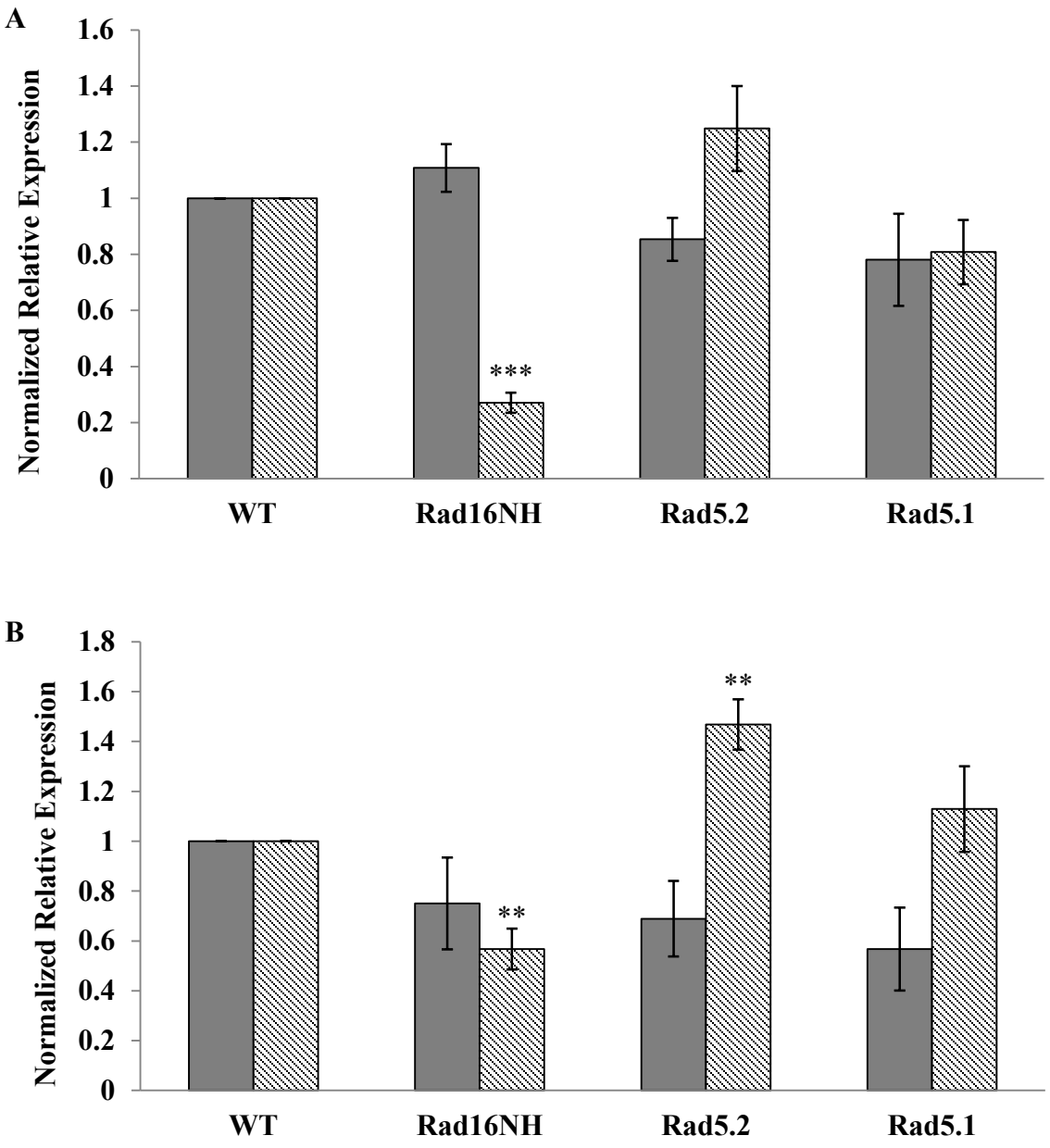

Figure 11: Gene Expression in shRad5.2 Strain. A) Transcript levels of Snf2/Swi2 ATPase homologs in the Rad5.2 knockdown strain three hours after 10 mM MMS treatment (striped), and three hours after mock treatment (gray). B) Transcript levels of Snf2/Swi2 homologs in the Rad5.2 knockdown strain two hours after 100 J/m^2 UV treatment (striped), and two hours after mock treatment (gray). Values represent the average expression relative to WT cells for five individual trials with error bars of ± SEM. *p<0.05, **p<0.01, ***p<0.001 vs. WT (CU522NC) samples as measured by two-tailed, equal variance t-test.

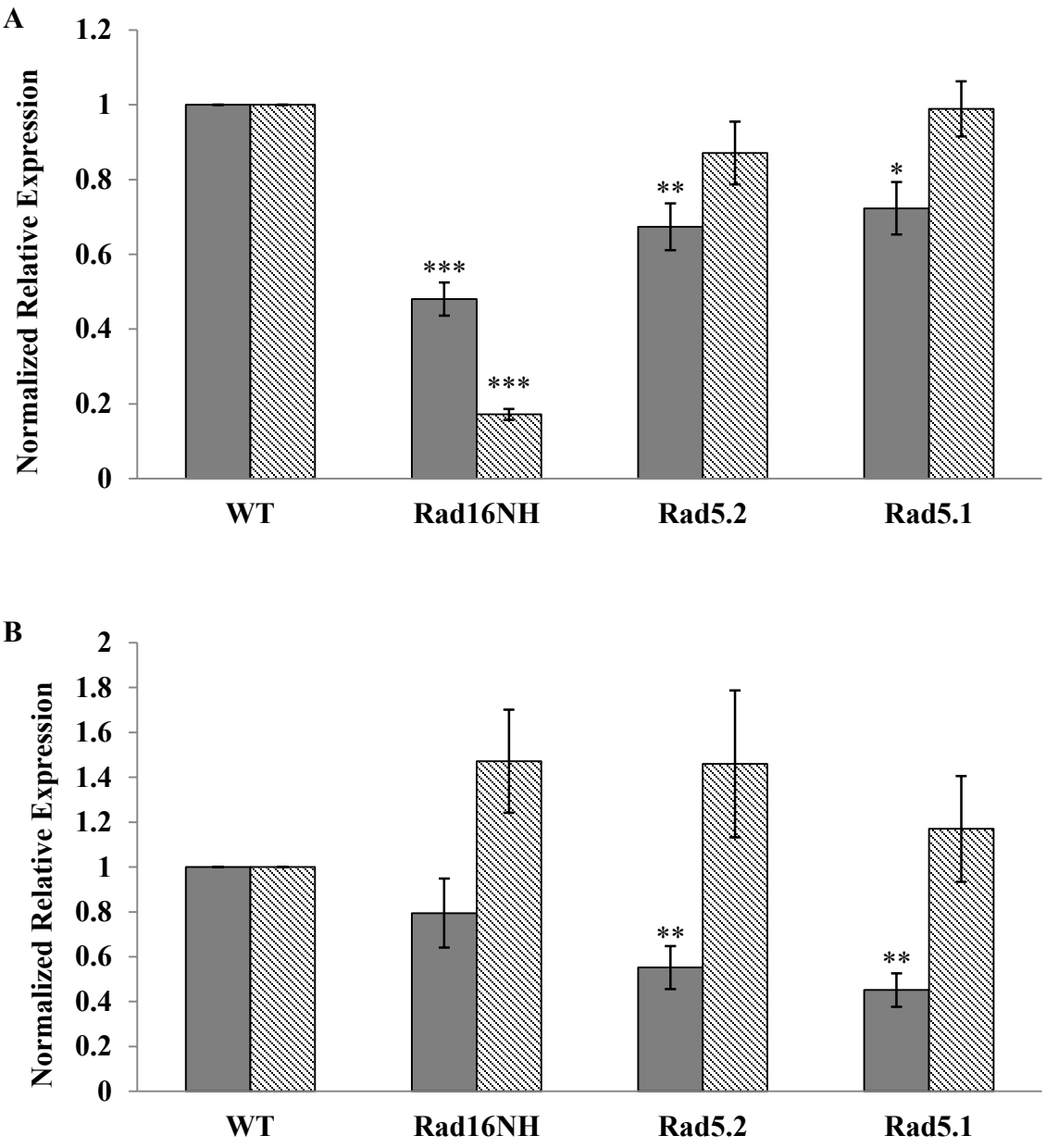

Figure 12: Gene Expression in shRad5.1 Strain. A) Transcript levels of Snf2/Swi2 ATPase homologs in the Rad5.1 knockdown strain three hours after 10 mM MMS treatment (striped), and three hours after mock treatment (gray). B) Transcript levels of Snf2/Swi2 homologs in the Rad5.1 knockdown strain two hours after 100 J/m^2 UV treatment (striped), and two hours after mock treatment (gray). Values represent the average expression relative to WT cells for five individual trials with error bars of ± SEM. *p<0.05, **p<0.01, ***p<0.001 vs. WT (CU522NC) samples as measured by two-tailed, equal variance t-test.

However, there is a significant decrease in the levels of Rad16NH after MMS to 17% of WT levels in the shRad5.1 knockdown strain.

The shRad16 strain had a number of different effects on mRNA levels of the three homologs before and after the different genotoxic stressors (Figure 13). In mock MMS treated cells the levels of Rad16NH were decreased to 66% of WT levels, while the levels of Rad16NH in mock UV treated cells were decreased to 31%. Expression of Rad5.2 was down to 79% in the mock MMS treated cells, and down to 55% of WT expression after mock UV treatment. Finally, levels of Rad5.1 were not significantly different from WT levels after mock MMS treatment but were down to 51% of the WT levels after mock UV treatment.

The dynamics are altered after treatment with MMS as well, with all three genes showing a significant decrease in expression in the shRad16 strain. Levels of Rad16NH were decreased to roughly 67%, with levels of Rad5.2 dropping to 76% of WT cells. Levels of Rad5.1 also decreased after MMS treatment to 67% of the expression in WT cells. After UV treatment the only significant change in expression for any of the genes was a 3.3-fold increase in the levels of Rad16NH when compared to the CU522NC strain.

Promoter and shRNA Expression

To further analyze the efficacy of the shRNA constructs, RNA extracts were made under the same damage conditions as the shRNA expression profiles. Those RNAs underwent Reverse Transcriptase PCR (RT-PCR) using a random hexamer primer to ensure all cellular RNAs were captured for conversion into cDNA to be analyzed by

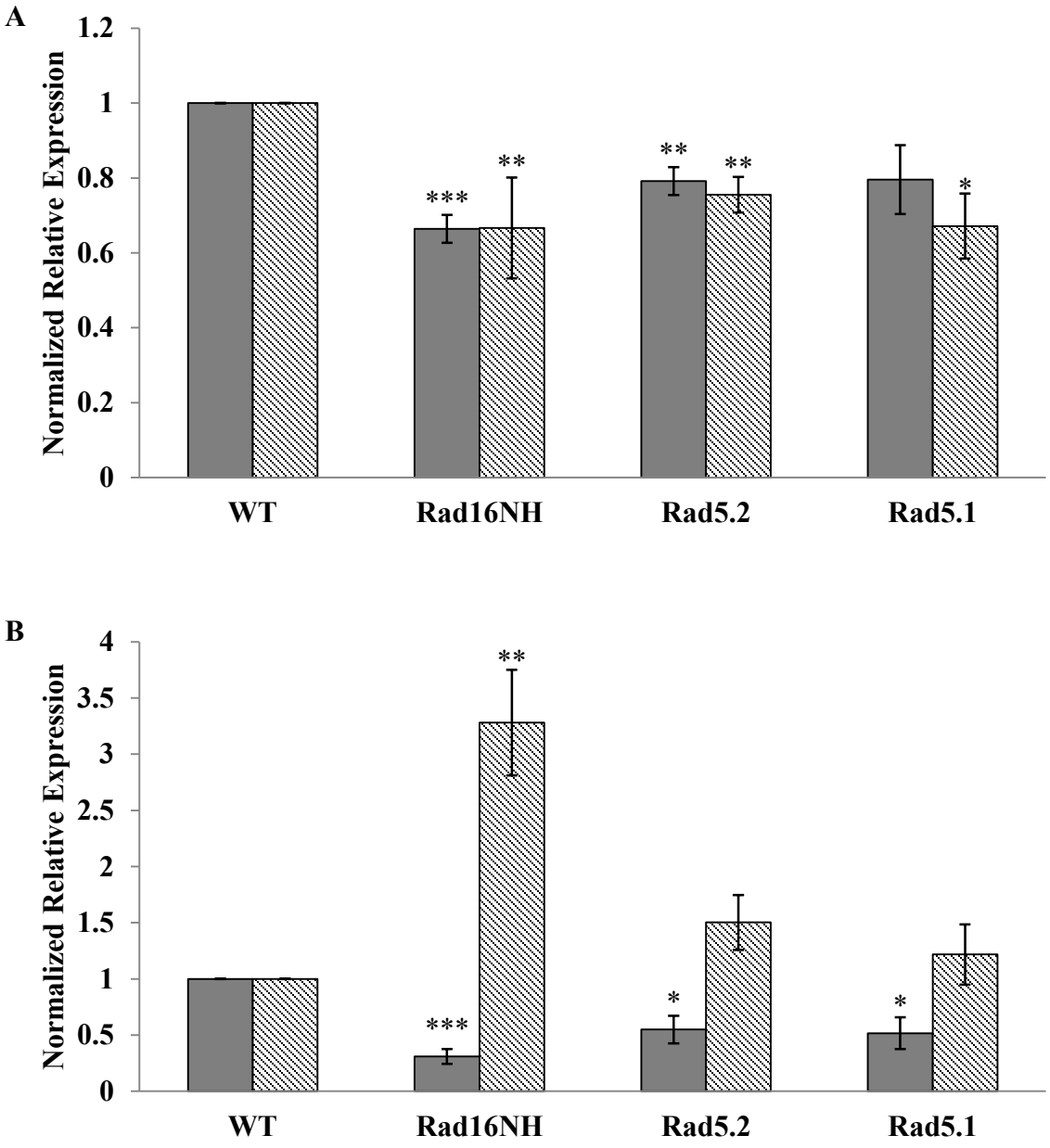

Figure 13: Gene Expression in shRad16 Strain. A) Transcript levels of Snf2/Swi2 ATPase homologs in the Rad16NH knockdown strain three hours after 10 mM MMS treatment (striped), and three hours after mock treatment (gray). B) Transcript levels of Snf2/Swi2 homologs in the Rad16NH knockdown strain two hours after 100 J/m^2 UV treatment (striped), and two hours after mock treatment (gray). Values represent the average expression relative to WT cells for five individual trials with error bars of ± SEM. *p<0.05, **p<0.01, ***p<0.001 vs. WT (CU522NC) samples as measured by two-tailed, equal variance t-test.

qRT-PCR. PCR primers were utilized to bind and amplify the newly generated cDNA products of *btu1-1*. This was done to analyze the activity of the promoter, under which the shRNA constructs are controlled, after the different damaging agents. Primers which recognize the boundaries of the shRNA constructs in the genome were also utilized to determine the amount of shRNA product being transcribed at these same timepoints.

In the shRad16 knockdown strain BTU1 expression after UV treatment was decreased to roughly 21% of untreated levels; with expression decreased to 1% of untreated levels after MMS. Levels of the shRNA construct in this strain were decreased to approximately 41% of untreated levels after UV and 9% of untreated levels after MMS exposure (Figure 14). In the shRad5.2 strain BTU1 levels after UV treatment were at 42.5% of untreated levels, while the expression of BTU1 was decreased to 3% of untreated levels after MMS exposure. The expression of the shRNA construct in this strain was also affected with expression after MMS at 49% of untreated levels and expression after UV at increasing by approximately 320% (Figure 15).

The shRad5.1 strain showed decreased expression of BTU1 to 41% after UV and to 0.6% of untreated expression after exposure to MMS. Similarly, levels of the shRNA hairpin were down to approximately 29% after UV treatment but were increased to roughly 213% after treatment with MMS (Figure 16).

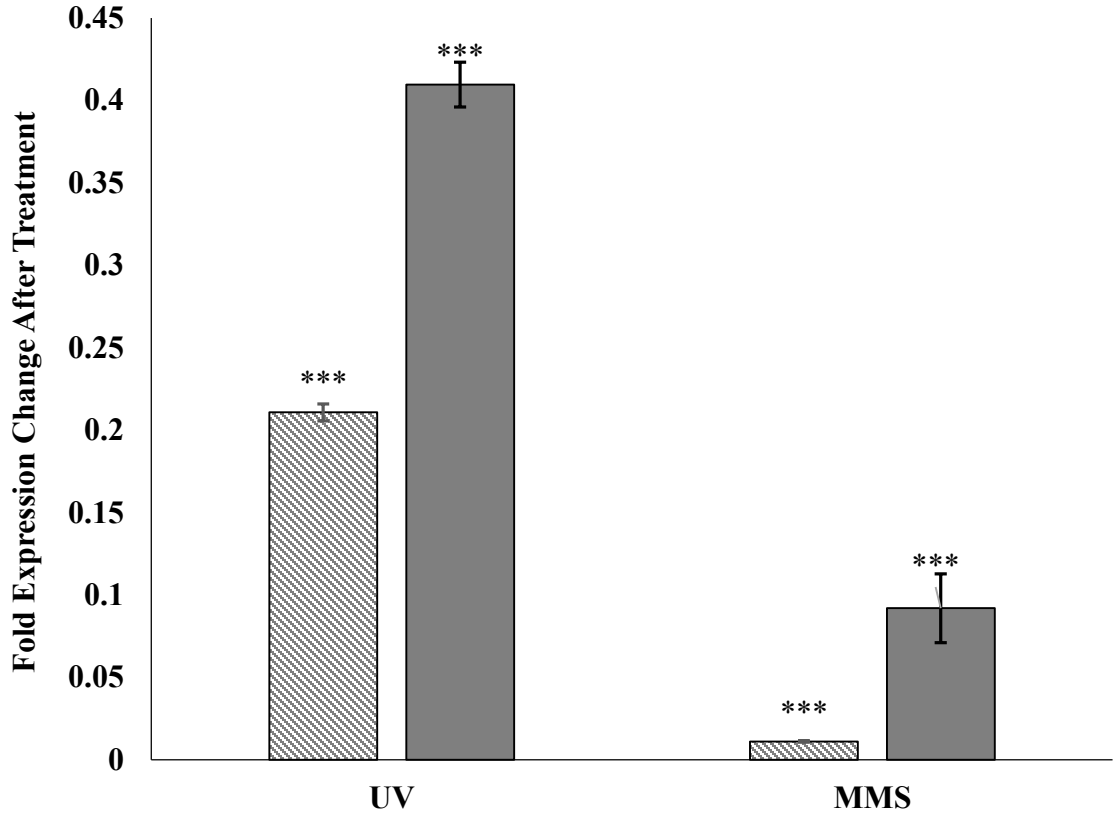

Figure 14: Hairpin and BTU1 Expression in shRad16 Strain. Expression of BTU1 (striped) or the shRNA hairpin (gray) two hours after UV treatment and three hours after MMS treatment. All values represent the expression relative to untreated WT cells. The shRNA hairpin values represent the average of five individual trials with error bars of ± SEM. *p<0.05, **p<0.01, ***p<0.001 vs. WT (CU522NC) values as measured by two-tailed, equal variance t-test. BTU1 values represent the average of three individual trials with error bars of ± SEM. *p<0.05, **p<0.01, ***p<0.001 vs. WT (CU522NC) values as measured by two-tailed, equal variance t-test.

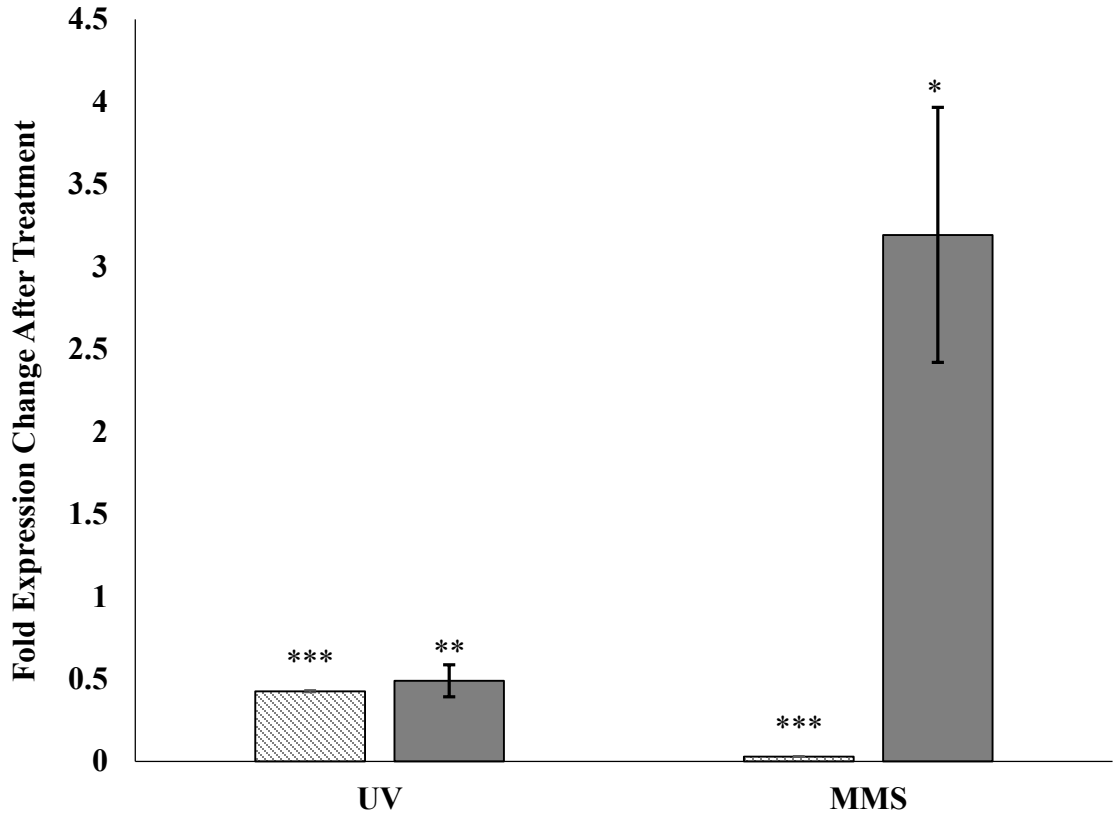

Figure 15: Hairpin and BTU1 Expression in shRad5.2 Strain. Expression of BTU1 (striped) or the shRNA hairpin (gray) two hours after UV treatment and three hours after MMS treatment. All values represent the expression relative to untreated WT cells. The shRNA hairpin values represent the average of five individual trials with error bars of ± SEM. *p<0.05, **p<0.01, ***p<0.001 vs. WT (CU522NC) values as measured by two-tailed, equal variance t-test. BTU1 values represent the average of three individual trials with error bars of ± SEM. *p<0.05, **p<0.01, ***p<0.001 vs. WT (CU522NC) values as measured by two-tailed, equal variance t-test.

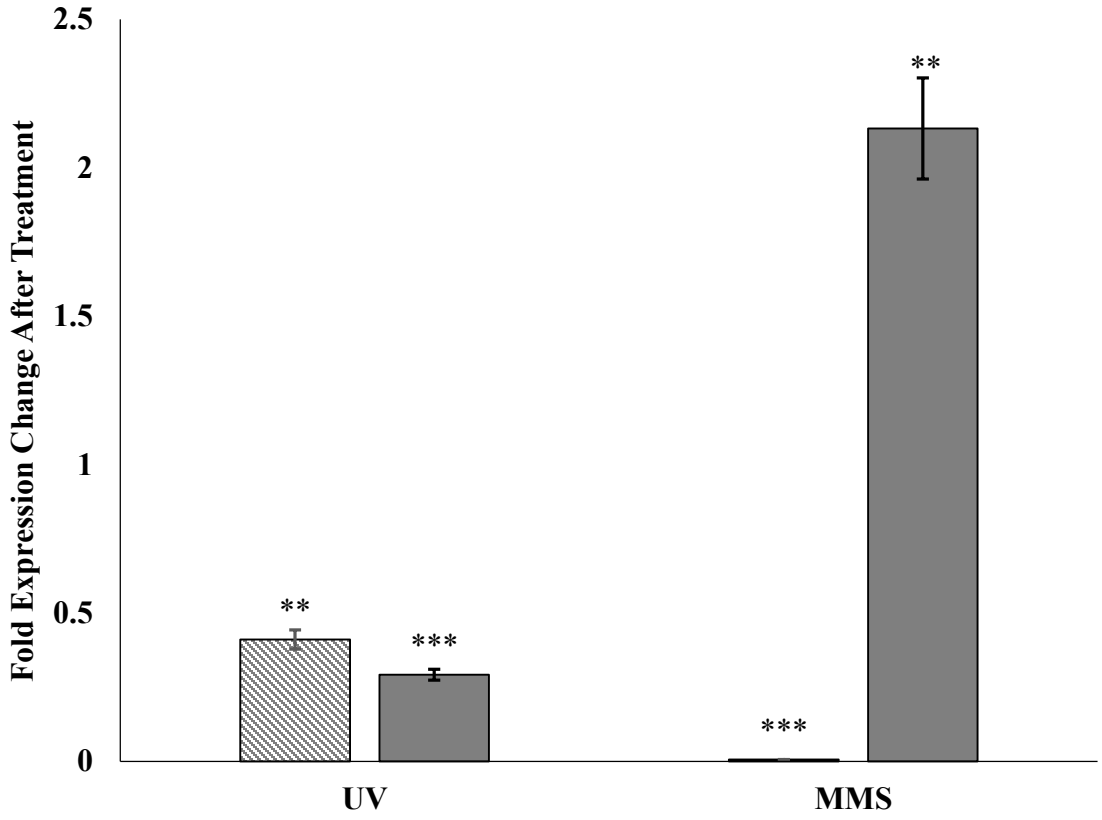

Figure 16: Hairpin and BTU1 Expression in shRad5.1 Strain. Expression of BTU1 (striped) or the shRNA hairpin (gray) two hours after UV treatment and three hours after MMS treatment. All values represent the expression relative to untreated WT cells. The shRNA hairpin values represent the average of five individual trials with error bars of ± SEM. *p<0.05, **p<0.01, ***p<0.001 vs. WT (CU522NC) values as measured by two-tailed, equal variance t-test. BTU1 values represent the average of three individual trials with error bars of ± SEM. *p<0.05, **p<0.01, ***p<0.001 vs. WT (CU522NC) values as measured by two-tailed, equal variance t-test.

DISCUSSION

Bioinformatics and Wild Type Strain Analyses

The initial bioinformatic data pointed to four potential homologs of Rad5/16, each contained the characteristic ATPase domains and the embedded E3 ubiquitin ligase domain. Only one of those four, Rad5.2, also contained a HIRAN DNA binding domain (Figure 1). Since all four of these proteins share the ATPase and ubiquitin ligase domains there is potential for shared or common functionality. However, knowing that these proteins contain the domains does not demonstrate how closely these *T. thermophila* homologs are related to the *S. cerevisiae* proteins. The alignments and analyses of the protein sequences in Figure 2 revealed interesting relationships.

When the *T. thermophila* proteins were aligned with *S. cerevisiae* Rad5 and Rad16 alone in Figure 2A, both Rad5.1 and Rad5.2 were most closely related to Rad16. Rad16NH was also more closely related to Rad5, despite the fact that Rad16NH lacks a HIRAN domain. The data also showed that Rad16.1 was very distantly related to every other Rad5 or Rad16 homolog. These relationships were changed by the inclusion of the SHPRH, HLTF, and SM3L1-3 in the analyses, seen in Figure 2B.

HLTF, SM3L1, SM3L2, and SM3L3 are Rad5-like proteins (the SM3L proteins are found in *Arabidopsis thaliana*) which have been found to have similar structures when compared to Rad5. However, these proteins tend to also be involved in transcription, where Rad5 has not been implicated. Curiously, Rad5.2, which had initially been identified as more closely related to Rad16 was shown to be much more closely related to the Rad5-like genes than to anything else. Rad5.1 branched more

closely to both *S. cerevisiae* proteins along with Rad16NH. Again, Rad16.1 was the most distant from the others, but it was also the most closely related to the higher eukaryotic SHPRH Rad5 homolog.

The relationships suggested by the phylogenetic analyses was, at times, contradictory; with relationships varying greatly depending on how many other proteins were considered in the analyses. Due to these inconsistencies another method of determining homology was necessary. Knowing that Rad16 exhibits activity only after UV damage, and that Rad5 can respond to a number of different genotoxic stressors allowed for a method to examine homology by function. Expression profiles of the four potential homologs were conducted under conditions that would lead to the use of nucleotide excision repair (NER), base excision repair (BER), and double-strand break (DSB) repair. This was done through treatment with UV light, Hydrogen Peroxide (H_2O_2), and methyl methanesulfonate (MMS), respectively.

The expression of Rad16.1, seen in Figure 8, was the most surprising of the four genes. After MMS treatment there was no significant change seen in expression, which indicated that Rad16.1 was not involved in DSB repair. There were significant changes in the expression of Rad16.1 after both UV and H_2O_2. In both cases, expression of Rad16.1 was significantly decreased from undamaged levels. After UV, expression of Rad16.1 decreased to 8% of the untreated levels, and was unable to return to untreated levels during the four hour timecourse. Decreases in expression were also seen after H_2O_2 treatment, where expression began decreasing two hours after exposure and continued to decrease to 30% of untreated levels four hours after damage.

These results strongly suggest that Rad16.1 is not involved in DNA repair and, as a matter of fact, may be involved in a process that is shut down after DNA damage. The process of DNA repair has profound effects on the processes that occur in the cell; with damage having the potential to stop normal cellular activity. When this occurs, a number of different transcription factors will be differently regulated to deal with the damage or to prevent continuation of the cell cycle. Since Rad16.1 contains all of the components to act on DNA and alter the local structure it is conceivable that it may be a transcription factor, one which gets downregulated in response to certain types of DNA damage. The fact that Rad16.1 did not appear to be upregulated by damage it was not studied beyond that experiment.

Expression of Rad5.1, seen in Figure 5, is far more characteristic of a DNA repair-involved gene. Levels of Rad5.1 increase dramatically within the first hour after H_2O_2 treatment, up to 40 times untreated levels, however this increase was short lived, and decreased to 10 times untreated levels after two hours, and finally down to roughly three times untreated levels at three and four hours after treatment. Similarly, expression of Rad5.1 after MMS increased early, to about 33 times the untreated levels one hour after treatment. However, levels of Rad5.1 remained that high for three hours after treatment before decreasing to approximately 18 times the untreated levels at four hours.

After treatment with UV there was no significant change in the expression of Rad5.1 until four hours after treatment, where the expression peaked at 33 times the untreated levels. These data suggest that Rad5.1 is involved in DNA repair, but that it more likely functions in DSB repair, as that was where a sustained increase was seen. While expression did change in H_2O_2 the response wasn't as robust, and levels returned

to the untreated expression much more quickly. This may be a more general initial response to a stressor, as H_2O_2 can cause oxidative damage not only to DNA but also to larger cellular structures such as organelles. Since Rad16 functions in an early step of NER it is unlikely that a reactionary increase of expression four hours after damage would be sufficient to fulfill the function of Rad16.

The expression of Rad5.2, seen in Figure 6, is also likely to be DNA repair related. After exposure to H_2O_2 Rad5.2 also shows a sharp increase to 40 times untreated levels at one hour which quickly begins to decrease down to three times untreated levels four hours after treatment. The response to MMS also shows a sustained increase after treatment with expression between 18 and 34 times untreated levels throughout the timecourse. Exposure to UV also had an effect with levels increasing to almost two times untreated levels immediately after treatment and continuing to increase throughout the four hours to 60 times untreated levels.

Again, the response to H_2O_2 appears to be a general reaction to a cellular stressor, as the response begins strong and then starts to taper off quickly. In contrast, the expression of Rad5.2 in response to MMS is more sustained over time, suggesting a continued need for Rad5.2 after DSB damage. Rad5.2 acts differently after UV than Rad5.1, with expression increasing immediately and continuing to increase throughout the trial. This would suggest that as the process of repair is continuing there is increased need for Rad5.2, which may implicate the use of Rad5.2 in a downstream step of repair. This could include a process like post-replication repair (PRR) or damage bypass which occur later after damage. Both of those processes would also be triggered by many different types of genotoxic agents.

The expression of Rad16NH in Figure 7 followed a different pattern than any of the other homologs, but it still appeared to be damage dependent. Again, after H_2O_2 treatment expression peaked at one hour and continued to decrease throughout the timecourse. In the case of MMS treatment levels were unaffected until four hours after treatment when the expression peaked at 1.65 times untreated expression. While statistically significant this is still a minor increase that occurred late in the timecourse which may be related to the repair of errors introduced by other repair methods. Finally, the expression changes for Rad16NH are most notable after UV treatment, with the largest increase of 10 times untreated expression occurring at two hours after treatment and decreasing to approximately three times the untreated levels at four hours. This seems to be a specific and finite response to UV, which is more indicative of how Rad16 would function.

Knockdown Strain Analyses

While the expression profiles were useful they were not enough to say that any protein was definitively Rad5 or Rad16. To help with further characterization, shRNA knockdown strains were made for Rad5.1, Rad5.2 and Rad16. The shRNA constructs were transformed into the *btu1-1* locus in strain CU522. As a result of this transformation, the cells developed resistance to paclitaxel, a microtubule stabilizing agent. After selection with paclitaxel, the resulting transformants were analyzed by whole cell PCR to confirm transformation (Figure 9). In the absence of the shRNA constructs the PCR primers are unable to amplify the target sequence, while the presence of the construct would lead to a PCR product of approximately 500 bp in size. The PCR

confirmed that neither the CU522, or the CU522NC strain (which was spontaneously resistant to paclitaxel) had an shRNA construct incorporated. The PCR also confirmed that all three shRNA constructs were transformed into the separate CU522 strain of *Tetrahymena thermophila*.

The generated shRNA knockdown strains were then used to identify the consequences of decreased expression of the genes for Rad16NH, Rad5.1, and Rad5.2. The shRNA strains were treated with 100 j/m^2 UV, or 20 mM MMS to induce the specific types of damage mentioned above. When considering Rad5 and Rad16 it has been shown that deficiencies in Rad16 lead to a decrease in survival after UV damage, while survival after MMS is unaffected. This differs from Rad5 deficiencies, which lead to decreases in survival after both UV and MMS damage. The results of the genotoxic challenges to each of the shRNA strains with these agents are seen in Figure 10.

Remarkably, after treatment with either UV and MMS, the shRad5.2 strain suffered no decreases in survivability. The same could not be said for the shRad5.1 or shRad16NH strains. After UV damage the shRad16NH strain had only 4.6 percent of cells surviving treatment compared to 57 percent of CU522NC cells surviving. Similarly, the shRad5.1 had only 10.5 percent of cells surviving UV damage. An identical trend was also seen after damage with MMS, where shRad16NH had only 62 percent of cells surviving treatment with MMS compared to approximately 94 percent of the CU522NC cells surviving. The shRad5.1 strain was more sensitive to MMS treatment, with only 54 percent of cells surviving the damage. These results alone would indicate that the knockdown strains for Rad16NH and Rad5.1 are damage responsive, while Rad5.2 is not. However, the fact that two genes, which are so similar to Rad5 and Rad16, have a role in

DNA repair after multiple types of damage is extremely different from the dynamics seen in *S. cerevisiae*.

The relationship of these knockdowns to DNA damage survivability favors a relationship that is more closely related to that of higher eukaryotic HLTF and SHPRH than that of Rad5 and Rad16. One characteristic of HLTF that distinguishes it from Rad5 is that HLTF can act as a transcription factor, where Rad5 has not been shown to function in this manner. This information, along with the data showing that the shRad5.2 strain does not have increased susceptibility to the DNA damaging agents, prompted a closer examination of the effectiveness of the shRNA knockdowns along with the potential effects that a knockdown in one gene may have on the others. In order to accomplish this the shRNA strains were treated with UV and MMS under the same conditions as the previous set of expression profiles, and mRNA samples were converted into cDNA for analysis at two hours after UV treatment and at three hours after MMS treatment.

The levels of expression for each of the three genes in the shRad5.2 strain is seen in Figure 11. Interestingly, despite the fact that the shRad5.2 strain was confirmed to have the shRNA construct inserted, there was no change in the basal expression of Rad5.2 in that strain. While this knockdown has no effect on Rad5.2 basal levels it also has no effect on the basal levels or Rad16NH or Rad5.1, but that is not to say that this strain has no effect whatsoever. After MMS damage, in the shRad5.2 strain there is a significant decrease in the levels of Rad16NH, down to just 27 percent of the CU522NC (WT) levels of Rad16NH at the same time after MMS damage. This decrease is also seen after UV, but to a lesser degree with expression at only 57 percent of WT levels.

These effects are highly unlikely to be random, as no other gene tested in this strain produced similar results, and these decreases were statistically significant across five replicates of the qRT-PCR. Additionally, levels of Rad5.2 in this knockdown strain did increase to roughly 150 percent of WT levels after treatment with UV. These results suggest that the shRad5.2 construct is having an effect on this strain. There seemed to be a relationship to the levels of Rad5.2 and Rad16NH, with higher levels of Rad5.2 leading to a decrease in the levels of Rad16NH, as seen in Figure 11 after both UV and MMS treatment. This is reminiscent of an interaction between HLTF and SHPRH after damage, where HLTF is degraded after MMS damage to allow SHPRH to function; and after UV where HLTF sequesters SHPRH to allow HLTF to function. In this case Rad16NH would act like HLTF, whose expression does not increase after MMS damage, as existing protein is degraded. High levels of unbound SHPRH, or in this case Rad5.2, would signal to the cell that SHPRH was being used instead of HLTF. This would prevent the cell from increasing levels of HLTF, which would explain why Rad16NH levels are decreased when Rad5.2 levels are elevated.

Figure 12 shows the results of the same experiment for the shRad5.1 strain, and those results are quite a bit more illuminating. The shRad5.1 construct does indeed significantly decrease basal levels of Rad5.1 in the knockdown strain, while at the same time causing significant decreases in the basal levels of both Rad5.2 and Rad16NH. Interestingly, again, we see a significant decrease in levels of Rad16NH in this knockdown strain after UV damage. However, other than this there are no decreases in the levels of the genes under any other circumstance after damage. These data demonstrate that the Rad5.1 knockdown construct is functioning during the normal stages

of cell growth, and more importantly that a decrease in the basal levels of Rad5.1 leads to a decrease in the basal levels of both Rad5.2 and Rad16NH. Again, we see that the knockdown construct is failing to decrease the post-damage levels of the knockdown target, despite the fact that the knockdown appears to have an effect on basal levels of expression.

The expression profiles for the shRad16 strain, seen in Figure 13, also provide interesting data which help to understand the relationship between these three genes. The shRad16 strain shows decreased basal expression levels of all three genes, while also showing decreased levels of expression of all three after MMS damage. While there were no decreases in expression after UV damage there was a large increase in Rad16NH levels after UV damage, similar to the increase of Rad5.2 after UV damage in the shRad5.2 strain.

These results indicated that both Rad16NH and Rad5.1 play a role in controlling the basal expression of all three genes, an effect which is entirely uncharacteristic of both Rad5 and Rad16, but which corresponds more closely to the activity of HLTF. In order to investigate these phenomena a two pronged analysis was conducted on the N-terminal regions of the proteins before the N-terminal ATPase domains (Figure 3) and the promoter regions of the genes (Figure 4). Previous work has shown that HLTF uses a DNA binding domain located at amino acids 38-287 to interact with a B-box promoter element to affect basal expression of certain genes. Upon alignment, all three homologs displayed sequence with extremely high similarity to the sequence of the DNA binding domain from the *H. sapiens* HLTF. Interestingly, there appears to be a higher degree of similarity between the N-terminal regions of Rad5.1 and Rad16NH than to the N-

terminal region of Rad5.2 (Supplementary Figure #). When the promoter regions of these genes were examined to identify potential B-box or B-box-like sequences all three homologs had at least one B-box like sequence.

The promoter regions of both Rad5.1 and Rad16NH have multiple B-box-like sequences, which are also highly similar to each other, while the promoter region of Rad5.2 contains only a single B-box-like sequence which is more similar to the full B-box sequence seen in Rad5.1. Together, these data suggest that the decreases in basal expression seen in the shRad5.1 and shRad16 strains is a direct result of a decrease in the basal levels of Rad5.1 and Rad16NH, which appear to have the capacity to act as transcription factors for each gene. This implies that there is an intricate network of regulation where the basal expression of each gene is determined by the expression of the others.

The shRad5.2 knockdown remains an outlier to this trend, largely because it would appear to have no effect on the expression of Rad5.2 at any point. While it can be inferred that the initiating factor for decreased basal expression in each strain is the transcript that the transformed shRNA is targeting (Rad5.1 in the shRad5.1 strain, Rad16NH in the shRad16 strain), there is no way of knowing how Rad5.2 fits into this pattern of expression. This is largely because we do not know what happens if Rad5.2 basal levels are the first to be decreased; while we do know what happens if either of the other two are the first to be decreased.

Still, the failure of the knockdowns to alter expression of the genes after damage, with the exception of the shRad16 strain, was curious. To address this, expression profiles were conducted with cDNA made from total RNA extracts of the shRNA strains

at the same conditions as described above. The targets for this series of qRT-PCR expression profiles were the BTU1 gene (whose promoter the shRNA constructs are under) and the hairpin created from the shRNA constructs. For the hairpin, the qRT-PCR would only be able to detect transcribed shRNA hairpins which had not been processed, since the primers for this qRT-PCR were designed on either side of the hairpin. This meant that a decrease in the shRNA hairpin levels would correspond to a decrease in the unprocessed transcripts, while an increase would correspond to an increase in the unprocessed transcripts.

In Figures 14, 15, and 16, we could see that BTU1 levels after both UV and MMS were greatly decreased in all strains. The data shows that the BTU1 gene itself has decreased expression after genotoxic stress, and this decrease should carry over to any other product under control of that promoter, which includes the shRNA constructs. In Figure 14, this trend is indeed carried out in the shRad16 strain, with decreased levels of BTU1 corresponding to decreased levels of the shRNA hairpin under both types of damage. This trend also holds after UV damage for both shRad5.2 in Figure 15, and shRad5.1 in Figure 16. These data help to explain why after UV, even when basal levels are decreased, we did not see a decrease in the levels of expression of those same genes.

Additionally, it is worth noting that the shRNA constructs do not abolish the expression of these genes during normal cellular growth. While they do have an effect, this effect is seen when levels are not elevated. After MMS and UV damage the levels of Rad5.1 increase roughly 20-40 fold when compared to the untreated levels in WT cells. When factoring this and the decrease in the level of shRNA hairpin made after damage it would mean that there were far more Rad5.1 transcripts available than hairpins to target

them. This would mean that for Rad5.1, after both UV and MMS there would be no noticeable effect on the expression of Rad5.1, which would allow the cells to correct the deficiencies in the levels of the other proteins.

This also helps to explain how the levels of Rad16NH remain decreased after MMS treatment. Since Rad16NH is not upregulated at three hours after MMS treatment there would be no process which would signal for an increase in Rad16NH levels, and thus they would remain low. While after UV damage the levels of Rad16NH do increase, which is why the Rad16NH could return to WT levels under those conditions.

This phenomenon is confirmed in Figure 13 when analyzing the effect of the Rad16NH knockdown after MMS. Decreased basal levels of Rad16NH led to decreases in the basal levels of the other two genes. When treatment with MMS occurred there may have been a decrease in the shRNA expression, but there was no increase in the level of Rad16NH because the expression of that gene was not upregulated after MMS damage. With levels of Rad16NH still low, the effect of these low Rad16NH levels (decreases in both Rad5.2 and Rad5.1) carried over, resulting in decreases at the same relative levels as the untreated levels. These data imply that Rad16NH may be a key player in the response of both Rad5.1 and Rad5.2 to both UV and MMS damage.

This BTU1 promoter downregulation allowed the cells to briefly return expression to basal levels under conditions where the genes were being upregulated. This would explain the post-UV damage increases seen in Rad5.2 and Rad16NH; because the cells would be overcompensating in an attempt to overcome the detriment in expression caused by the constructs, and once the constructs were downregulated the over-compensation would lead to an increase in the expression of those proteins.

The expression of the constructs after MMS damage is a little more convoluted, but must be examined as a whole in order to be understood. When analyzing the expression of the shRNA hairpins after MMS treatment it is important to take into account that there is a limited pool of the proteins which process these hairpins. In the case of shRad16, after MMS there is no increase in gene expression, but a decrease in the amount of hairpin being made. In total, there would be no more Rad16NH than there had been previously, so the shRNA machinery would be able to continue to function properly, preventing a buildup of the unprocessed products. This is why there was not an increase in the shRNA hairpin for shRad16 after MMS damage.

When looking at Figures 15 and 16 for shRad5.2 and shRad5.1, respectively, there are significant increases in the shRNA hairpins after MMS damage. This was most likely the result of increased gene expression after damage combined with diminished, but not abolished, expression of the shRNA hairpins. It is likely that, as the expression of the target mRNAs were increased, more shRNA machinery was utilized, and since this machinery was being utilized in so many places at once it was increasingly unable to process all of the hairpins being generated. This led to an increase of the unprocessed product after MMS damage as seen in both Figures 15 and 16.

This effect would not likely be seen after UV damage for any of the strains, since the increases in expression after UV by two hours after damage are much smaller than those seen after MMS damage. Increases of approximately 10-fold for Rad16NH, Rad5.1, and Rad5.2 were observed after UV damage. In contrast, increases of approximately 30-fold were seen for both Rad5.1 and Rad5.2, with no increase in Rad16NH levels after MMS treatment. Much larger increases in expression like these

would have a greater potential to lead to an excess of unprocessed shRNA hairpins, especially if those increases occurred early after damage and the cells had a longer time to develop a backlog of unprocessed hairpins. Both Rad5.1 and Rad5.2 had early expression increases after MMS which remained high through the three hour time point, which provided more targets for a longer period of time than what would have been possible to produce after UV damage.

Between the final three potential homologs: Rad5.1, Rad5.2, and Rad16NH, there was much more evidence to suggest that the homologs were more closely related to SHPRH and HLTF than to Rad5 and Rad16. The fact that there is complex interplay between the three genes in the knockdown strains; combined with the data showing that Rad16NH and Rad5.1 are very likely to be able to act as transcription factors for the other potential homologs, strongly suggests functional similarity to SHPRH and HLTF. Additionally, the way in which survivability is affected for both Rad16NH and Rad5.1 after both UV and MMS is highly uncharacteristic of Rad16.

Rad5.2 remains an unknown when looking at this trend, as we were unable to decrease basal levels of Rad5.2 to analyze what effect, if any, that would have had on the other genes or survivability after damage. It remains unclear why this was the case, although it could be the result of alternative splicing for this gene which would remove the target sequence for the shRNA. While the target sequence was designed in a transcribed region, this region may have an alternatively spliced variant which is transcribed at the same time as the version containing the target site. In the absence of damage this could result in a diminished effect, which would not significantly decrease basal expression but may have some effect after damage.

It is likely that *Tetrahymena thermophila* has a series of DNA repair systems which are more similar to those in higher eukaryotes than to those in *Saccharomyces cerevisiae*. However, more experimentation is necessary to be certain of the extent of the similarities and differences between the function of Rad16NH, Rad5.1, and Rad5.2 when compared to Rad5, Rad16, HLTF, and SHPRH. At most, it has been shown that Rad16NH plays a major role in controlling basal and post-damage expression of both Rad5.1 and Rad5.2, while Rad5.1 would appear to have an extremely similar function. Rad5.2 also appears to be able to regulate the expression of Rad16NH, at least indirectly, which implies that a signaling pathway is utilized in determining how the expression of the different proteins are regulated.

Future Directions

In order to better understand the relationship of these proteins it will be necessary to tag these proteins with an HA tag, both in WT strains and in the shRNA strains which have already been produced. The tagging should be done endogenously, on the C-terminal end of the proteins for a number of reasons. First, with the complex network of interactions, and the apparent ability of these proteins to act as transcription factors, it would be best to ensure that the proteins are under their own control and that they are expressed as they would normally be expressed. Second, the activity of these proteins to function as transcription factors is more likely to be dependent on the N-terminal regions of the proteins, and adding extraneous sequence could interfere with this functionality.

The tagging itself would be useful in three regards. First, the ability to precipitate tagged proteins would allow us to measure how the expression levels from the shRNA

strains correlate to protein levels, which would provide valuable information about protein concentrations and stability. Second, by performing co-immunoprecipitation we would be able to determine what proteins are interacting with the homologs under which conditions, and those interactions are well document for Rad5, Rad16, SHPRH, and HLTF. Another method of analysis would be to damage the cells with the various DNA damaging agents and then track the ability of the *Tetrahymena* to mate and produce viable progeny. The reasoning behind this would be that any deficiencies in repair of silenced areas of the genome would have specific and more drastic effects on the heterochromatinized micronucleus. *Tetrahymena* with damaged micronuclei would, most likely, be unable to complete mating, as large scale damage of the DNA would prevent the replication of the micronuclear DNA. Finally, the ability to isolate functional versions of these proteins would allow them to be used in an *in vitro* NER assay, which would provide direct evidence for the function of these proteins.

REFERENCES

Arslanyolu M, Doerder FP. Genetic and environmental factors affecting mating type frequency in natural isolates of *Tetrahymena thermophila*. J Eukaryot Microbiol. 2000 Jul-Aug;47(4):412-8.

Becker, P.B. and Horz, W. (2002) ATP-dependent nucleosome remodeling. Annu. Rev. Biochem., 71, 247–273.

Caruthers, J.M. and McKay, D.B. (2002) Helicase structure and mechanism. Curr. Opin. Struct. Biol., 12, 123–133.

Chalker DL. Transformation and strain engineering of *Tetrahymena*. Methods Cell Biol. 2012; 109: 327-45. doi: 10.1016/B978-0-12-385967-9.00011-6.

Chen S, Davies AA, Sagan D, Ulrich HD. The RING finger ATPase Rad5p of *Saccharomyces cerevisiae* contributes to DNA double-strand break repair in a ubiquitin-independent manner. Nucleic Acids Res. 2005 Oct 13;33(18):5878-86.

Cole, E. S. (2006). The *Tetrahymena* conjugation junction. In ‘‘Cell–cell channels,’’ (F. Baluska, D. Volkmann, P. W. Barlow, eds.), pp. 39–62. Springer, New York.

Collins K, Gorovsky MA. *Tetrahymena thermophila*. Curr Biol. 2005 May 10;15(9): R317-8.

Davis, J.L., Kunisawa, R. and Thorner, J. (1992) A presumptive helicase (MOT1 gene product) affects gene expression and is required for viability in the yeast *Saccharomyces cerevisiae*. Mol. Cell. Biol., 12, 1879–1892.

Ding H, Descheemaeker K, Marynen P, Nelles L, Carvalho T, Carmo-Fonseca M, Collen D, Belayew A. Characterization of a helicase-like transcription factor involved in the expression of the human plasminogen activator inhibitor-1 gene. DNA Cell Biol. 1996 Jun; 15(6): 429-42.

Ding H, Benotmane AM, Suske G, Collen D, Belayew A. Functional interactions between Sp1 or Sp3 and the helicase-like transcription factor mediate basal expression from the human plasminogen activator inhibitor-1 gene. J Biol Chem. 1999 Jul 9; 274(28): 19573-80.

Dürr H, Flaus A, Owen-Hughes T, Hopfner KP. Snf2 family ATPases and DExx box helicases: differences and unifying concepts from high-resolution crystal structures. Nucleic Acids Res. 2006; 34(15): 4160-7. Epub 2006 Aug 25.

Eisen, J.A., Sweder, K.S. and Hanawalt, P.C. (1995) Evolution of the SNF2 family of proteins: subfamilies with distinct sequences and functions. Nucleic Acids Res., 23, 2715–2723.

Flaus, A. and Owen-Hughes, T. (2001) Mechanisms for ATP-dependent chromatin remodelling. Curr. Opin. Genet. Dev., 11, 148–154.

Flaus, A., Martin, D.M., Barton, G.J. and Owen-Hughes, T. (2006) Identification of multiple distinct Snf2 subfamilies with conserved structural motifs. Nucleic Acids Res., 34, 2887–2905.

Gangavarapu V, Haracska L, Unk I, Johnson RE, Prakash S, Prakash L. Mms2-Ubc13-dependent and -independent roles of Rad5 ubiquitin ligase in postreplication repair and translesion DNA synthesis in *Saccharomyces cerevisiae*. Mol Cell Biol. 2006 Oct; 26(20): 7783-90.

Greider, C. W., and Blackburn, E. H. (1985). Identification of a specific telomere terminal transferase activity in *Tetrahymena* extracts. Cell 43, 405–413.

Hoege C, Pfander B, Moldovan GL, Pyrowolakis G, Jentsch S. RAD6-dependent DNA repair is linked to modification of PCNA by ubiquitin and SUMO. Nature. 2002 Sep 12; 419(6903): 135-41.

Iyer LM, Babu MM, Aravind L. The HIRAN domain and recruitment of chromatin remodeling and repair activities to damaged DNA. Cell Cycle. 2006 Apr; 5(7): 775-82.

Krijger PH, van den Berk PC, Wit N, Langerak P, Jansen JG, Reynaud CA, de Wind N, Jacobs H. PCNA ubiquitination-independent activation of polymerase η during somatic hypermutation and DNA damage tolerance. DNA Repair (Amst). 2011 Oct 10; 10(10): 1051-9. doi: 10.1016/j.dnarep.2011.08.005.

Kumar R, Whitehurst CB, Pagano JS. The Rad6/18 ubiquitin complex interacts with the Epstein-Barr virus deubiquitinating enzyme, BPLF1, and contributes to virus infectivity. J Virol. 2014 Jun; 88(11): 6411-22. doi: 10.1128/JVI.00536-14.

Le May N, Egly JM, Coin F. True Lies: The Double Life of the Nucleotide Excision Repair Factors in Transcription and DNA Repair J Nucleic Acids. 2010 Jul 25. pii: 616342.

Lee KY, Myung K. PCNA modifications for regulation of post-replication repair pathways. Mol Cells. 2008 Jul 31; 26(1): 5-11. Epub 2008 Jun 4. Review.

Lehmann AR, Fuchs RP. Gaps and forks in DNA replication: Rediscovering old models. DNA Repair (Amst). 2006 Dec 9; 5(12): 1495-8.

Lehmann AR, Niimi A, Ogi T, Brown S, Sabbioneda S, Wing JF, Kannouche PL, Green CM. Translesion synthesis: Y-family polymerases and the polymerase switch. DNA Repair (Amst). 2007 Jul 1; 6(7): 891-9. Epub 2007 Mar 23. Review.

Li Y, Zhou Z, Chen C. WW domain-containing E3 ubiquitin protein ligase 1 targets p63 transcription factor for ubiquitin-mediated proteasomal degradation and regulates apoptosis. Cell Death Differ. 2008 Dec; 15(12): 1941-51. doi: 10.1038/cdd.2008.134.

Limoli CL, Giedzinski E, Bonner WM, Cleaver JE. UV-induced replication arrest in the xeroderma pigmentosum variant leads to DNA double-strand breaks, gamma-H2AX formation, and Mre11 relocalization. Proc Natl Acad Sci U S A. 2002 Jan 8; 99(1): 233-8.

Lin JR, Zeman MK, Chen JY, Yee MC, Cimprich KA. SHPRH and HLTF act in a damage-specific manner to coordinate different forms of postreplication repair and prevent mutagenesis. Mol Cell. 2011 Apr 22; 42(2): 237-49. doi: 10.1016/j.molcel.2011.02.026.

Lukin M, de Los Santos C. NMR structures of damaged DNA. Chem Rev. 2006 Feb; 106(2): 607-86.

McGrath JP, Jentsch S, Varshavsky A. UBA 1: an essential yeast gene encoding ubiquitin-activating enzyme. EMBO J. 1991 Jan; 10(1): 227-36.

Motegi A, Liaw HJ, Lee KY, Roest HP, Maas A, Wu X, Moinova H, Markowitz SD, Ding H, Hoeijmakers JH, Myung K. Polyubiquitination of proliferating cell nuclear antigen by HLTF and SHPRH prevents genomic instability from stalled replication forks. Proc Natl Acad Sci U S A. 2008 Aug 26; 105(34): 12411-6. doi: 10.1073/pnas.0805685105.

Nouspikel T. DNA repair in mammalian cells : Nucleotide excision repair: variations on versatility. Cell Mol Life Sci. 2009 Mar; 66(6): 994-1009. doi: 10.1007/s00018-009-8737-y. Review.

Orias E, Newby CJ. Macronuclear genetics of *Tetrahymena*. II. Macronuclear location of somatic mutations to cycloheximide resistance. Genetics. 1975 Jun; 80(2): 251-62.

Rajagopalan,V., Subramanian, A.,Wilkes,D. E., Pennock,D. G., and Asai,D. J. (2009). Dynein-2 affects the regulation of ciliary length but is not required for ciliogenesis in *Tetrahymena thermophila*. Mol. Biol. Cell. 20, 708–720.

Satoh MS, Jones CJ, Wood RD, Lindahl T. DNA excision-repair defect of xeroderma pigmentosum prevents removal of a class of oxygen free radical-induced base lesions. Proc Natl Acad Sci U S A. 1993 Jul 1; 90(13): 6335-9.

Shuck SC, Short EA, Turchi JJ. Eukaryotic nucleotide excision repar: from understanding mechanisms to influencing biology. Cell Res. 2008 Jan; 18(1): 64-72. Review

Sinha RP, Häder DP. UV-induced DNA damage and repair: a review. Photochem Photobiol Sci. 2002 Apr; 1(4): 225-36. Review.

Smirnova M, Klein HL. Role of the error-free damage bypass postreplication repair pathway in the maintenance of genomic stability. Mutat Res. 2003 Nov 27; 532(1-2): 117-35. Review.

Strahl, B.D., Ohba, R., Cook, R. G., and Allis, C.D. (1999). Methylation of histone H3 at lysine 4 is highly conserved and correlates with transcriptionally active nuclei in *Tetrahymena*. Proc. Natl. Acad. Sci.U.S.A. 96, 14967–14972.

Sugai T, Hiwatashi K. Cytologic and autoradiographic studies of the micronucleus at meiotic prophase in *Tetrahymena pyriformis*. J Protozool. 1974 Oct; 21(4): 542-8.

Sun L, Chen ZJ. The novel functions of ubiquitination in signaling. Curr Opin Cell Biol. 2004 Apr; 16(2): 119-26.

Tapias A, Auriol J, Forget D, Enzlin JH, Schärer OD, Coin F, Coulombe B, Egly JM. Ordered conformational changes in damaged DNA induced by nucleotide excision repair factors. J Biol Chem. 2004 Apr 30; 279(18): 19074-83.

Wang TC, Smith KC. Postreplication repair in ultraviolet-irradiated human fibroblasts: formation and repair of DNA double-strand breaks. Carcinogenesis. 1986 Mar; 7(3): 389-92.

Yao MC, Blackburn E, Gall JG. Amplification of the rRNA genes in *Tetrahymena*. Cold Spring Harb Symp Quant Biol. 1979;43 Pt 2:1293-6.

Zhao GY, Sonoda E, Barber LJ, Oka H, Murakawa Y, Yamada K, Ikura T, Wang X, Kobayashi M, Yamamoto K, Boulton SJ, Takeda S. A critical role for the ubiquitin-conjugating enzyme Ubc13 in initiating homologous recombination. Mol Cell. 2007 Mar 9; 25(5): 663-75.

APPENDICES

Appendix A. *Tetrahymena* Strains, PCR Primers, and shRNA Constructs

Genotypes and phenotypes for the various *Tetrahymena thermophila* strains utilized in this work are listed in Appendix A1. The genotype for the CU522NC strain remains unknown, as does the exact nature of the mutation that led to Paclitaxel resistance. This is due to the fact that the strain spontaneously developed the drug resistance but was shown to lack an inserted product like the other drug resistance strains which carried the shRNA knockdown constructs.

The PCR primers utilized throughout this work are listed in Appendix A2 and sorted by DNA or RNA target. In all instances, both a forward and reverse primer are listed, and the subsequent annealing temperature was calculated by multiplying the number of A or T bases by two, multiplying the number of G or C bases by three, and adding the two numbers together. When annealing temperatures were not identical, the two temperatures were averaged to determine a usable temperature in between the two optimal annealing temperatures.

Constructs for the shRNA knockdowns are seen in Appendices A3-5, each construct was identical in the blue and black areas, while the segment in red is the variable region that targets the specific mRNA molecules. Each red segment is expanded and shown in nucleotides, with the black nucleotides representing either the loop of the shRNA, or the sites on either end used for ligating the insert into the vector.

Appendix A1: *Tetrahymena* Strains

Name	Genotype	Phenotype	Description
CU522	MIC: *mpr1-1/mpr1-1, btu1-1::btu1-1M350K/btu1-1::btu1-1M350K* MAC: *btu1-1::btu1-1M350K*	6-methylpurine resistant, paclitaxel sensitive, vinblastine resistant	*BTU1* mutant used for transformation of shRNA knockdown constructs
CU428	MIC: *mpr1-1/mpr1-1*	6-methylpurine resistance	Used as a WT strain for expression profiles
CU522NC	MIC: *mpr1-1/mpr1-1, btu1-1::btu1-1M350K/btu1-1::btu1-1M350K* MAC: *btu1-1::btu1-1M350K*^{NC*}	6-methylpurine, paclitaxel, vinblastine resistant	Used as a WT control for shRNA expression profiles and survivability
shRNA-*RAD16*	MAC: *btu1-1M350K::shRNA-RAD16*	Paclitaxel resistant	Knockdown of *RAD16NH* by short-hairpin RNA, under the *BTU1* promoter, CU522 background
shRNA-*RAD5.1*	MAC: *btu1-1M350K::shRNA-RAD5.1*	Paclitaxel resistant	Knockdown of *RAD5.1* by short-hairpin RNA, under the *BTU1* promoter, CU522 background
shRNA-*RAD5.2*	MAC: *btu1-1M350K::shRNA-RAD5.2*	Paclitaxel resistant	Knockdown of *RAD5.2* by short-hairpin RNA, under the *BTU1* promoter, CU522 background

* Sequence of MAC mutation resulting in drug resistance unknown at this time

Appendix A2: PCR Primers

Target	Primer Sequence (5'-3')
RAD16NH	Forward: CTCCACGAAGAAATGAACACACTT Reverse: TATGTGAATCTTGTTGCCTTCTTTCG
RAD16.1	Forward: TAGAGGAAGCTGGAAACAGTAATCC Reverse: AATCTGCCAACACCTTTAGAGAGAG
RAD5.1	Forward: CTATTCCAGCCATACTTACACCAATA Reverse: GAAGGAATGAATGAGAAAAGAGGTCC
RAD5.2	Forward: ATTTACCATCTATCTTGAGACGCCC Reverse: GAGGTTTTGCAGTATAACTTTGAGGA
BTU1	Forward: GATAGAATCATGGAAACCTTCTC Reverse: CAAGTGGTTAAGATCACCATAAG
ACT1	Forward: TGAATTAAAGGCTTACAAGGAATC Reverse: CACACTTCATGATAGAGTTGAAGG
HHP1	Forward: GGAAAGGCTACTCTCTCAAATAAG Reverse: TTTAGGAGTAGATTTAGGATTAGATGC
shRNA Confirmation	Forward: ATGAATGATATAAATGAAGAGTGGC Reverse: TGTTATGTGAATGAAGTTAATTGGG
shRNA Hairpin	Forward: TTAAAAAATGGCAAGCTTCGCGAG Reverse: CGATTCAGTTCCGAGATCTCACC

A

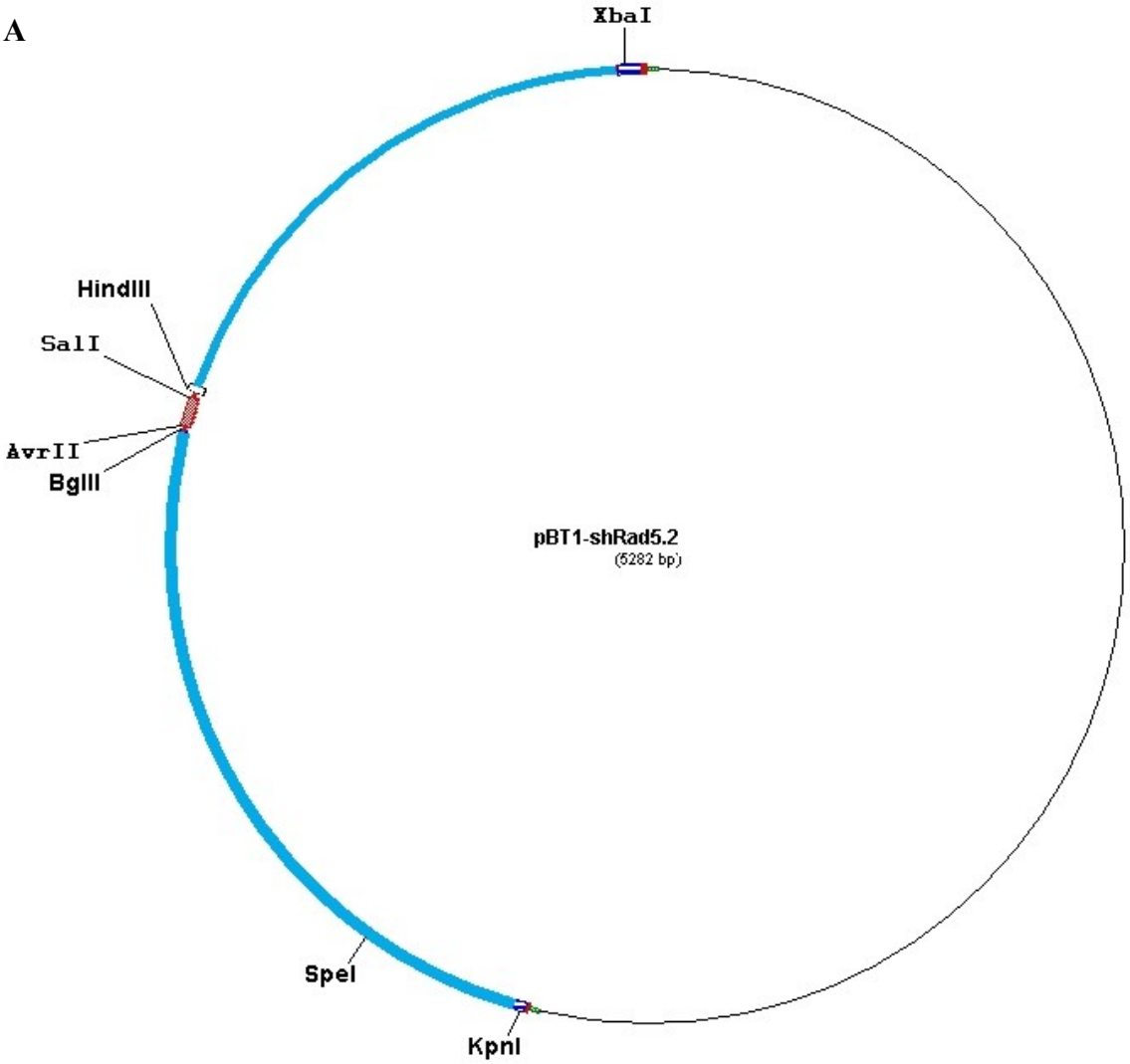

B

5′-CTAGGGGGCATGATGGACTTATTTTCTCGAGTAAATAAGTCCATCATGCCCG-3′

3′-CCCCGTACTACCTGAATAAAAGAGCUCATTTATTCAGGTAGTACGGGCAGCT-5′

Appendix A3: Plasmid Map and Sequence of the Rad5.2 Knockdown Construct. A) Plasmid map of pBT1-shRad5.2, the red denotes the specific small hairpin RNA (shRNA) sequence while the blue represents the *btu1-1* target recombination sequence, and black represents the plasmid backbone. B) Sequence for the shRad5.2 knockdown, red sequence is either identical or complimentary to the genomic sequence for Rad5.2, the black sequence in the middle represents the defined loop sequence while the black nucleotides at the end are the specific overhangs used to ligate the construct into the vector.

A

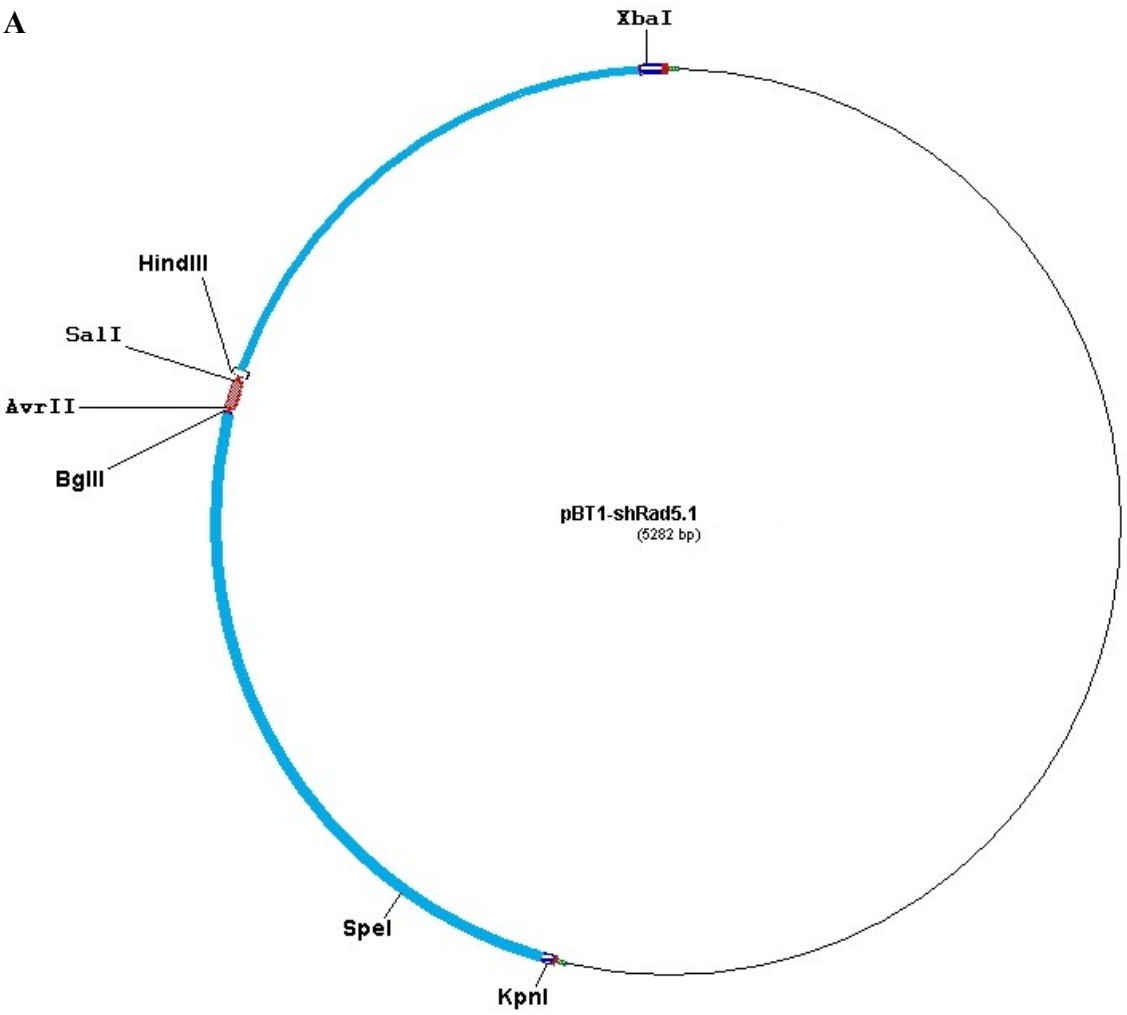

B

5′-CTAGGGCTGGTGCATTTGGTCTAATCTCGAGTTTAGACCAAATGCACCAGCG-3′

3′-CCGACCACGTAAACCAGATTAGAGCUCAAATCTGGTTTACGTGGTCGCAGCT-5′

Appendix A4: Plasmid Map and Sequence of the Rad5.1 Knockdown Construct. A) Plasmid map of pBT1-shRad5.1, the red denotes the specific small hairpin RNA (shRNA) sequence while the blue represents the *btu1-1* target recombination sequence, and black represents the plasmid backbone. B) Sequence for the shRad5.1 knockdown, red sequence is either identical or complimentary to the genomic sequence for Rad5.1, the black sequence in the middle represents the defined loop sequence while the black nucleotides at the end are the specific overhangs used to ligate the construct into the vector.

A

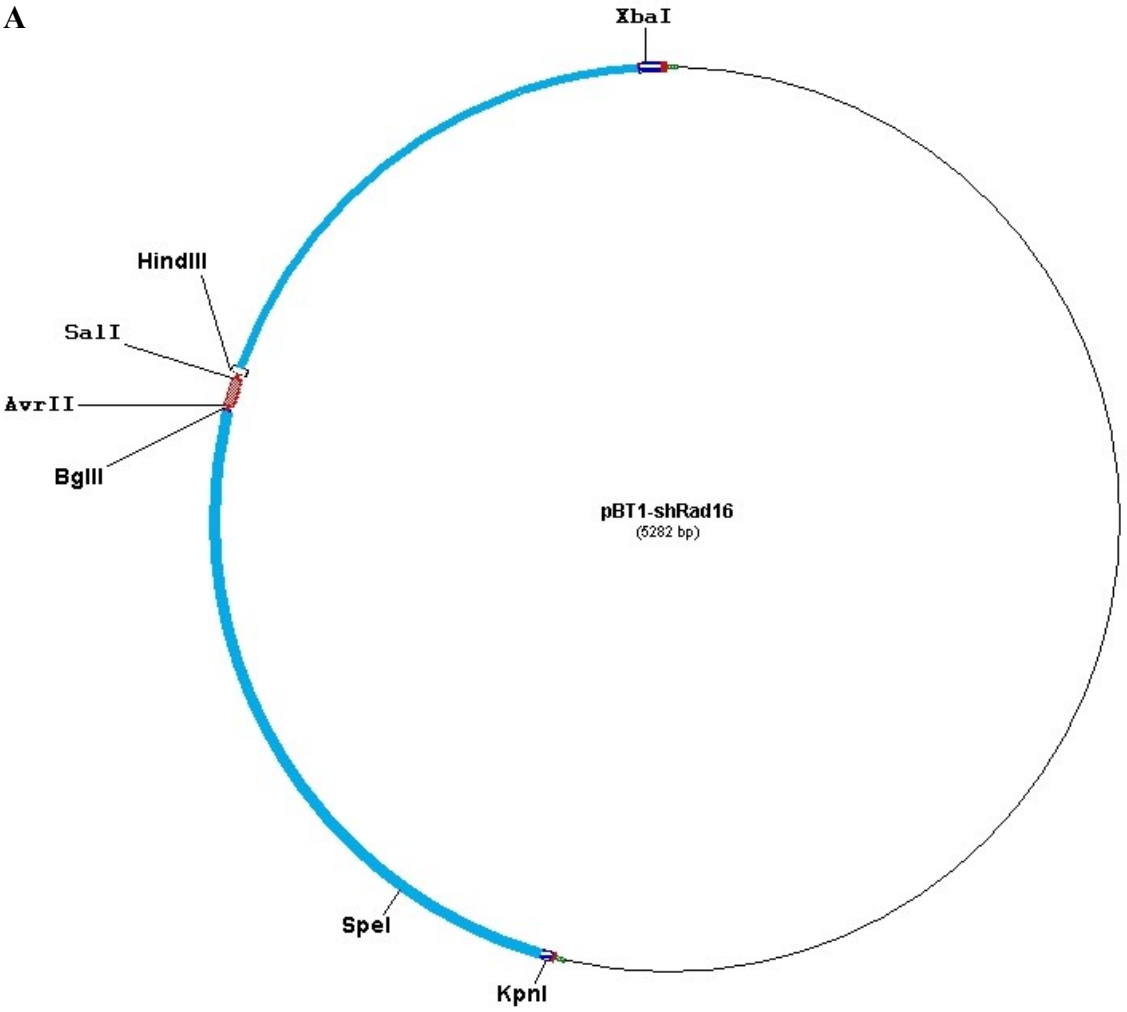

B

5′-CTAGGGCGCCTTGTAAACGACATTTCTCGAGTAATGTCGTTTACAAGGCGCG-3′

3′-CCGCGGAACATTTGCTGTAAAGAGCUCATTACAGCAAATGTTCCGCGCAGCT-5′

Appendix A5: Plasmid Map and Sequence of the Rad16NH Knockdown Construct. A) Plasmid map of pBT1-shRad16, the red denotes the specific small hairpin RNA (shRNA) sequence while the blue represents the *btu1-1* target recombination sequence, and black represents the plasmid backbone. B) Sequence for the shRad16NH knockdown, red sequence is either identical or complimentary to the genomic sequence for Rad16NH, the black sequence in the middle represents the defined loop sequence while the black nucleotides at the end are the specific overhangs used to ligate the construct into the vector.

.

Appendix B. qRT-PCR Confirmation

In order to verify the success of the qRT-PCR, a representative sample was taken after qRT-PCR from each condition and the samples were analyzed via agarose gel electrophoresis. In each instance a gDNA control was also run on the gel to allow for a comparison of size for the cDNA products versus the gDNA products. This allowed for a determination of any potential gDNA contamination in samples. The melt peaks for an average of three (for BTU1) or five (all other samples) different qPCR runs were graphed as well. Different peaks would indicate multiple qRT-PCR products and the potential of gDNA contamination. Appendix B1 shows both the melt peaks and the gel electrophoresis of all BTU1 PCR products. There is no significant size variation between any of the BTU1 samples, with the exception of the gDNA, and there are only single melt peaks present. These data strongly suggest that only a single product is being made from cDNA and not from gDNA.

Appendix B2 shows similar results for the qRT-PCR of the shRNA hairpins, with similar sizes and consistent melt peaks between all samples tested. This indicates that only a single product was made, and that this product was consistent across strains, as it should have been. Appendix B3 shows the melt peak results for the Rad16.1 expression profiles, with consistent single peaks present. While Appendix B4 confirms these results with consistently sized products displayed on the agarose gel. Appendix B5 shows the melt peaks for all of the Rad5.1 targeted samples. In all instances the products maintain a single melt peak, which is indicative of a single PCR product. When looking at the gel electrophoresis in Appendix B6 there is a clear abundance of products which are the same size, with the only deviation being seen in the expression profile samples related to zero

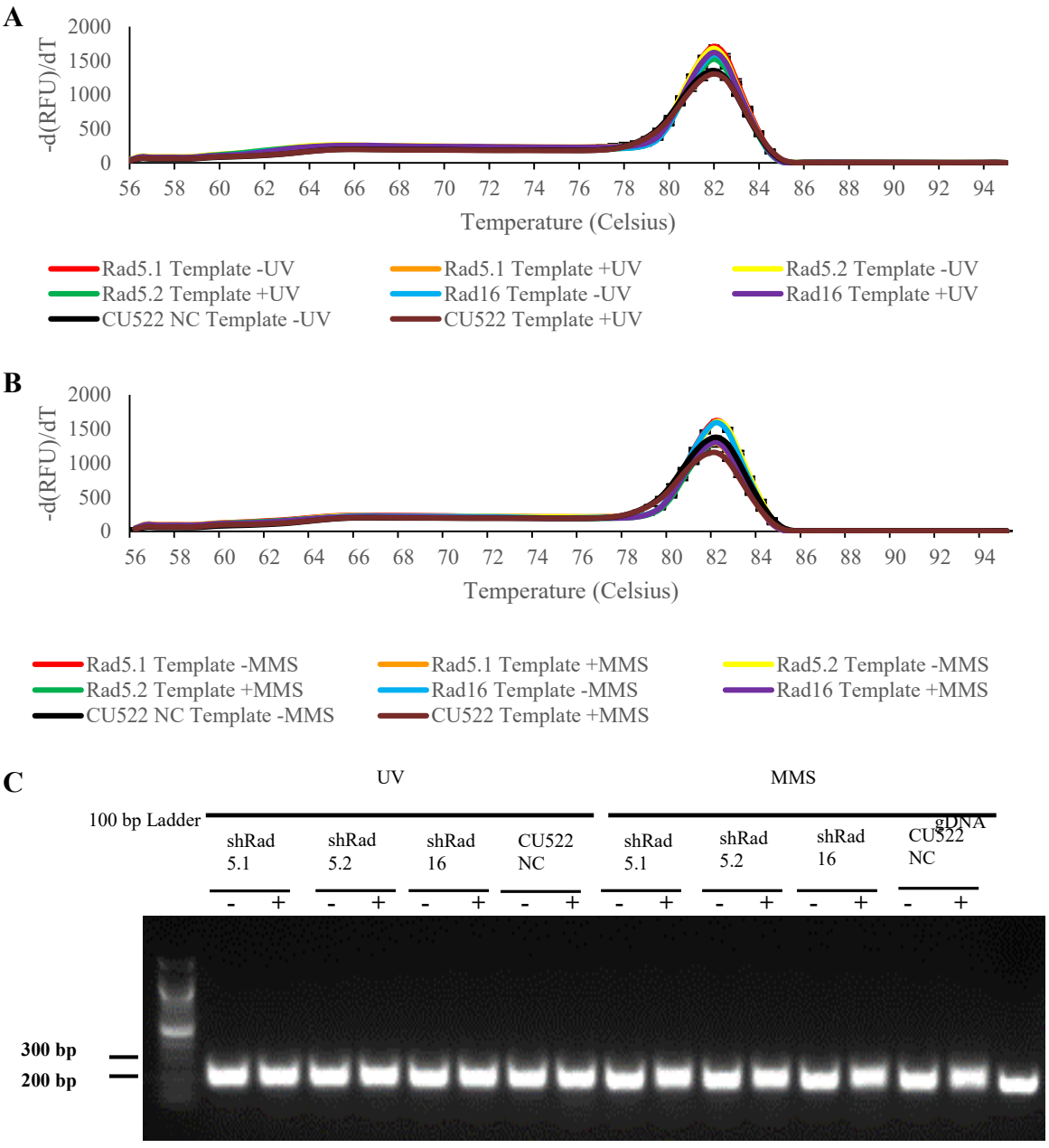

Appendix B1: qPCR Melt Peaks and Products for BTU1. Values for melting point of the products after the completion of qPCR were taken by the BioRad Mj mini Personal thermocycler and the resulting data points were taken for three trials and averages were graphed to display the melt peaks. Error bars represent ± SEM for the three trials A) Melting temperatures of BTU1 qPCR products in the shRNA strains two hours after treatment with 100 J/m^2 UV or mock treatment as indicated. B) Melting temperatures of BTU1 qPCR products in the shRNA strains three hours after treatment with 20 mM MMS or mock treatment as indicated. C) Representative qPCR samples were analyzed by agarose gel electrophoresis along with a genomic DNA (gDNA) control to confirm the presence of products as indicated by the melt peaks.

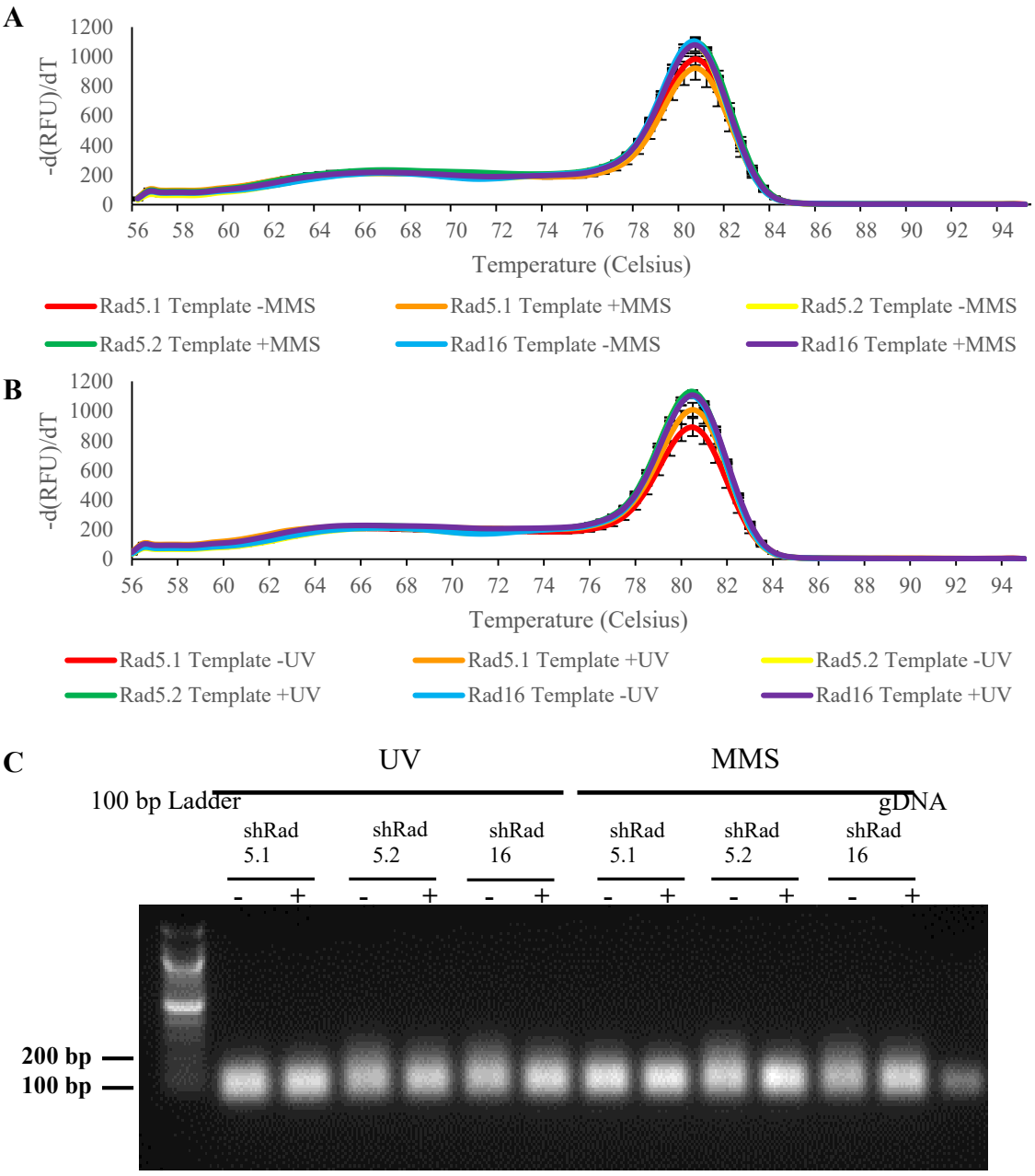

Appendix B2: qPCR Melt Peaks and Products for the shRNA Hairpin. Values for melting point of the products after the completion of qPCR were taken by the BioRad Mj mini Personal thermocycler and the resulting data points were taken for five trials and averages were graphed to display the melt peaks. Error bars represent ± SEM for the five trials A) Melting temperatures of the shRNA hairpin qPCR products in the shRNA strains two hours after treatment with 100 J/m^2 UV or mock treatment as indicated. B) Melting temperatures of the shRNA hairpin qPCR products in the shRNA strains three hours after treatment with 20 mM MMS or mock treatment as indicated. C) Representative qPCR samples were analyzed by agarose gel electrophoresis along with a genomic DNA (gDNA) control to confirm the presence of products as indicated by the melt peaks.

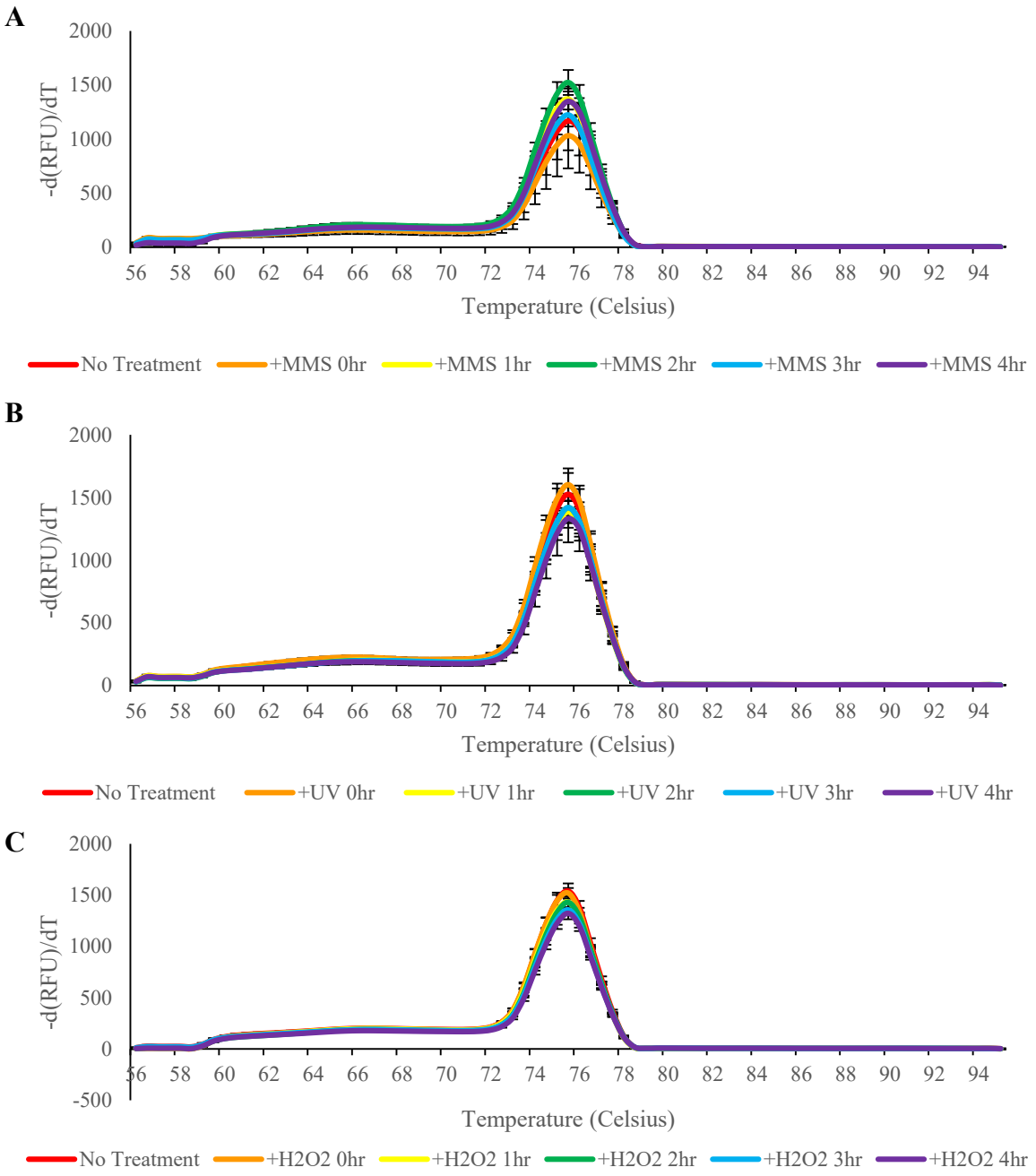

Appendix B3: qPCR Melt Peaks for Rad16.1 Expression Profiles. Values for melting point of the products after the completion of qPCR were taken by the BioRad Mj mini Personal thermocycler and the resulting data points were taken for five trials and averages were graphed to display the melt peaks. A) Melting temperatures of the Rad16.1 qPCR products in the CU428 strain after treatment with 20 mM MMS or mock treatment as indicated. B) Melting temperatures of the Rad16.1 qPCR products in the CU428 strain after treatment with 100 J/m^2 UV or mock treatment as indicated. C) Melting temperatures of the Rad16.1 qPCR products in the CU428 strain after treatment with 10 mM H_2O_2 or mock treatment as indicated. Error bars represent ± SEM for the five trials.

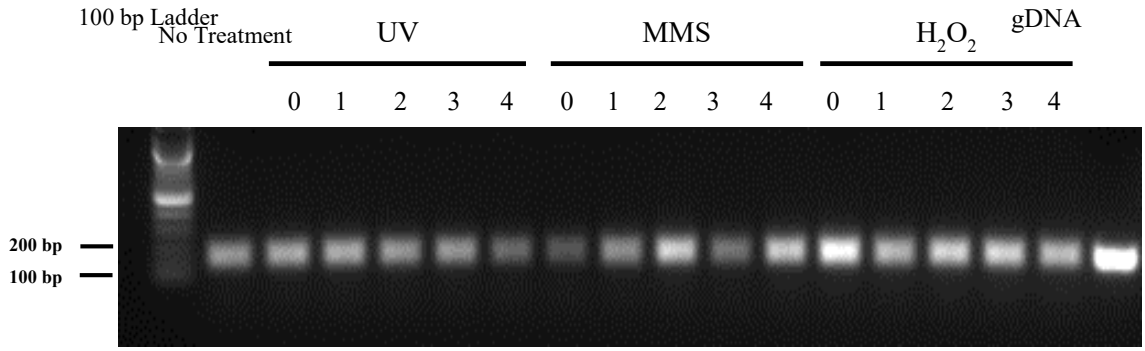

Appendix B4: Rad16.1 qPCR Products. Representative qPCR samples from the CU428 expression profiles for Rad16.1 were analyzed along with a genomic DNA (gDNA) control by agarose gel electrophoresis to confirm the presence of products as indicated by the qPCR data.

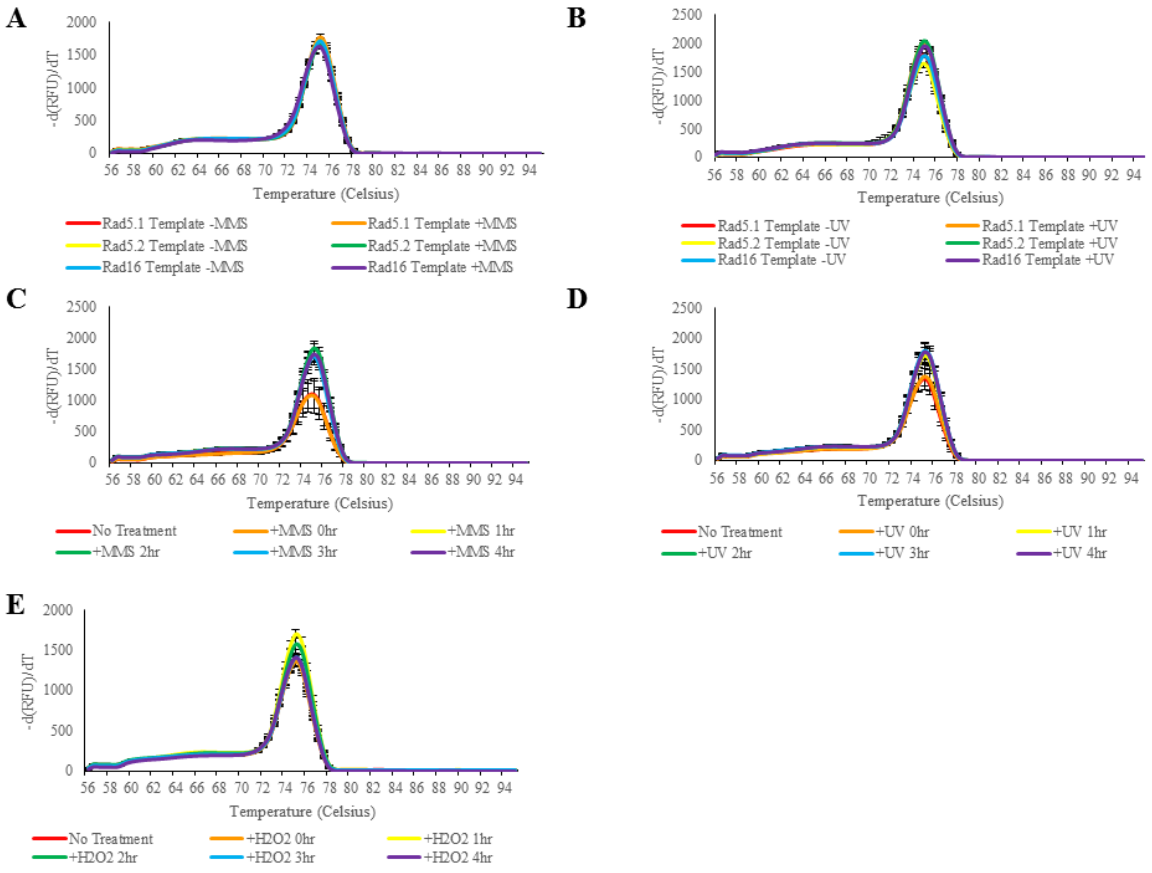

Appendix B5: qPCR Melt Peaks for Rad5.1 Expression Profiles. Values for melting point of the products after the completion of qPCR were taken by the BioRad Mj mini Personal thermocycler and the average of five trials was graphed to display the melt peaks. A) Melt peaks of the Rad5.1 qPCR products in the shRNA strains two hours after treatment with 100 J/m^2 UV or mock treatment as indicated. B) Melt peaks of the Rad5.1 qPCR products in the shRNA strains three hours after treatment with 20 mM MMS or mock treatment as indicated. C) Melt peaks of the Rad5.1 qPCR products in the CU428 (WT) strain after treatment with 20 mM MMS or mock treatment as indicated. D) Melt peaks of the Rad5.1 qPCR products in the WT strain after treatment with 100 J/m^2 UV or mock treatment as indicated. E) Melt peaks of the Rad5.1 qPCR products in the WT strain after treatment with 10 mM H_2O_2 or mock treatment as indicated. Error bars represent ± SEM for the five trials.

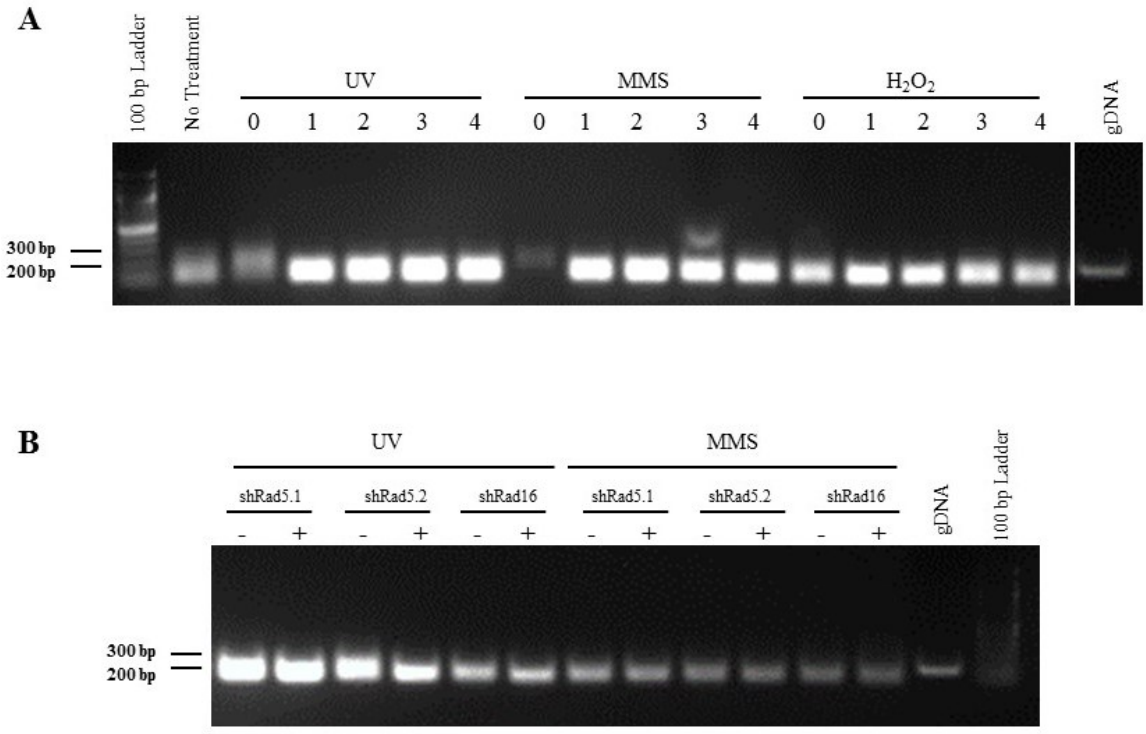

Appendix B6: Rad5.1 qPCR Products. A) Representative qPCR samples from the CU428 expression profiles were analyzed along with a genomic DNA (gDNA) control by agarose gel electrophoresis to confirm the presence of products as indicated by the qPCR data. B) Representative qPCR samples from the indicated shRNA knockdown strains two hours after treatment with 100 J/m^2 UV, three hours after treatment with 20 mM MMS, or mock treated at the same timepoints.

hours after UV treatment, and at zero and three hours after MMS treatment. In all instances there is a varying amount of product seen at the cDNA size, with a separate product seen slightly higher and closer to the gDNA size. However, these cDNA samples did not show gDNA contamination in any other qRT-PCR, and so it is likely that these larger bands are different isoforms of the same mRNA that contains a different set of introns and exons.

The melt peak results for Rad5.2 products are shown in Appendix B7, in most instances there is a single peak, however there is a consistent second peak at the no treatment points which become a more dulled second peak at zero hours, before disappearing at one hour after treatment. The gel in Appendix B8 confirms these results, as two bands are clearly seen at no treatment. While two more blurry bands are seen at zero hours after treatment. These results are indicative of two products, but again, the same samples did not show gDNA contamination when looking for other targets. It is more likely that there are two different isoforms of Rad5.2 made during the normal cell cycle and that after damage one version is preferred.

Appendices B9 and B10 show the results for the Rad16NH qRT-PCR products. While almost all of the melt peaks are largely consistent (with exceptions matching the following gel loaded samples) there are some variations in the three and four hour samples after MMS and at the one hour sample after hydrogen peroxide. Again, these templates were the same ones that were used for all of the other qRT-PCR experiments, which lacked gDNA contamination at these specific timepoints. It is more likely that another isoform of Rad16NH exists, and that the specific isoform is favored under those conditions, although the exact sequence of these remain a mystery as do their purposes.

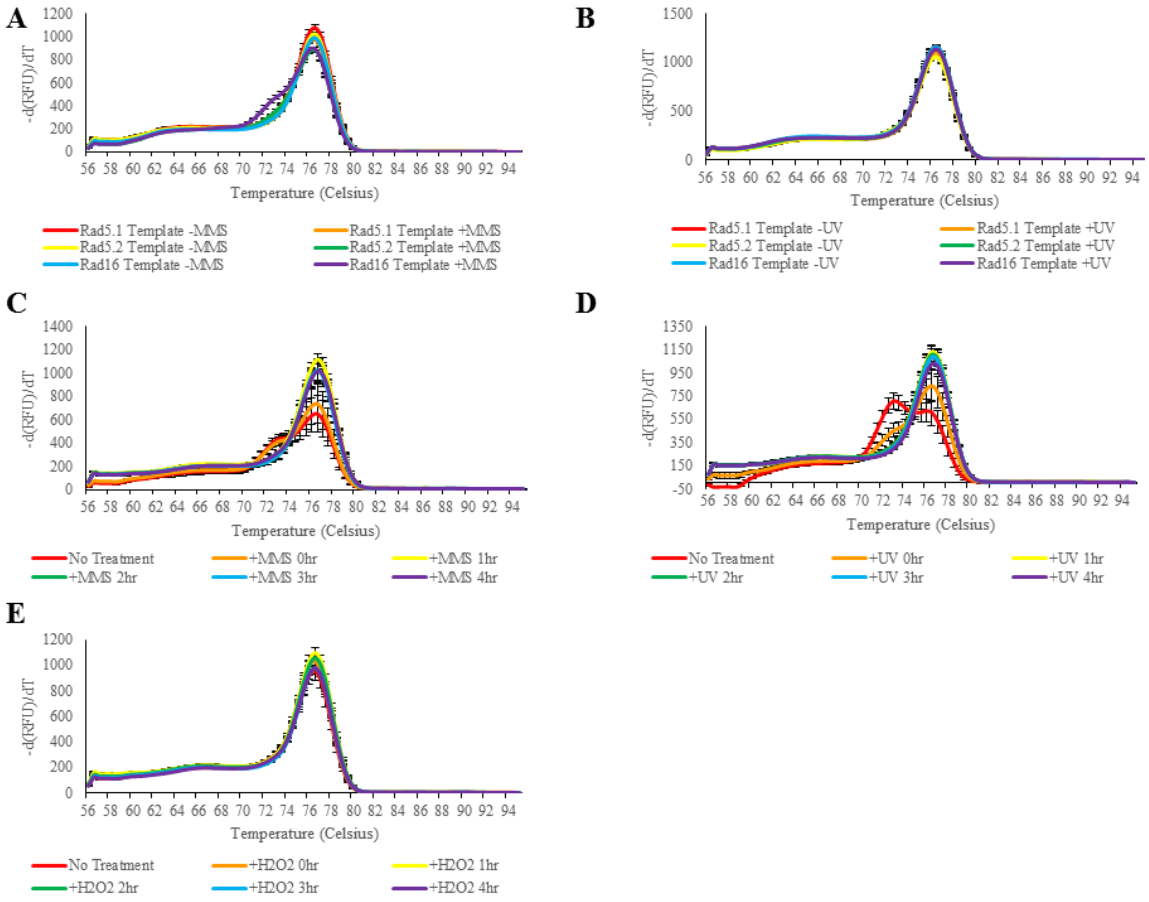

Appendix B7: qPCR Melt Peaks for Rad5.2 Expression Profiles. Values for melting point of the products after the completion of qPCR were taken by the BioRad Mj mini Personal thermocycler and the average of five trials was graphed to display the melt peaks. A) Melt peaks of the Rad5.2 qPCR products in the shRNA strains two hours after treatment with 100 J/m^2 UV or mock treatment as indicated. B) Melt peaks of the Rad5.2 qPCR products in the shRNA strains three hours after treatment with 20 mM MMS or mock treatment as indicated. C) Melt peaks of the Rad5.2 qPCR products in the CU428 (WT) strain after treatment with 20 mM MMS or mock treatment as indicated. D) Melt peaks of the Rad5.2 qPCR products in the WT strain after treatment with 100 J/m^2 UV or mock treatment as indicated. E) Melt peaks of the Rad5.2 qPCR products in the WT strain after treatment with 10 mM H_2O_2 or mock treatment as indicated. Error bars represent ± SEM for the five trials.

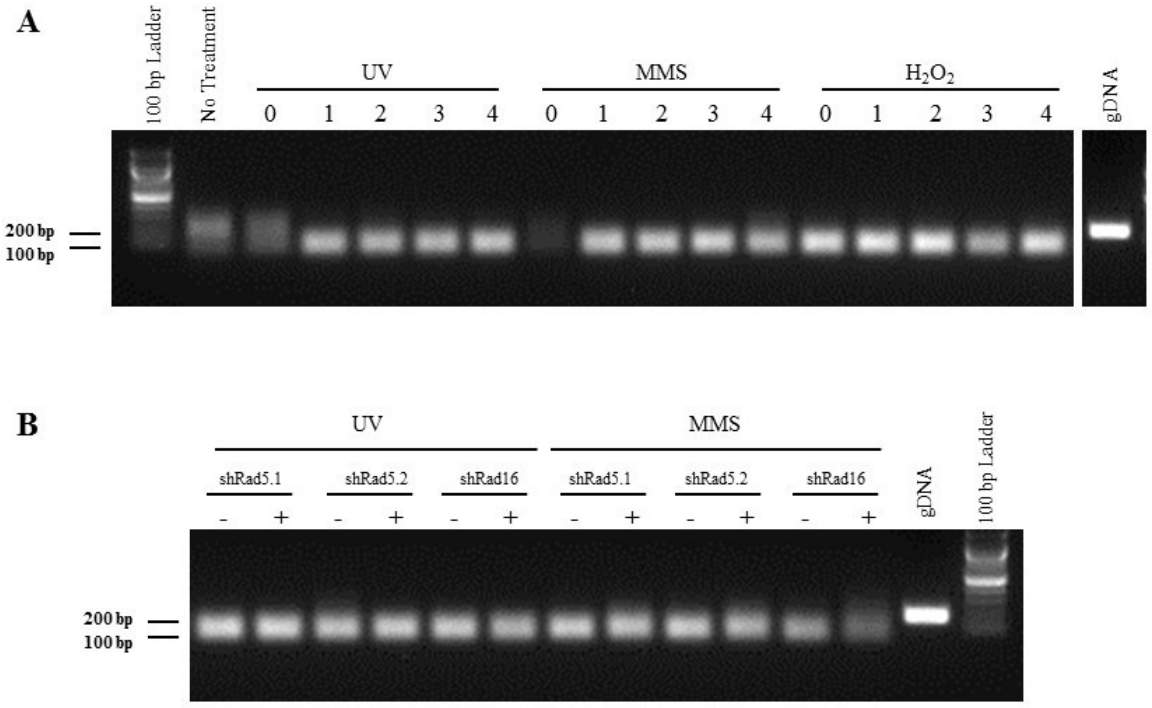

Appendix B8: Rad5.2 qPCR Products. A) Representative qPCR samples from the CU428 expression profiles were analyzed along with a genomic DNA (gDNA) control by agarose gel electrophoresis to confirm the presence of products as indicated by the qPCR data. B) Representative qPCR samples from the indicated shRNA knockdown strains two hours after treatment with 100 J/m^2 UV, three hours after treatment with 20 mM MMS, or mock treated at the same timepoints.

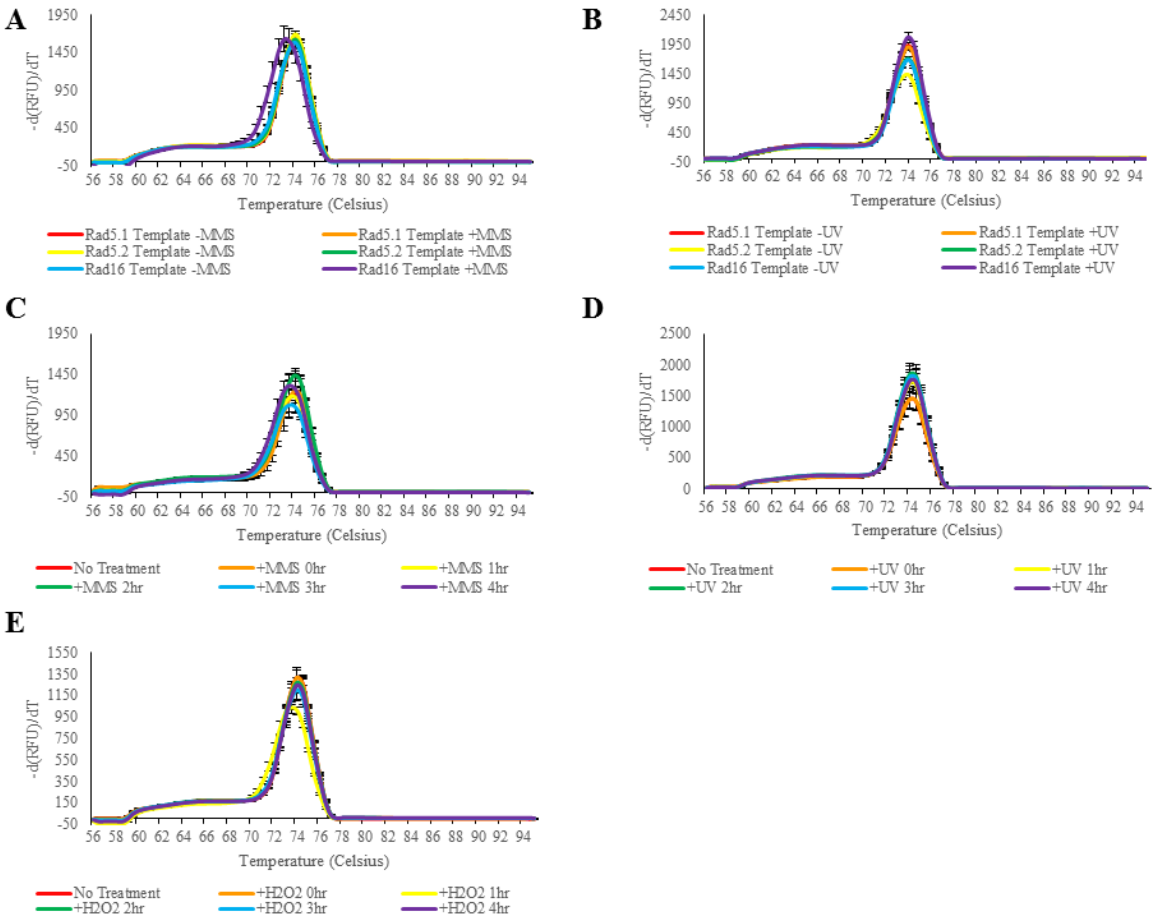

Appendix B9: qPCR Melt Peaks for Rad16NH Expression Profiles. Values for melting point of the products after the completion of qPCR were taken by the BioRad Mj mini Personal thermocycler and the average of five trials was graphed to display the melt peaks. A) Melt peaks of the Rad16NH qPCR products in the shRNA strains two hours after treatment with 100 J/m^2 UV or mock treatment as indicated. B) Melt peaks of the Rad16NH qPCR products in the shRNA strains three hours after treatment with 20 mM MMS or mock treatment as indicated. C) Melt peaks of the Rad16NH qPCR products in the CU428 (WT) strain after treatment with 20 mM MMS or mock treatment as indicated. D) Melt peaks of the Rad16NH qPCR products in the WT strain after treatment with 100 J/m^2 UV or mock treatment as indicated. E) Melt peaks of the Rad16NH qPCR products in the WT strain after treatment with 10 mM H_2O_2 or mock treatment as indicated. Error bars represent ± SEM for the five trials.

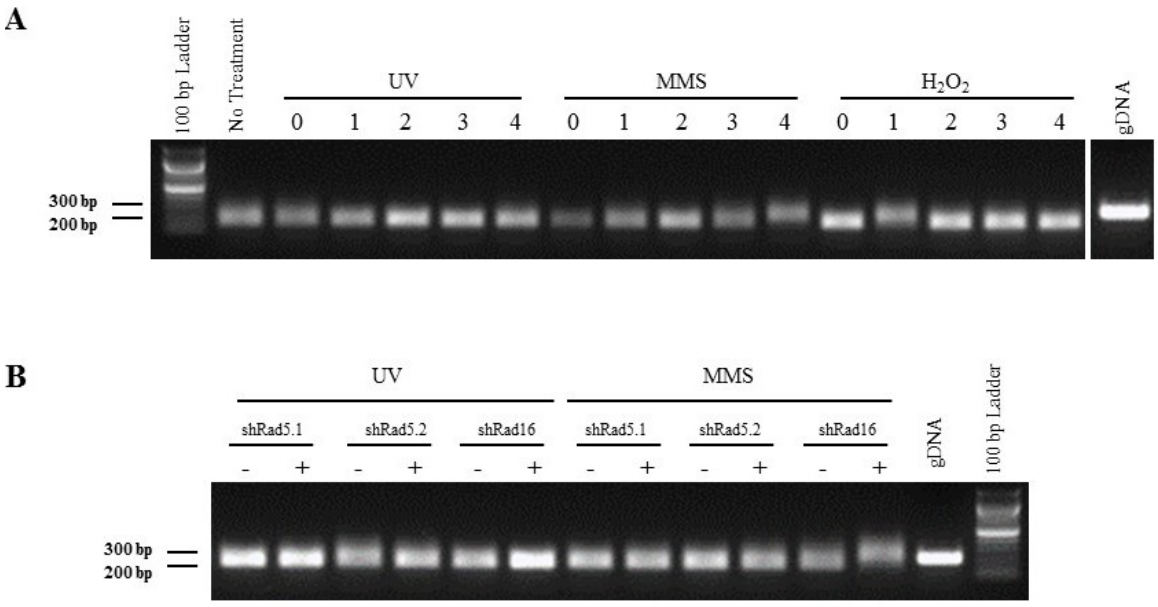

Appendix B10: Rad16NH qPCR Products. A) Representative qPCR samples from the CU428 expression profiles were analyzed along with a genomic DNA (gDNA) control by agarose gel electrophoresis to confirm the presence of products as indicated by the qPCR data. B) Representative qPCR samples from the indicated shRNA knockdown strains two hours after treatment with 100 J/m^2 UV, three hours after treatment with 20 mM MMS, or mock treated at the same timepoints.

Appendix C. *In vitro* NER Assay

To assess the efficacy of nucleotide excision repair (NER) in the different knockdown strains an *in vitro* NER assay was developed. A portion of the BTU1 gene was amplified by PCR from *Tetrahymena* genomic DNA and utilized as the repair substrate for this assay. The PCR fragment (1.7 kb) contained a single Ase1 restriction site (ATTAAT) at approximately 1.1 kb into the sequence. Samples were treated with $AgNO_3$ for 30, 60, or 120 minutes prior to exposure to 254 nm UV light at doses of 0, 50, 100, 200, or 400 j/m^2. The samples were then treated with Ase1, or mock treated, for 30 minutes prior to visualization by agarose gel electrophoresis (Appendix C1).

The percentage of digested substrate, represented by one fragment at approximately 0.6 kb and another at approximately 1.1 kb, were compared to the amount of the undigested product at 1.7 kb. The intensities of the bands were measured and their percentages of the total intensity of all bands in the well were graphed. When compared to untreated samples there was a visually significant increase in the amount of undigested product after treatment with 50 j/m^2 of UV. The percentage of undigested product continued to increase up to approximately 45% of the total product in the lane. In mock digested samples no abnormalities were seen in the banding size of the substrate on the gel when compared to the untreated sample, regardless of UV dosage.

Analysis of the effects of repetitive treatment with 50 j/m^2 (leading to a total of 600 j/m^2) were also conducted (Appendix C2), and the results were similar to those from the direct treatment with higher doses of UV.

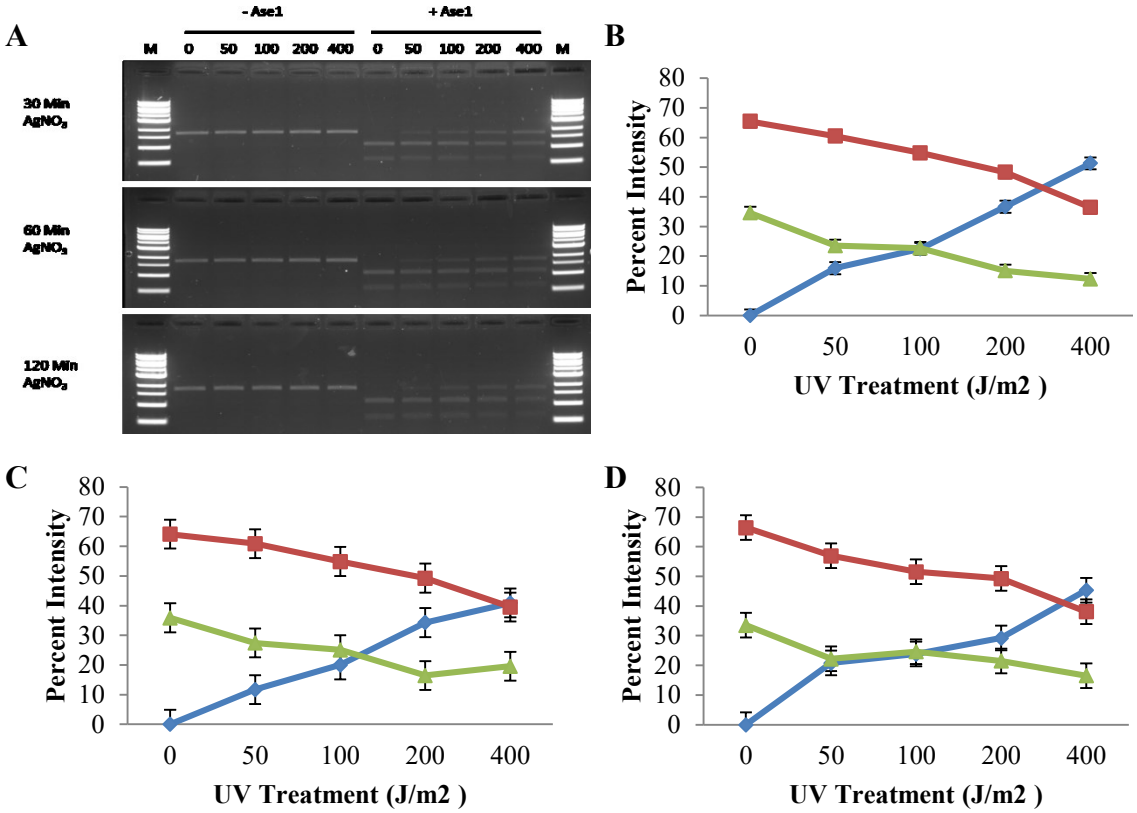

Appendix C1: Inhibition of Ase1 Digestion by UV Damage**.** A) Agarose gel electrophoresis of UV treated 100 ng of BTU1 gene fragment. UV dosages and +/- Ase1 treatment conditions above images and time of $AgNO_3$ treatment listed to the left of images. B) Graphical representation of the intensity of bands for the 30 minute $AgNO_3$ treatment. C) Graphical representation of the intensity of bands for the 60 minute $AgNO_3$ treatment. D) Graphical representation of the intensity of bands for the 120 minute AgNO3 treatment. Red lines represent the intensity of the cut 1.1 kb fragment, green represents the intensity of the cut 0.6 kb band, and blue represents the intensity of the uncut 1.7 kb band. All intensities were measured by Kodak MI software and graphed as the percentage of the total intensity from each lane. Error bars represent ± SE of total intensities from all of the digested samples from the corresponding $AgNO_3$ treatment.

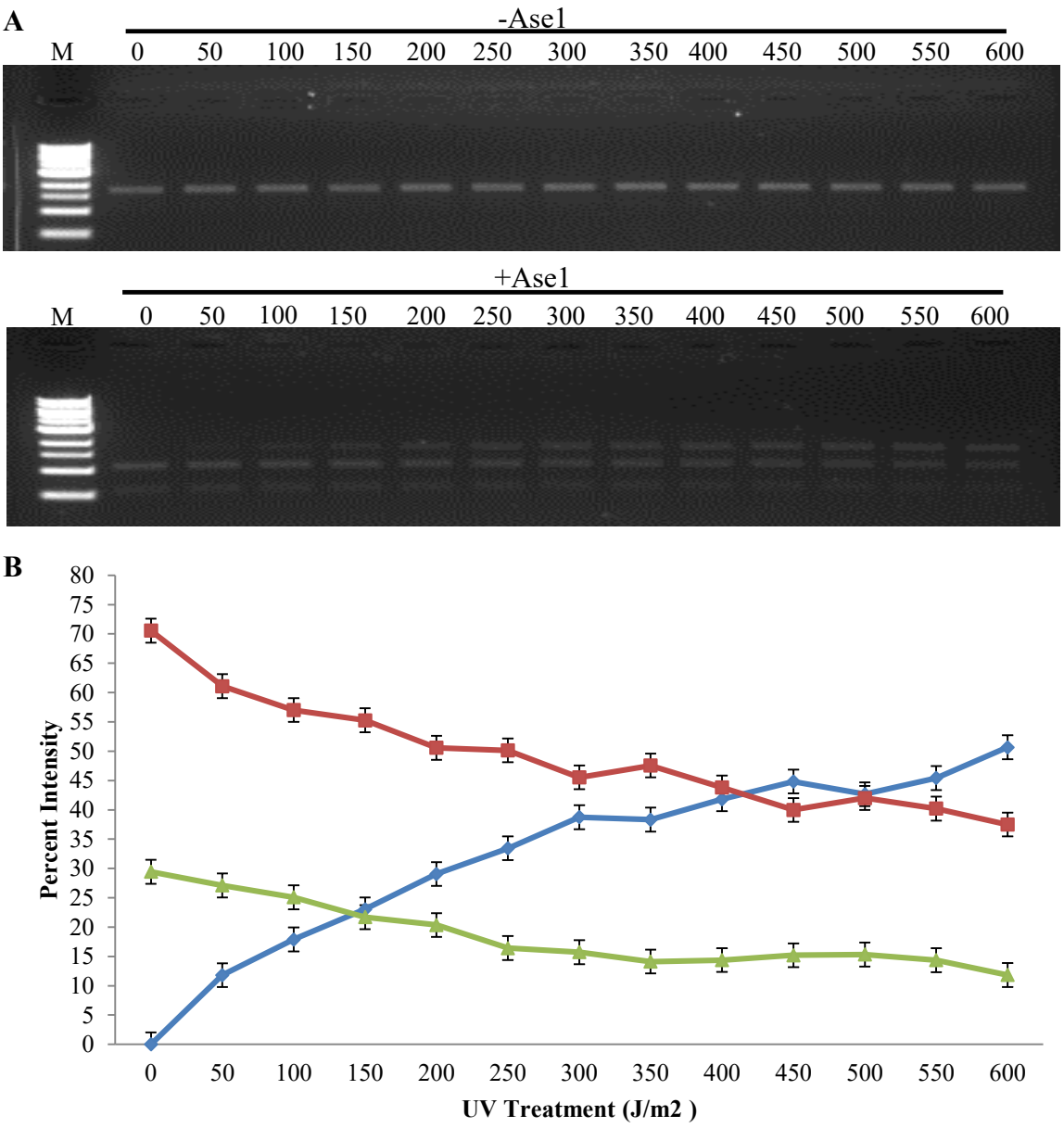

Appendix C2: Inhibition of Ase1 by Repetitive UV Treatment**.** A) Samples of BTU1 fragment DNA were treated with repetitive dosages of 50 J/m^2 of UV totaling the doses indicated above the lanes. Samples were mock treated (-Ase1) or treated (+Ase1) with Ase1 and analyzed via agarose gel electrophoresis to determine the ability of the enzyme to digest the DNA substrate. B) Graphical representation of the intensity of bands for the Ase1 treated samples. Red lines represent the intensity of the cut 1.1 kb fragment, green represents the intensity of the cut 0.6 kb band, and blue represents the intensity of the uncut 1.7 kb band. All intensities were measured by Kodak MI software and graphed as the percentage of the total intensity from each lane. Error bars represent ± SE of total intensities from all of the digested samples from the various UV treatments.